Analysis, Design, and Control of a Single-Phase Single-Stage Grid-Connected Transformerless Solar Inverter

Manisha Verma

A Thesis

In the Department

of

Electrical and Computer Engineering

Presented in Partial Fulfillment of the Requirements

For the Degree of Master of Applied Science at

Concordia University

Montreal, Quebec, Canada.

June 2019

CONCORDIA UNIVERSITY
SCHOOL OF GRADUATE STUDIES

This is to certify that the thesis prepared

By: Manisha Verma

Entitled: Analysis, Design, and Control of a Single-Phase Single-Stage Grid-Connected Transformerless Solar Inverter

and submitted in partial fulfillment of the requirements for the degree of

Master of Applied Science

Complies with the regulations of this University and meets the accepted standards with respect to originality and quality.

Signed by the final examining committee:

_____ Chair
Dr. Luiz A. C. Lopes

_____ Examiner, External
Dr. Anjali Awasthi (CIISE) To the Program

_____ Examiner
Dr. Luiz A. C. Lopes

_____ Supervisor
Dr. Akshay Kumar Rathore

_____ Co-Supervisor

Approved by: _____
Dr. Yousef R. Shayan, Chair
Department of Electrical and Computer Engineering

_____20_____ _____
Dr. Amir Asif, Dean
Gina Cody School of Engineering and Computer Science

ABSTRACT

Analysis, Design, and Control of a Single-Phase Single-Stage Grid-Connected Transformerless Solar Inverter

Manisha Verma

As energy utilization is increasing with the rise in the world's power demand, the traditional energy sources are depleting at a high pace. It has led to attention drawn towards inexhaustible energy resources. There is a huge augmentation in the power generation from renewable energy sources (RES) like wind, solar, hydropower, biomass, etc. to reduce the stress on conventional energy sources like fossil fuels, oil, gas, etc. There has been a steep increase in interest for wind and solar energy systems. PV energy has been growing swiftly in the past two decades which made it most demanded power generation system based on RES. This worldwide requirement for solar energy has led to an immense amount of innovation and development in the Photovoltaic (PV) market. The Conventional grid-connected PV inverter was either with DC/DC converter or without DC/DC converter. These inverters were isolated using a transformer either on the grid (AC) side as a low-frequency transformer or as a high-frequency transformer on the DC side. Elimination of the transformer leads to a galvanic connection between the grid and PV module. This gives rise to the flow of leakage current which is disastrous for the system when it exceeds a specific value. Thus, minimization of this leakage current after the removal of the transformer has been an interesting topic explored by many researchers. Many topologies have been proposed targeting reduction in this leakage current either by 1.) Directly connecting the PV negative with neutral of utility grid or 2.) Disconnecting the PV panel side from AC side. This generally involved addition of more switches or diodes or supplementary branches to disconnect during the freewheeling period. Generally, the above-mentioned ways lead to a reduction in efficiency due to increased losses or complex circuitry.

The motivation of this thesis is to design a transformerless inverter for single-phase PV grid-tied system with a smaller number of devices and still has minimum ground current. It discusses the prevailing inverter topologies in detail and then explains the modes of operation of the proposed inverter. A simple control strategy has been derived and passive elements of the inverter are designed. The simulation results presented have validated the theoretical claims. The experimental results which are similar to simulation results are evidence that the proposed topology is suitable for PV grid-tied systems.

Also, the dynamic modeling of the inverter has been done to derive the plant transfer function. Then, the Proportional Resonant (PR) controller has been designed to ensure the flow of sinusoidal current into the grid with zero steady-state error and constant sinusoidal grid voltage irrespective of load change. The simulation and experimental results achieved high performance which makes this topology successful and promising for grid-tied PV systems.

I dedicate this work to my family…

Acknowledgments

First of all, I would like to express my deepest gratitude to the almighty for his grace and bestowing his blessings upon me throughout this journey. I am thankful to my supervisor, Prof. Akshay Kumar Rathore, for giving me this opportunity.

The members of Power Electronics and Energy Research (PEER) became my small family in no time. I am grateful to all my colleagues for helping in one or another way. To be specific, special thanks to Sivanagaraju, Lucas, Karin, and Amit for solving all sorts of doubts numerous times. I have always looked upon them in times of trouble. Not to mention my friends Bigyan, Sumeet and Yupeng who made this research a bit light and fun and life became beautiful with their company.

Last but not least, I am highly obliged to my family because they believed in my ambition and stood by me to accomplish it. It would not be possible without my parents. Thank you for your faith and encouragement.

Table of Contents

Table of Figures

List of Tables

Chapter 1 **Introduction**

1.1 Renewable Energy Sources (RES)

It is a well-known fact that the major contributors to greenhouse emissions on the earth are power generation and transportation sectors. The continuous usage of conventional power plants has proven to be unsuitable for the environment. The excessive use of fossil fuels has resulted in shrinking of its reserves, thereby adversely affecting the environment as well as alarming the users. The soaring demand from power generation sectors has led to the exhaustion of non-replenishable conventional resources. It is crucial to reduce these emissions by incorporating renewable sources as they lead to a less contaminated world [1]. The increment in the usage of RES is also due to expansion in electricity grids with rising load demand. The various types of RES include hydropower, wind, geothermal, biomass, wave/tidal and solar energy. As per the Renewables Global Status Report (GSR), a fifth of the world's power production is derived from renewable energy sources. These are contributing to 18% of net primary energy supply in Canada, where wind and solar energy are rapidly growing sources of electricity. Wind energy has contributed to 4% of the electricity generation whereas solar energy accounts for 3.5% of energy generation in Canada. Figure 1.1 shows the contribution of various renewable energy sources for generation of electricity, heat, and biofuels [2].

1.1.1 Applications of Power Electronics in Renewable energy Systems

Power electronics is the link for power conversion by utilizing semiconductor devices. The constant urge for improvement in our standard of living has increased the consumption of electrical energy by leaps and bounds [3]. This hike in energy consumption, draining of fossil fuels and degrading global environment has led to the invention of the green power generation systems. These RES need power electronics technology for load interactive power conditioning.

Recently, the focus has shifted to the development of the small and medium scale power plants integrating renewable energy sources in the field of power distribution. It is known as Distributed Generation (DG) plant [4]. Power electronic converters are responsible for aligning the RES based plant with the distribution grid. Although these resources are abundant in nature, still the expense of power electronics and conversion efficiency are of main interest.

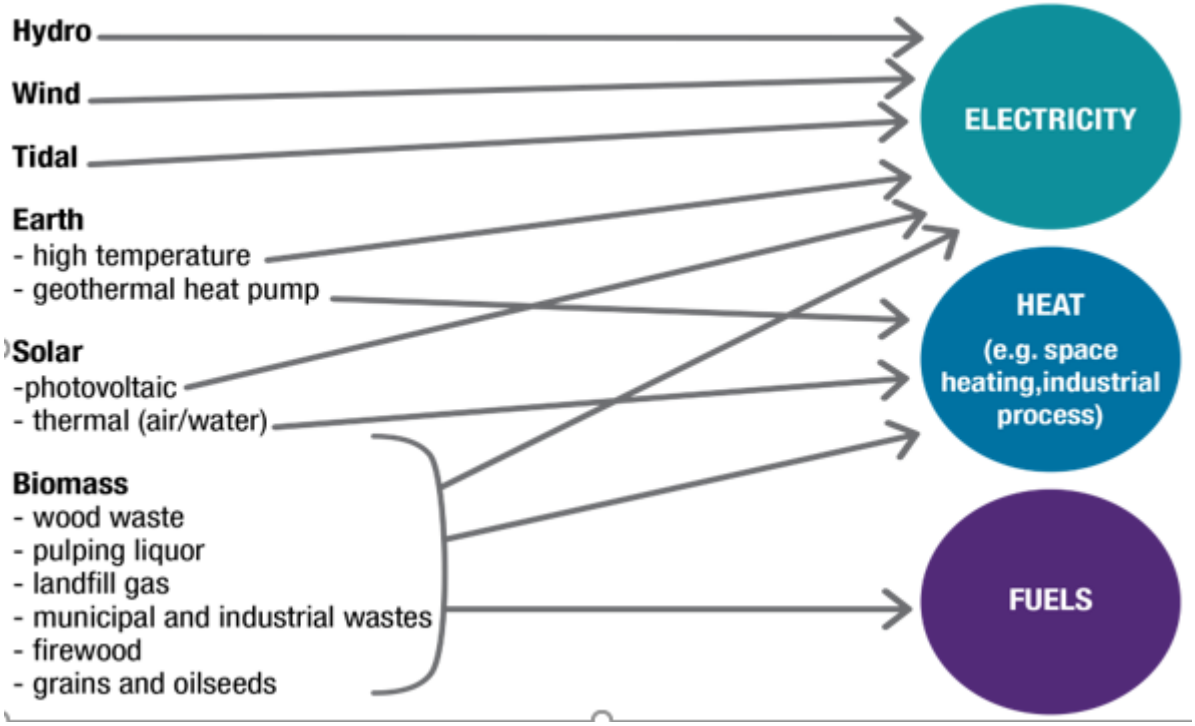

Figure 1.1 Various Renewable Energy Sources

In the course of the kickoff period, these RES were critically costlier than conventional fuels. However, their cost dropped in an exponential manner in the past ten years [5]. During the previous few years, power electronic technology has gone through tremendous transformation for amalgamation of renewable energy sources into the electrical grid. It is mainly due to the advancement of fast semiconductor devices and the establishment of real-time controllers [6]. Among available clean energy resources, wind energy, solar energy, and hydrogen energy have gained the most worldwide attention. While wind energy is considered to be most economical, photovoltaic is the utmost eco-friendly and the fuel cell has the topmost energy conversion efficiency so far. Their operation has steadily improved and the price has reduced simultaneously.

The inverter interfacing the PV panel to the utility grid is considered as a potential element. The major issue associated with the global acceptance of the PV panels on a large scale has been its cost. But a falling pattern has been observed in terms of cost of solar panels due to immense production of solar panels over the years. Such a graph is depicted in illustrating the expansion of solar energy from a corner market to mainstream source of electricity, as a potential alternative to conventional energy resources. For instance, the cost of crystalline cells was 77 USD /watt in 1977 and in 2018, it was worth 0.33 USD/watt which

means 600 times drop in rate in forty years [7]. Thus, to further contribute in addressing this concern, various attempts have been made on the PV inverter. It is an integral part of PV power generation as the PV panel and inverter are considered as a system such that the cost reduces but the performance and efficiency remain intact.

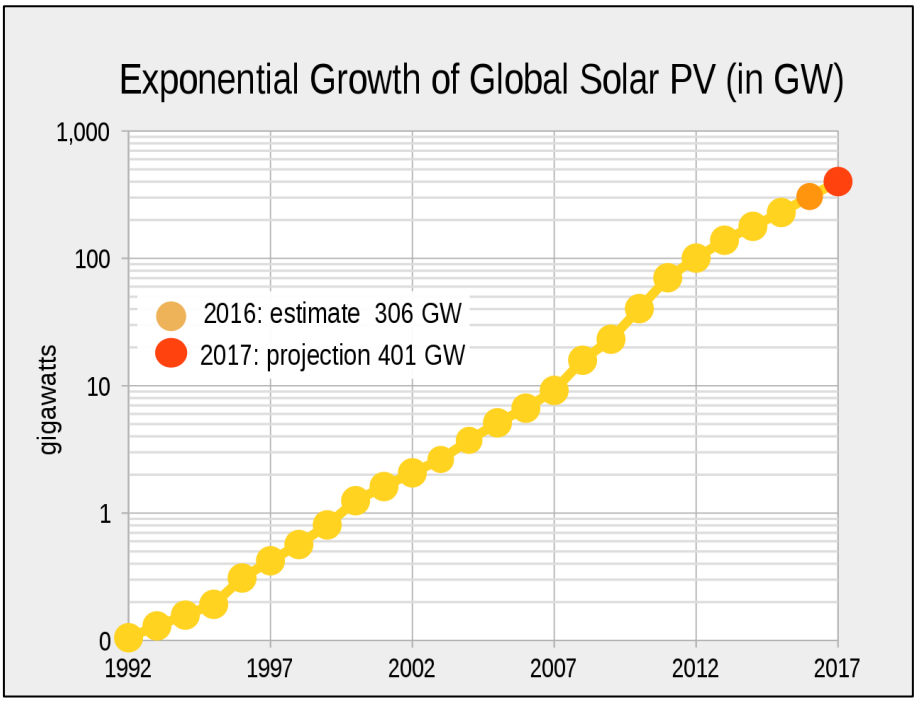

Figure 1.2 Photovoltaic (PV) Growth from 1992-2017 [7]

Main functionalities of power electronic converters are:

1. Power conditioning from an available form of electric power to another form.
2. Voltage regulation with respect to source variability.
3. Power flow control with respect to source availability.

1.2 Overview of Photovoltaic (PV) Systems

The trending improvements in the power and digital electronics market led to the tremendous growth in small scale distributed generation systems integrating RES like wind, hydro and solar energy. The reason behind unprecedented attention gained by PV systems is its presence in abundance and the existence of global concern about the extinction of fossil fuels with the growing demand. Initially, the cost was a major hurdle but now the PV modules are economical and comprise of a power electronic converter for ac grid interfacing distributed generation (DG) systems. It is a well-known fact that solar power is the most abundant energy. Interestingly, solar energy is evaluated equally to 15,000 times the annual energy consumption

of the earth. PV technology could be a promising RES for the upcoming electric demand with the reduction in cost.

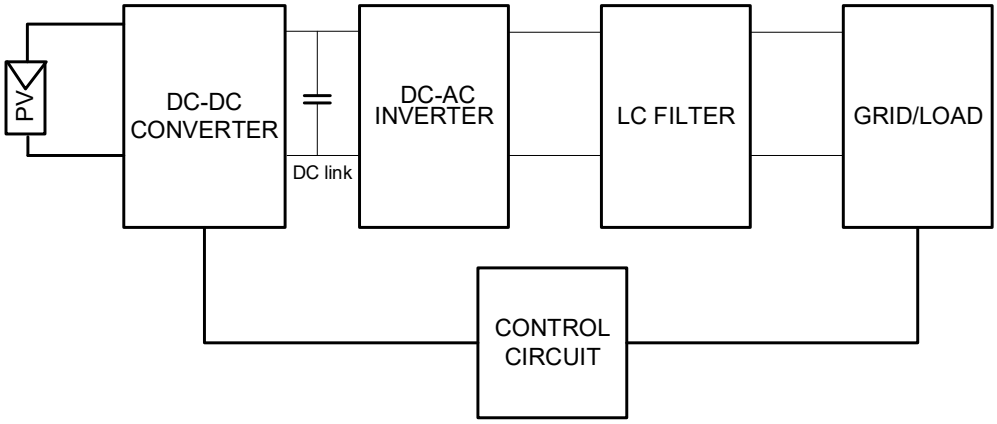

Figure 1.3 Energy flow process from source to main load (grid)

As the sunlight strikes over the PV panel, Electromotive Force (EMF) is produced due to transfer in the momentum of sunlight photon. This results in the conversion of solar energy into electric energy and current passes from the PV array to an electrical load. The solar panel generates electricity in DC form. The PV application can be categorized into stand-alone, grid-connected and hybrid based on the load configuration. In the case of grid-connected PV systems, all the energy produced is directly fed to the utility grid. The standalone PV systems are known to function irrespective of AC grid and are generally designed for specific DC/AC electrical load. The hybrid renewable energy system can be utilized for both islanding mode or connected to grid mode.

When sun radiates heat on the solar PV array, then solar panels generate DC electricity. Since the most appropriate approach to increase power in power systems is by elevating the voltage levels thereby curbing current and minimizing losses. Hence, the inclination is shifting from low voltage to medium voltage by using series connected solar panels in PV systems [8]. It is fed to a DC-DC converter which is then followed by an inverter for transmitting solar power to the utility grid. The inverter is the main component of grid-tied PV systems as it converts DC power produced by the PV array into AC form. Nowadays, grid-tied PV systems with energy storage (ES) devices are trending. The battery bank is often used as an energy reserve for the same. It can be charged during off-peak hours and excess energy generated can be utilized by grid during peak load hours [3]. Figure 1.3 illustrates the above-mentioned process of solar energy flow from PV panels in DC form to load in AC form.

1.2.1 Grid-Connected (GC) PV Systems

Grid-connected PV systems are generally single-phase rooftop systems with a power range of up to 10 kW [6]. Grid-interfaced PV systems are preferred over standalone systems as former are cost-effective, needs low maintenance and do not require batteries for storage. It is considered to consume PV power in an efficient way and yield more energy. Their prime requirement is to produce sinusoidal output, which is congruent with the grid voltage waveform. The outline of a grid-tied system comprises of the PV system and a number of peripheral modules such as transformers, filters and conversion technologies. The fundamental element in the grid-tied PV System is power electronics based DC/AC inverter. It is mainly classified into string inverter, centralized inverter, and microinverter or AC-module inverter [9].

It could be categorized based on application, power rating, and system configuration. Figure 1.4 explains the classification of various grid-connected power inverters. The microinverter interfacing PV modules have to guarantee that the modules are operated at Maximum Power Point (MPP) and sinusoidal current must be injected into the grid. The PV microinverter can also be sorted as follows: 1) Types of power decoupling 2) a number of power processing stages in cascade 3) with transformer or without a transformer and 4) type of grid-connected power stage [10].

1.2.2 Stand-alone Photovoltaic (PV) Systems

A stand-alone, also known as the off-grid solar system is not connected to the grid and operates in self-sustained mode. It consists of PV modules, which are used to charge the batteries. These rechargeable lead batteries act as storage devices and supply stored power to electrical loads. It also comprises a charge controller as a control unit and a DC/AC converter for AC loads [11]. It can be used for applications like cabins in remote areas where the grid is not present, recreational vehicles, solar-powered water pumps, emergency phones and many more. As per given estimation by the International Energy Agency (IEA), the surplus population of 1.7 billion added to urban areas would increase the global demand by more than a quarter by 2040 [12]. Till today, grid installation is not feasible in rural areas of developing countries.

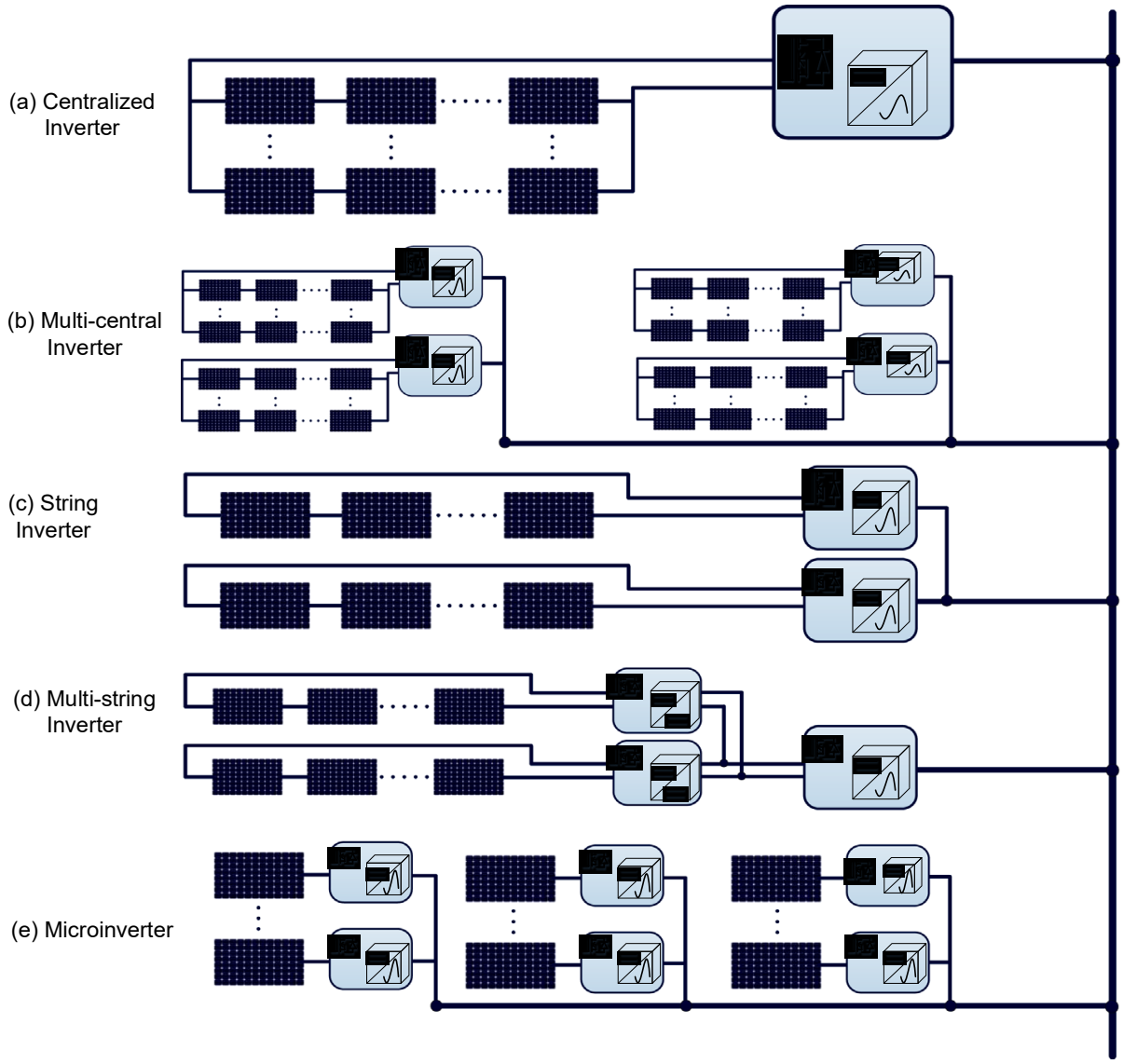

Figure 1.4 Grid-connected PV technologies [8]

Thus, Stand-alone PV systems have been fruitful for rural electrification, solar home systems. The number of people deprived of electricity has gone below 1 billion in 2017. Although they are advantageous due to low cost, more efficient, longer life span, robust and low maintenance, they require a high initial investment which is a hindrance. Thus, the share of grid-tied PV systems is 99% of net installed capacity whereas the remaining 1% is derived from standalone systems [9]. It has proven to be the best alternative for fulfilling the electricity demands of isolated areas. Figure 1.5 explains stand-alone PV systems.

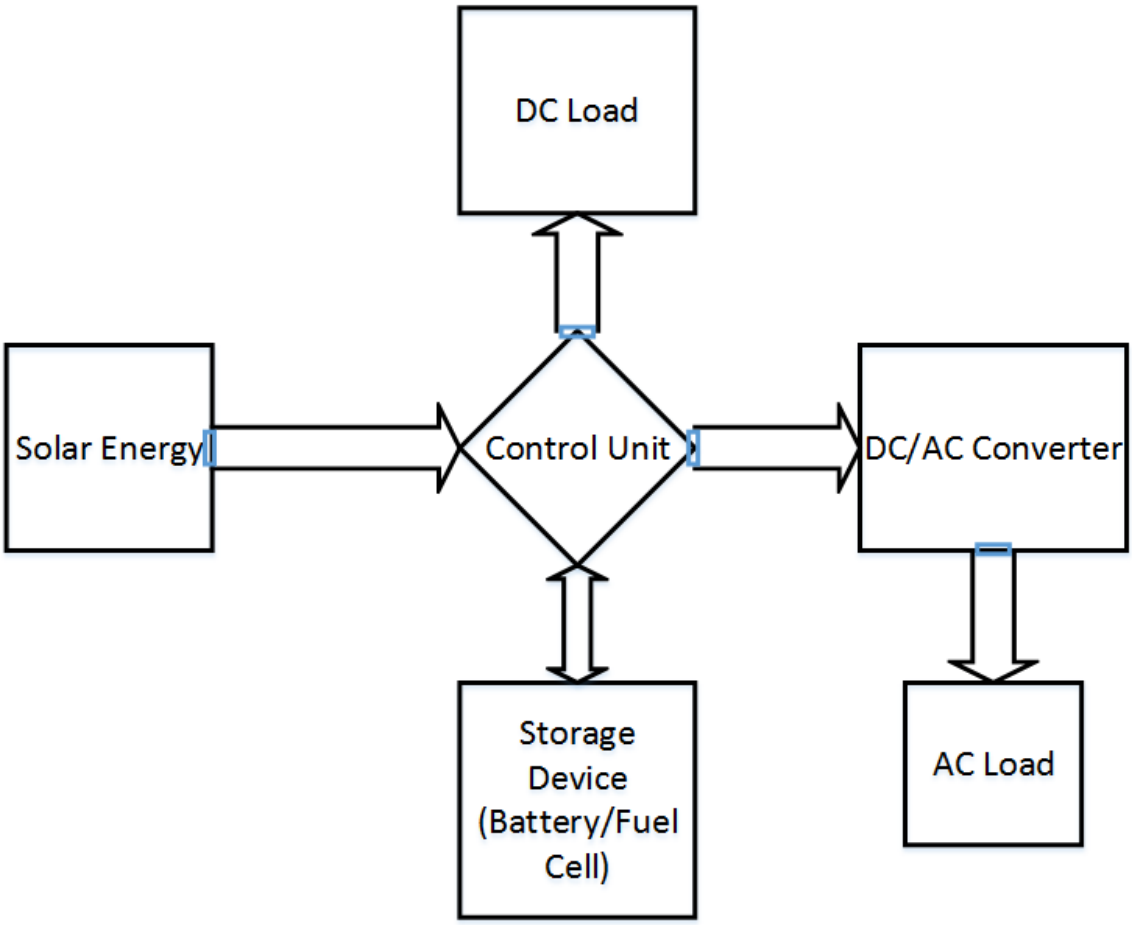

Figure 1.5 Block diagram of the stand-alone PV system

1.3 Types of Grid-Connected PV Inverter

The inverter is considered the most vital element for converting the DC electricity produced by solar panels into AC electricity for residential purposes or to the grid. Around the mid-1970s, grid-connected PV inverter was introduced. As per the architecture, they are categorized as centralized, string and microinverter. Microinverters are low power rating inverter ranging from 150 to 400W. They are assigned to individual PV module of the system. The central inverter has a life span of ten years and it has replacement cost almost twice that of PV microinverter. The multi-central inverter could be comprehended as a parallel connection of output from numerous central inverters. This has led to microinverter becoming an alternative solution to central inverter [13]- [14]. The inverter interfacing AC grid and PV panel must have the following characteristics:

- The dynamic response should be fast.
- Unity factor close to unity.
- Output should have fewer harmonics.

Various topologies have been experimented to evaluate and improve the inverter's performance and efficiency. They are characterized based on cost and high-quality output voltage and current.

1.3.1 Central Inverter

This inverter has a configuration of a series connection of PV panels to form a string of PV panels in order to increase the voltage rating of the inverter. These PV strings are then connected in parallel sharing the same voltage to increase the power level as shown in Figure 1.4 (a). By end of the 1980s, they became prominent and various projects incorporating it began. The topology implied was line-commutated inverters [9]. Later, it changed to switch mode inverters due to access to the high-frequency switching devices. Although this configuration provides common MPPT for PV array, it is disadvantageous as MPP operation is not present for each module due to shading and clouding effects. It is generally considered for large scale power generation. Despite its advantages such as low initial capital, high efficiency, it has some loopholes like more noise, bigger in size and a fault at any single point is sufficient for entire unit failure [15]. Moreover, the presence of high voltage DC cables might cause several losses including power losses, mismatch losses among the PV modules due to which profit of mass production could not be achieved.

1.3.2 String Inverter

A string inverter is a scaled down topology of the centralized inverter. It is most commonly used an inverter for the grid-tied PV system. Since it has a configuration of a number of PV modules connected in series to form a string as shown in Figure 1.4 (c), it provides more precise MPPT [16]. They are suitable for medium scale (up to 5 kW) PV power generation systems. It would lead to lower partial shading or clouding effect. Thus, string inverter provides higher efficiency by delivering higher power to the utility grid and is considered superior to the centralized inverter. Still, it has some shortcomings like the shading in one of the modules would hamper the entire operation of that PV string.

An extension of this topology is multi-string inverter as shown in Figure 1.4 (d). It comprises of each string with individual MPPT followed by a low power DC-DC converter, which is connected to a central inverter via DC bus. It could be utilized for larger power systems as well. Thus, independent MPP tracker at each PV string optimizes power output and provides the benefit of controlling each string exclusively. It is considered a hybrid topology comprising of central and string inverter topologies.

1.3.3 Microinverter/AC Module Inverter

Microinverter emerged as a topology to overcome the loopholes of centralized and string inverter by diminishing clouding and shading effect of the PV system in the 1990s. It is composed of an integrated module having an inverter with independent MPPT for each PV module as shown in Figure 1.4 (e) [16]. Therefore, in case of partial shading in one of the modules, other modules remain unaffected. In addition, since the inverter is connected to only one PV module inside the AC module, it can be directly attached to the utility grid. Henceforth, they are popularly known as "*plug and play*" device. This eliminates the need for DC wiring and proves to be beneficial. It is worth mentioning that DC-AC conversion, voltage amplification, and MPPT are performed in a single module. The warranty of microinverter is 25 years as provided by the manufacturer. On the contrary, in terms of cost, it is considered expensive as compared to standard string and centralized inverter. The tensility of the microinverter could be tested by voltage amplification as it has low voltage rating (30-45 V). It is possible either with an isolated high-frequency transformer or a non-isolated boost converter, which presents a supplementary DC-DC stage for stepping up the voltage. DC-DC boost converter also provides MPPT. It can be isolated or non-isolated, have single or multiple power processing stages as shown in Figure 1.6 (a) and (b). The center-tapped transformer shown in single-stage inverter in Figure 1.6(b) is responsible for not only raising the voltage level but also for producing rectified AC at the secondary end [9].

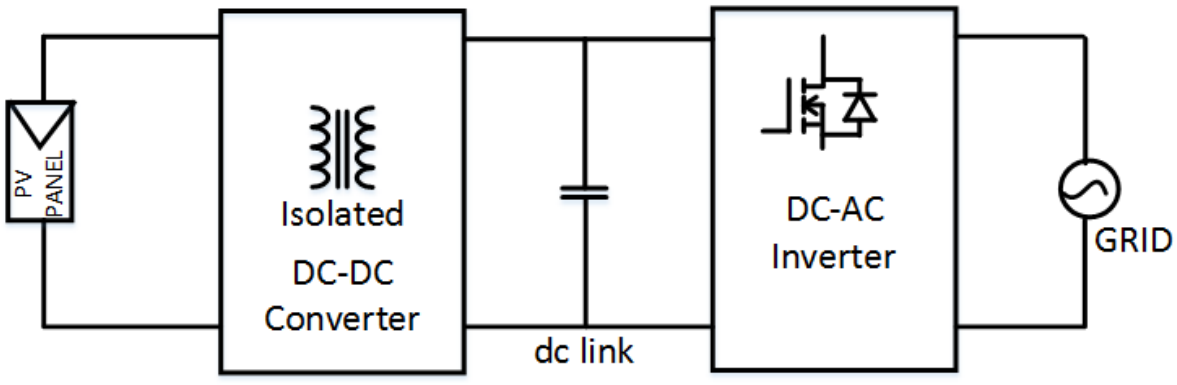

(a)

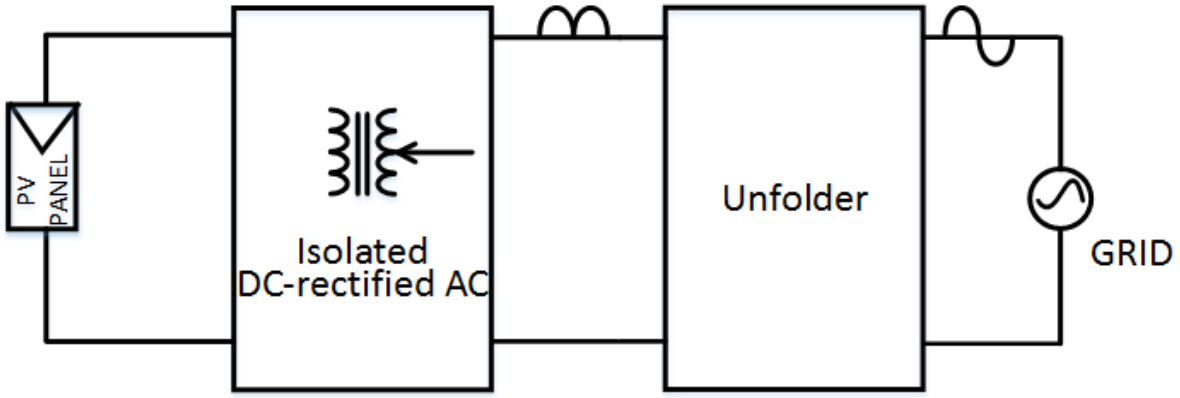

(b)

Figure 1.6 (a) Multi-stage isolated Microinverter; (b) Single-stage isolated Microinverter [9]

The single-stage isolated microinverter could be either flyback or interleaved flyback converter for stepping up the DC voltage level. The two-stage configuration is simple and direct with the DC-DC boost converter in the first stage for voltage amplification and inverter in the second stage providing the high-quality current to AC grid, it has certain drawbacks as well. Despite this fact, it has claimed to have more efficiency than the single-stage isolated microinverter. Maximum efficiency of 94% for single-stage isolated topology, 96.2% for multi-stage isolated and 99.01% for multistage non-isolated transformerless inverter has been stated [9]. It proves inclination towards the multistage non-isolated inverter. The power decoupling techniques could be among the following: PV side decoupling, DC link decoupling, and AC side decoupling.

1.4 Conclusion

In this Chapter, with the rapidly increasing energy demand, the consumption of traditional energy resources at a distressing rate is highlighted. Due to this, renewable sources are gaining popularity at a high pace, which has been discussed in detail. It is followed by focusing solar energy being used as an alternative to conventional energy sources such as fossil fuels, oil, and gas which are degrading quickly. In addition to it, the two most common configurations in a PV system and its various types have been discussed in this Chapter. The further explanation of PV inverter and introduction of transformerless PV inverter is detailed in the next chapter. Also, the prevailing topologies of transformerless PV inverter are discussed in Chapter 2.

Chapter 2 **Literature Review of Non-isolated Solar Inverters**

2.1 Introduction

In the past few decades, there has been a major drift towards energy production from renewable energy resources, also known as clean sources of energy. The pollution, CO_2 emission and global warming hampering the environment caused by the consumption of traditional energy resources cannot be neglected. This has increased the focus on the production of power from solar energy i.e. solar cells or PV cells. There is a multitude of ways in which sunlight energy can be transformed and utilized through solar cooker, water heater, etc. [17]. The tremendous growth in the solar market is evident from the fact that the power generation from PV has touched 512 GW in 2018 end, which is 3% of net global electricity demand. It is calculated that gross power generation from renewable energy sources would be the same as power generation from coal by 2040, in which half of the contribution comes from solar and wind [4]. As estimated by the International Energy Agency (IEA), solar power is anticipated to be the world's largest source of electricity by 2050 [7]. As discussed in the previous Chapter, the PV system can operate in stand-alone (off-grid) or grid-interfaced system. With respect to the grid-tied system, the inverter has to ensure that maximum power is seized by the PV system through MPPT strategies and power is fed to the utility grid with minimum losses [18]. A literature study has been done to understand the reason behind the evolvement of transformerless inverter and various transformerless PV inverter trending in the market. Their requirements, advantages over the isolated PV inverter and the loopholes in the existing topologies have been analyzed.

Based on the galvanic isolation, PV microinverter can be transformerless and transformer isolated configuration. Generally, transformers are employed to provide voltage gain and galvanic isolation. The high-frequency transformer on the DC side or a low-frequency transformer on the AC grid side in microinverter adds to isolation. The transformerless inverter became significant in the low power distributed PV generation systems once the benefits due to transformer elimination got highlighted. Their omission reduces size, weight and the losses in the inverter, thereby increasing the overall efficiency of the system. However, removal of the transformer leads to eradication of galvanic isolation between the PV array and grid. The aftereffect is the flow of leakage current, also known as DC current due to the parasitic

capacitance of PV panels to ground caused by the galvanic connection between PV panels and the utility grid. It is depicted in Figure 2.1

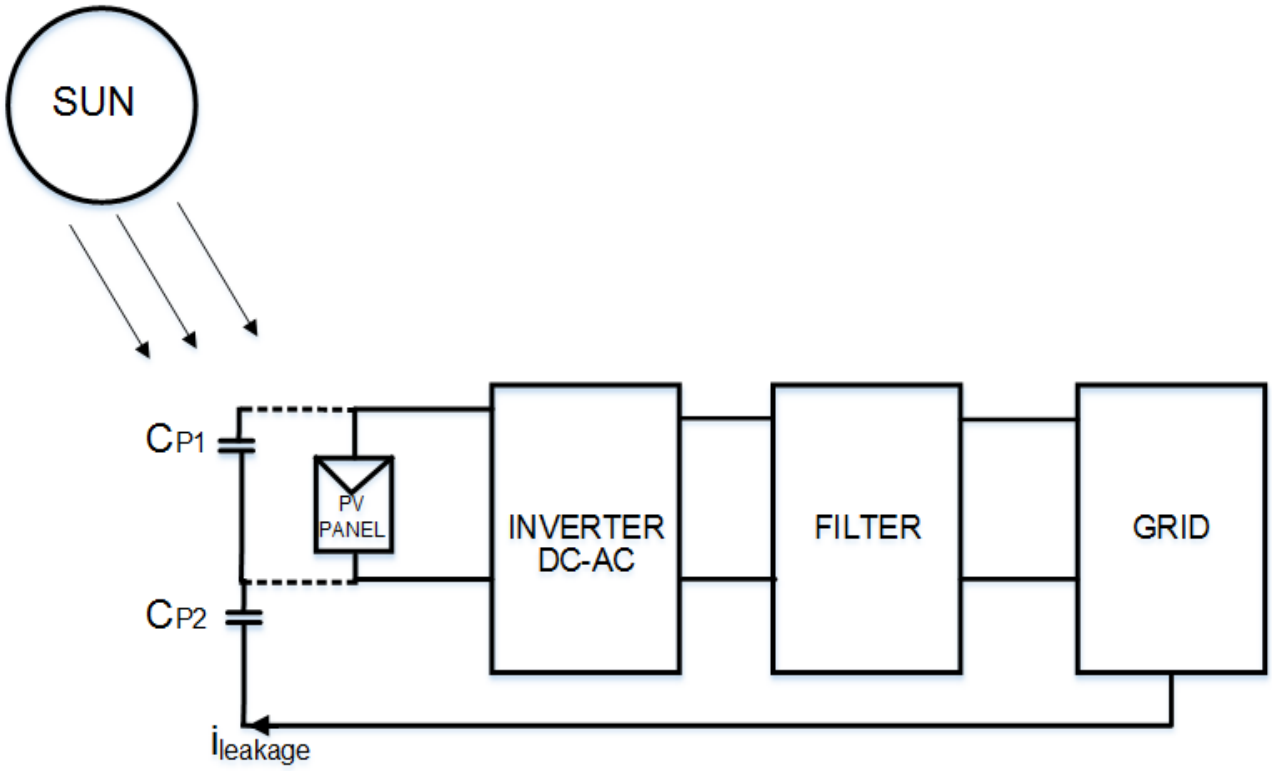

Figure 2.1 Block diagram of transformerless PV inverter [11]

These ground currents are produced by varying common-mode (CM) voltage and are injected into the ground through parasitic capacitance that is responsible for the rise in electromagnetic interference (EMI) and harmonics being injected into the grid [19]. This gives rise to capacitance formation whose one electrode is from PV cells and the other is from the earth. One issue that cannot be ignored is that it makes a CM resonant circuit comprising of DC source ground parasitic capacitance, inverter, filter and grid impedance [20]. In the presence of the transformer, this current flow through the stray capacitance of the transformer. Transformerless PV inverters can be classified in numerous ways based on the number of power processing stages, use of the transformers, location of power coupling capacitors and types of interface with the grid [6].

2.2 Standards of Inverters for Grid-connected PV System

The objective of PV inverter is to feed sinusoidal current into the grid. Now, the galvanic connection formed due to the removal of the transformer leads to flow of leakage current from PV to ground parasitic capacitance forming a conducting path to the inverter. In

the presence of the transformer, this current flows through the stray capacitance of the transformer. The circulation of ground leakage current is responsible for the increase in harmonic content which leads to Electromagnetic Interference (EMI) between the PV panel and the grid.

There are some standards, which are governed by national and international committees like the International Electro-Technical Commission (IEC) and IEEE which deal with topic like power quality, islanding situation (continuous operation of inverter even after grid is disconnected due accident, damage), grounding etc. to ensure uninterrupted operation between PV panel and the grid [16]. These standards put limits on the DC current that might be injected into the grid and lead to saturation of distribution transformers. As per German VDE 0126-1-1, when leakage current exceeds 30 mA, then the grid is disconnected from inverter within 0.3 seconds. Table 2.1 explains relation between peak value of leakage current and its disconnection time (VDE-4105, IEEE-929-2000, IEC 61727, IEEE 1547, and EN 61000-3-2) [21]. It could vary between 0.5 and 1% of rated current.

Table 2.1 Correlation between allowed maximum leakage current and disconnection time [21].

Leakage Current (in mA)	**Disconnection time(sec.)**
30	0.3
60	0.15
100	0.04

2.3 Evolution of Single-Phase Transformerless Photovoltaic (PV) Inverter

The grid-connected PV inverter can be categorized as follows:

a) Number of power processing stages
b) Inclusion or exclusion of transformer
c) Power decoupling between the PV panel and the AC grid
d) Types of grid interfaces

(a) Types of processing stages - PV inverter could have single or dual power processing stage as shown in Figure 2.2.

In the case of single-stage, the MPPT, voltage amplification and grid current control are done by an inverter. In dual-stage, DC-DC converter does the stepping up of the voltage and MPPT, while inverter converts DC output current to sinusoidal AC current by pulse-width modulation (PWM) switching to feed into the grid. As per the control strategy employed, either DC-DC converter would generate a pure DC voltage or a rectified sine wave [10].

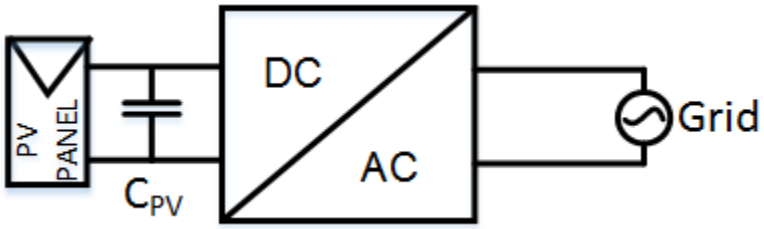

(a) Single power processing stage

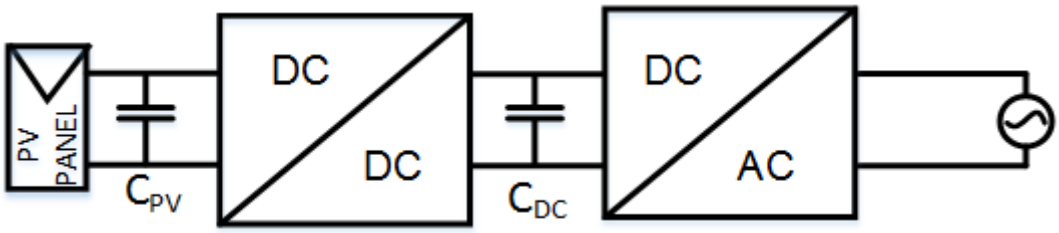

(b) Dual power processing stage

Figure 2.2 Types of power processing stages [10]

(b) With or without transformer - As mentioned earlier, PV inverter utilize either high-frequency transformer at DC side or line frequency transformer at grid side. These transformers help in the elimination of the DC current injection from the PV array to the grid. The grid frequency (line frequency) transformer is not recommended as they are bulky, costly and hard to install whereas the high-frequency transformers which are small in size and lightweight if used, decreases the overall efficiency due to leakage in transformer and are pretty complex because of multiple power stages [21]. Although they ensure isolation between the PV panels and grid, eliminating the transformer helps in reducing the size, weight, cost, and complexity. Thus, few high input voltage transformerless inverters have been discussed later in this Chapter in which input and output side can be grounded together.

(c) Power decoupling – Power decoupling is a process of allowing the DC component of input PV source and filtering out the voltage spikes. For the same, a decoupling capacitor is usually positioned either in parallel to PV modules or between DC link DC-DC converter and inverter as shown in Figure 2.2 (b). Since inverter converts DC to AC power at the high switching

frequency, it gives rise to switching transients. Thus, a DC-link capacitor ensures that these transients do not hamper the PV side by flowing in a backward direction. Generally, electrolytic capacitors are used but the film capacitor has been preferred due to the small size and capacitance is calculated by (2.1)

$$C = \frac{P}{2 * w_g * V_C * v_C} \tag{2.1}$$

where P = nominal power of PV modules

w_g = grid frequency

V_C = mean voltage across capacitor

v_C = ripple amplitude [10]

In addition to it, current drawn from PV modules is pure DC and that from the grid-connected inverter is a $Sin^2(w_{grid}.t)$ waveform. In case of the dual stage, both processing stage should be designed to handle twice the nominal power given by (2.2)

$$p_{grid} = 2.P_{grid}.Sin^2(w_{grid}.t) \tag{2.2}$$

(d) Types of grid interfaces – It could be:

1. Line frequency commutated current source inverter (CSI).
2. Voltage source inverter (VSI) with a decoupling capacitor.
3. VSI with unfolding inverter.

2.4 Types of Transformerless PV Inverter

After years of research to address the issue of minimizing leakage current by keeping CM voltage constant, a few renowned topologies have been successful, which are discussed next. They aimed at mitigating the high-frequency leakage current by either directly connecting PV negative terminal to the neutral of the grid or connecting negative PV terminal to the earth. A review of existing topologies is listed, it is not a comparison. It includes Half-bridge and Full-Bridge, Highly Efficient and Reliable Inverter Concept (HERIC), H5, H6, Neutral Point Clamped (NPC) and Karschny (Flying Inductor) Inverter. There are many companies manufacturing these PV inverters like REFU, Danfos solar, Ingeteam, Conergy, Sunways and SMA.

a) Half-Bridge Inverter:

The key elements comprise two switches (S_1, S_2), a capacitor divider at the input side and an output inductor. The working principle is simple: when S_1 is ON, the output grid voltage is $V_g = V_{Bus} = \frac{V_{in}}{2}$, while when S_2 is ON, the output voltage is$V_g = V_{Bus} = \frac{-V_{in}}{2}$. While the DC link voltage must be twice the maximum grid voltage. It provides zero ground current by generating a constant CM voltage [22]. Still, it has two drawbacks: firstly, the output voltage being modulated between $\frac{V_{in}}{2}$ and $\frac{-V_{in}}{2}$ produces current ripple and secondly, switching of semiconductors decreases the efficiency. The basic topology is reflected in Figure 2.3.

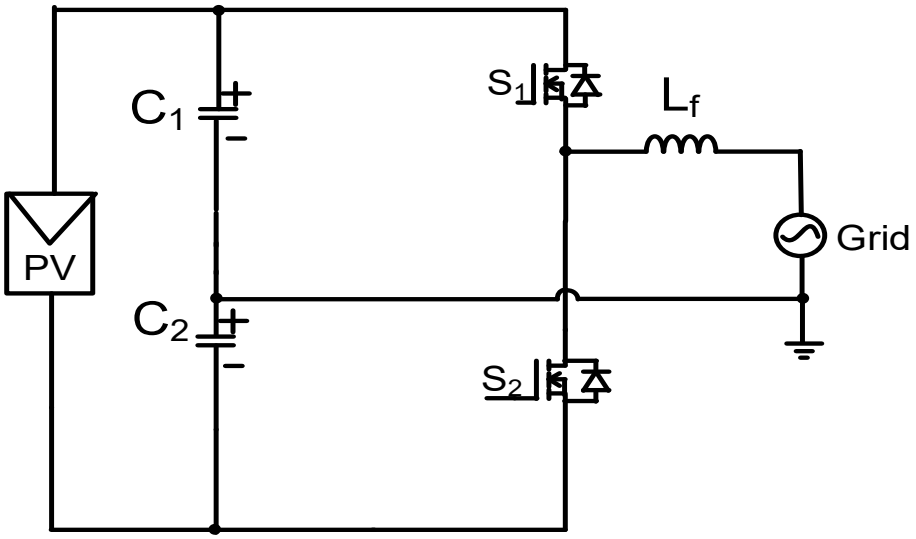

Figure 2.3 Half-bridge transformerless inverter

b) Full-Bridge Inverter:

Full Bridge Inverter (H-Bridge inverter) is the most widespread inverter, which can have both unipolar and bipolar PWM switching. In bipolar switching, a sinusoidal reference is given to diagonal switches while the other set gets the complementary signal. Output voltage gets modulated giving rise to high ripple current across the inductor. In unipolar switching, two sinusoidal references with a phase difference of 180° modulates the diagonal pair of switches. Output voltage alters with double of switching frequency. Therefore, it has ripple reduction and small filter size due to twice of switching frequency. Thus, unipolar modulation is preferred over bipolar modulation. The H-bridge inverter is illustrated in Figure 2.4.

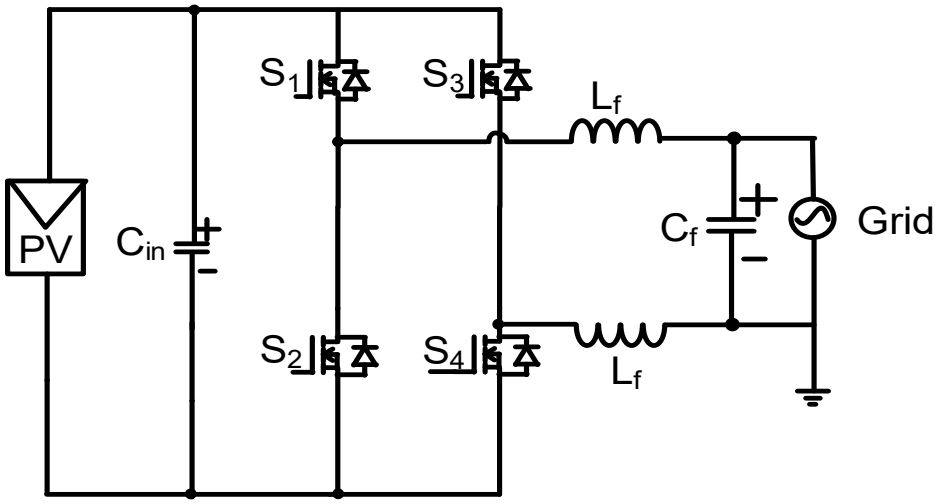

Figure 2.4 Full-bridge transformerless inverter

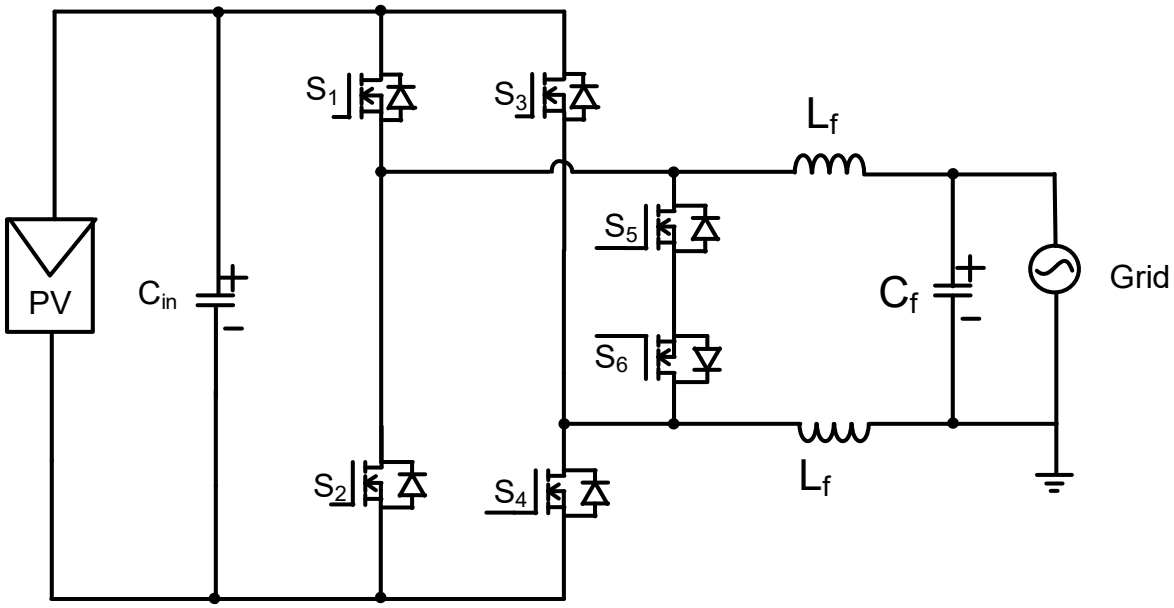

Figure 2.5 HERIC transformerless inverter

c) Highly Efficient and Reliable Inverter Concept (HERIC) Inverter:

This topology is derived by introducing additional switches, which are in the opposite direction in parallel to the filter of well-known full bridge inverter. It allows three-level output voltage, excludes reactive power flow and reduces CM voltage [23]. The pair of diagonal switches operate in the high-frequency during one half-wave cycle. One of these two extra switches is turned on during one half-wave to create a disconnection between the grid and PV array to decrease leakage current but higher switch count is still a concern. The topology is shown in Figure 2.5.

d) H5 Inverter:

This topology could be related to a conventional full-bridge inverter with an extra switch at DC side as presented in Figure 2.6. The lower pair of switches (S_2,S_4) work at high frequency whereas the upper pair of switches (S_1,S_3) operate at grid frequency. The supplementary switch S_5 operating at high-frequency aids in disconnecting the PV array from the utility grid during the freewheeling mode by interrupting the leakage current path and thus output inverter voltage is zero. Although three switches ON together during active mode is a major concern as it gives higher conduction losses than HERIC topology ([19], [24]).

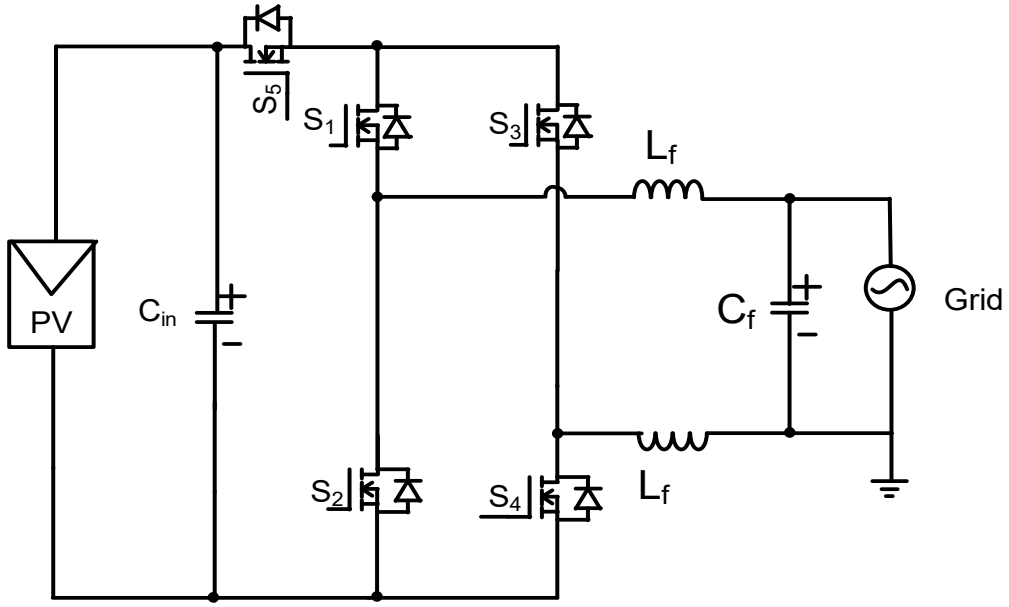

Figure 2.6 H5 transformerless inverter

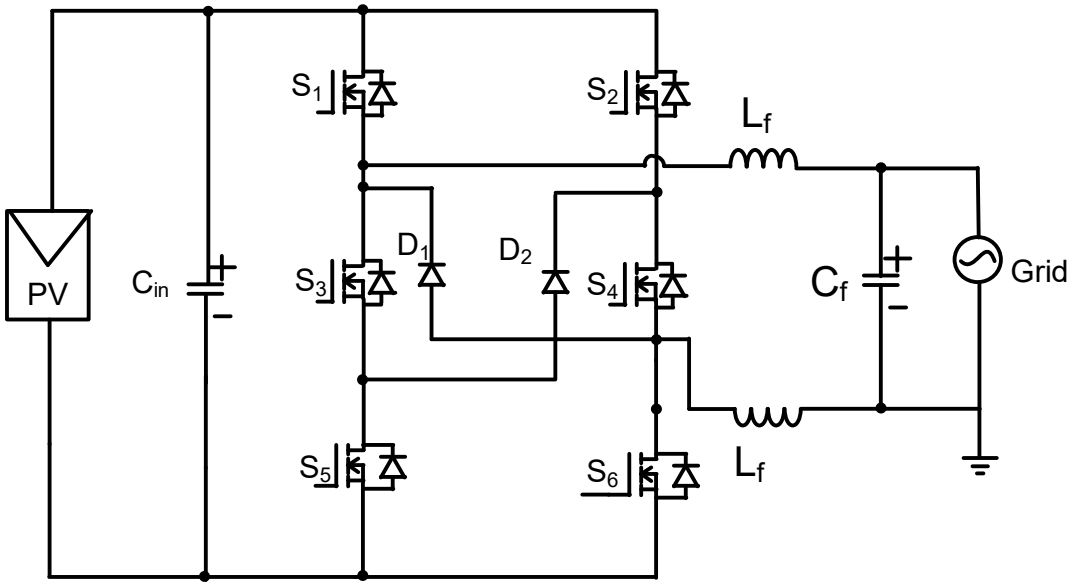

Figure 2.7 H6 transformerless inverter

e) H6 Inverter:

This inverter comprises of six power MOSFETs, two freewheeling diodes and a low pass filter composed of two split inductors and a capacitor. It could be analyzed as H5 inverter with an extra switch and two diodes shown in Figure 2.7. In the positive semi-cycle, switches (S_1, S_4, and S_6) are active and in its freewheeling period, S_4 and D_1 detach the grid from PV array. In addition to it, ground leakage currents are reduced as there are only low-frequency components in voltage across parasitic capacitance. Although the additional components increase the cost as compared to conventional H-bridge inverter [19].

f) Neutral Point Clamped (NPC) Inverter:

It is one of the established solutions in traction applications. The midpoint of dc- Link capacitor is linked to the neutral of the utility grid. Although, it is advantageous in terms of three levels inverter output voltage and minimum voltage oscillations of PV array, one of the issues of this circuit is that it undergoes higher transient voltages at middle switches as these are not clamped to dc-link capacitors ([19], [23]). Along with this, the requirement of input voltage is twice that of the input voltage required by H-bridge inverter. Also, the higher number of switches and diodes makes it complex. Figure 2.8 shows the topology of the NPC inverter.

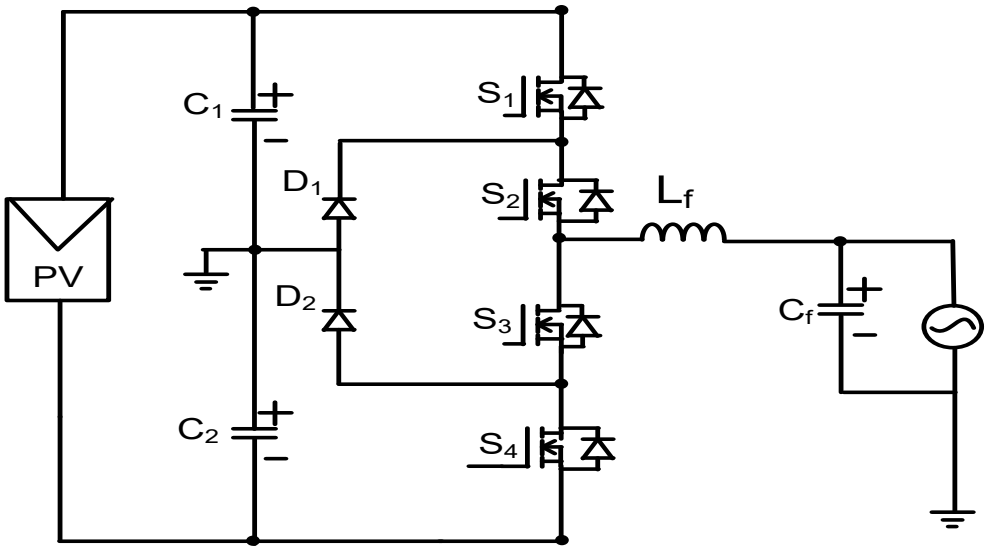

Figure 2.8 NPC transformerless inverter

g) Karschny Inverter :

It is also known as *Flying Inductor* topology. It is basically a buck-boost converter with supplementary switches, diodes, and passive elements to store energy. On one hand, it is beneficial as it connects negative PV array with the neutral of the grid and removes the voltage oscillations. On the other hand, the supplementary switches and large inductor to store entire

inductive energy contributes to depreciation in efficiency and an increase in cost and losses. Figure 2.9 reflects its topology and positioning of switches and passive elements [19].

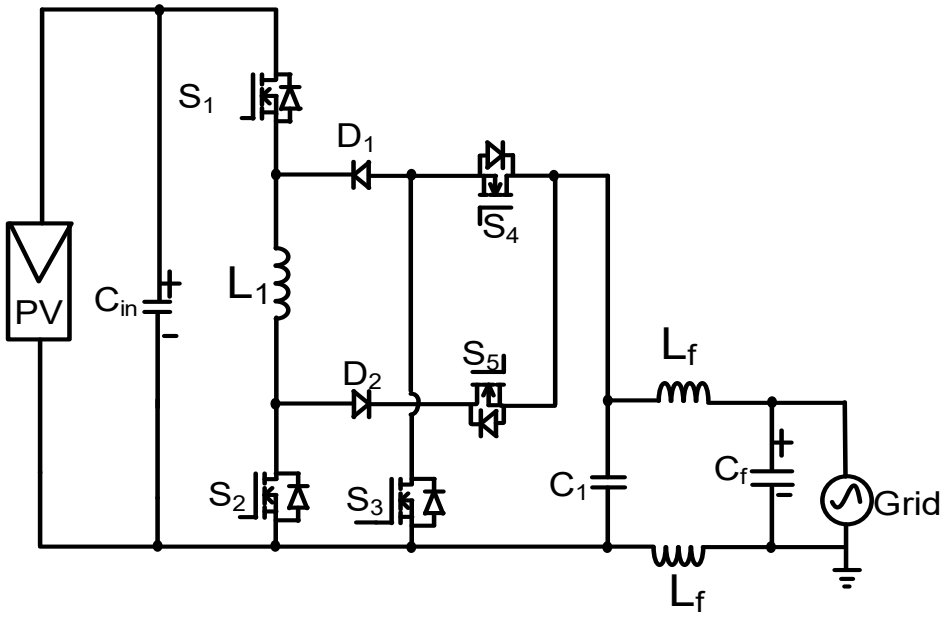

Figure 2.9 Karschny transformerless inverter

2.5 Problem Statement and Proposed Solution

All the aforementioned transformerless PV inverter topologies have targeted to minimize the CM leakage current by approaching two solutions:

I. Connect the utility grid neutral with PV negative terminal directly.
II. Separate the DC and AC sides of the inverter in the freewheeling modes.

The flow of CM leakage currents through the loop comprising parasitic capacitance (between PV panel and ground), bridge, filters and ground impedance of the grid forms a resonant circuit in series with CM voltage. Henceforth, this CM voltage must be constant to ensure the absence of leakage current [25]. This CM voltage is an average of the output voltages and a common reference and can be calculated from (2.3) as

$$V_{cm} = \frac{V_{AN} + V_{BN}}{2} \tag{2.3}$$

where v_{AN} and v_{BN} are voltages between outputs of inverter and point N as displayed in Figure 2.10. They vary during the switching of the inverter.

2.5.1 Leakage Current Estimation

The CM current is a function of CM voltage. When V_{cm} is maintained constant, then $\frac{dV_{cm}}{dt}$ will be zero and no leakage current will be generated as presented in (2.4).

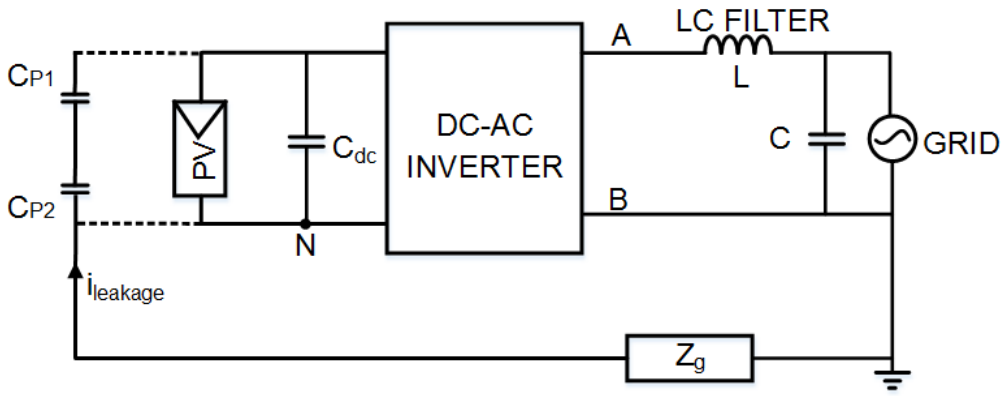

Figure 2.10 Leakage current flow for transformerless PV inverter

Since the utility grid is directly connected to negative of PV array in the proposed converter for both modes using bipolar sinusoidal PWM (SPWM), the leakage current is completely eliminated.

$$I_{cm} = C_{PV} \frac{dV_{cm}}{dt} \tag{2.4}$$

2.6 A Comprehensive Review on Transformerless PV Inverter

After analyzing the prevailing work in the field of transformerless PV inverters at PV's chain end, the common issue that came into the picture is that there is often an additional branch containing switches being used for disconnecting PV source from the grid. All inverter topologies have experimented in different ways to curb the capacitive earth current, for e.g. by adding passive elements to dampen the resonant circuit. The objective is to have a constant CM voltage because if it varies, then leakage current is produced [20]. These extra branches not only affects the efficiency by increasing the losses, but the additional circuitry increases cost and complexity as well. Thus, the main objective is to propose a converter with a lesser number of switches and without supplementary branches. A brief description of the topologies with a number of switches, diodes and passive elements is presented in Table 2.2 below.

Table 2.2 Review of PV transformerless topologies [19]

Topology	**Advantages**	**Disadvantages**	**No. of Semiconductors**		**Passive elements used**
			Switches	*Diodes*	
Full and Half Bridge topology	Simple design	Leakage current is high.	4	-	4
HERIC Topology	Reduced leakage current	Supplementary switches	6	-	4
H5 Topology	Decoupling between PV array and grid	Extra switch increasing conduction losses	5	-	4
H6 Topology	Low leakage current and prevents high frequency voltage	High cost due to extra switches and diodes	6	2	4
Neutral-point-clamped (NPC) multilevel inverter	Reduced leakage current and no internal reactive power flow	Increased losses and size due to input voltage twice as higher than other inverters	4	2	5
Karschny Inverter	Negative PV array connected to neutral of grid	More cost and less efficiency due to more switches and diodes	4	2	6
Proposed Inverter			4	-	6

2.7 Conclusion

A literature survey is presented focusing on prevailing PV transformerless inverters and its types. It has also explained the categories based on which inverter can be bifurcated. In addition to it, standards have been discussed in brief. Taking a cue from the above-mentioned topologies and considering the loopholes in them, a novel transformerless PV inverter is

proposed. This topology is a combination of DC-DC boost converter followed by flying inductor inverter. The detailed analysis of the principle of operation along with the control strategy adopted is explained in Chapter 3.

Chapter 3 **Analysis and Design of a Transformerless Inverter Topology**

3.1 Introduction

The power inverter has been a crucial element in many types of equipment like uninterruptable power supply (UPS), induction motor drive and automatic voltage regulator (AVR) systems. Since fuel cells, PV arrays and battery storage devices generate a low voltage, thus either a number of PV panels in series or a boost converter with high voltage gain should be employed. The presence of transformers at grid side (line frequency transformers) are bulky, expensive and restricts the freedom to control grid current, the transformerless inverters have become considerably popular in grid-connected solar systems in past few years. Therefore, inverter proposed in this Chapter is single-stage inverter for PV-grid interface which comprises of DC-DC boost converter integrated with a flying inductor inverter. For proper functioning of an inverter, the input voltage must be twice the peak grid voltage in order to inject current into ac mains. This first stage comprising boost converter provides power conditioning, MPPT and also generates voltage level compatible with the grid voltage [22].

3.2 Principal of Operation

In the previously discussed prevailing topologies in Chapter 2, there is often an additional branch containing auxiliary switches being used for disconnecting PV source from the grid. Their prime objective was to either decouple DC from the AC side or clamp the CM voltage. Several topologies attempted for common ground configurations for minimizing leakage current flow. The addition of switches leads to a rise in total on-state resistance $R_{DS,on}$ leading to higher conduction losses in the converter [26]. This extra leg not only affects the efficiency by increasing the losses, but the additional circuitry increases cost and complexity as well. It is to be highlighted that the leakage current appears if the CM voltage is not constant. Thus, the main aim of the proposed converter is

I. CM voltage should be maintained consistently to obtain zero leakage current.
II. Output current generated must be sinusoidal in nature ensuring high power quality.

With the proposed inverter, the above-mentioned objectives are achieved and hence leakage current is maintained at minimum value. The circuit diagram of the proposed converter is shown in Figure 3.1. It comprises of four switches ($S_1, S_2, S_3$and S_4) with two switches (S_1,S_3) conducting in first the interval and other two switches(S_2,S_4) conducting in the second

interval. The circuit has three inductors (L_{in}, L_{fly} and L_f) and three capacitors (C_{in}, C_{out} and C_f).

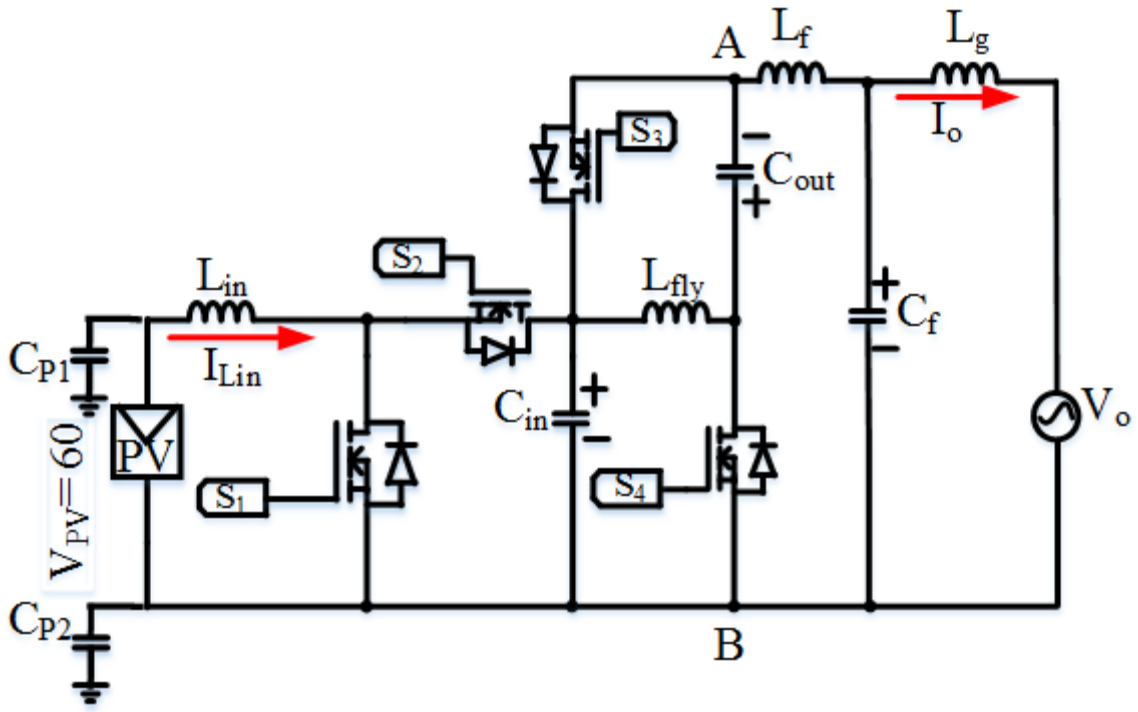

Figure 3.1 Proposed Transformerless converter

The basic steady-state operation of this topology is divided into two intervals. The converter operates in the following modes:

Mode 1 (0<t<DT_s): At the beginning of this mode, the switches S_1 and S_3 are turned ON and switches S_2 and S_4 are turned OFF. The inductor L_{in} is charged to store energy from input DC source and DC link capacitor C_{in} discharges through filter inductor L_f while L_{fly} discharges into the output capacitor C_{out}. Thus, L_f is storing energy. During this interval, the voltage across the capacitor C_{in} appears across the terminals 'AB' i.e. before the low-pass filter. The voltage difference between C_{in} and C_{out} will be reflected in the output voltage V_o. The current flow can be understood from Figure 3.2 (a)

Mode 2 (DT_s<t<T_s): During this mode, the switches S_2 and S_4 are turned ON and S_1 and S_3 switches are turned OFF. The PV panel and magnetized inductor L_{in} transfers its stored energy and to charge the capacitor C_{in} and magnetizes inductor L_{fly}. The filter inductor L_f releases energy through grid and C_{out} also discharges to flow through S_4. During this interval, the voltage across the capacitor C_{out} appears across the terminals 'AB' i.e. before the low-pass

filter. The voltage difference between C_{in} and C_{out} will be output voltage for this mode as well. Figure 3.2 (b) explains the current flow in mode 2.

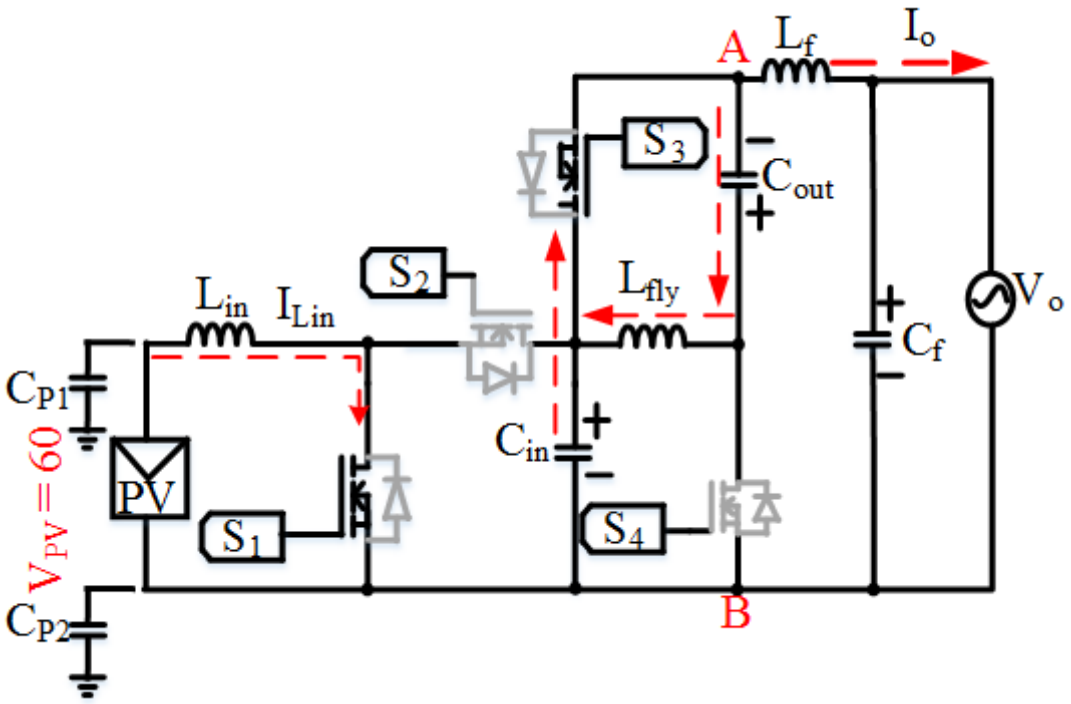

(a)

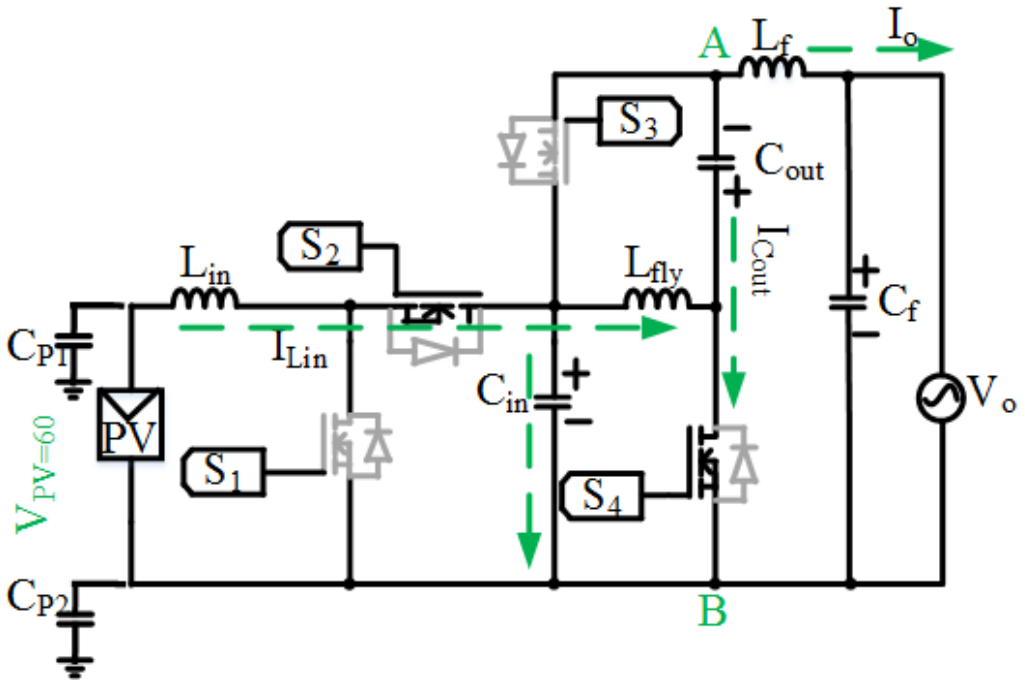

(b)

Figure 3.2 Equivalent circuit of proposed converter (a) Mode 1 (b) Mode 2

Table 3.1 expresses the mathematical equations of voltages across inductor and current through the capacitor in each interval. This behavior of charging and discharging of inductors and capacitors has been detailed.

Table 3.1 Mathematical Expressions for Inductor voltages and capacitor currents in both interval

Interval	Switch Status	Equations
$0 < t < DT_s$	S_1 and S_3 ON S_2 and S_4 OFF	$I_{Lfly} = I_{Cout}$ $I_{C_{in}} = -I_{L_f}$ $I_{L_f} = I_O$ $V_{Lf} = (V_{Cin} - V_o)$ $V_{PV} = V_{Lin}$
$DT_s < t < T_s$	S_2 and S_4 ON S_1 and S_3 OFF	$V_{Lin} = V_{PV} - V_{Cin}$ $V_{Lfly} = V_{Cin}$ $I_{L_f} = I_{Cout}$ $V_o = -(V_{Cout} + V_{Lf})$

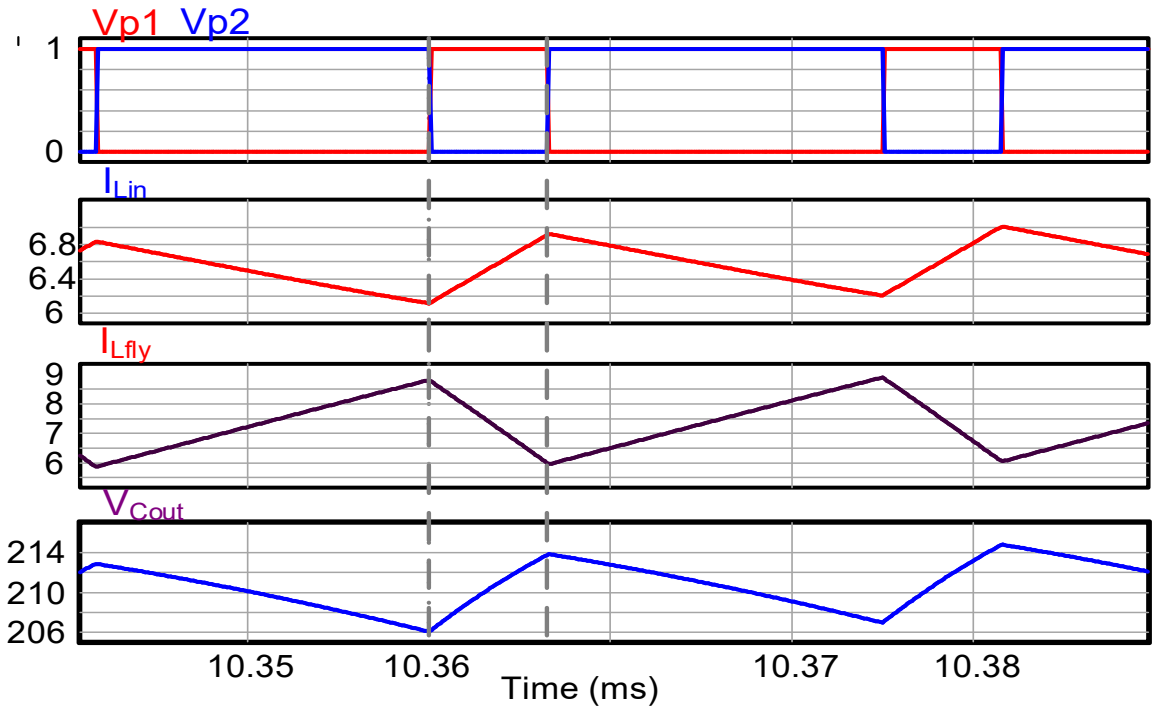

Figure 3.3 Converter waveforms at steady state

The steady-state waveforms of the inverter for a few switching cycles are depicted in Figure 3.3. It is to be noted that the voltage across terminals 'AB' is bipolar i.e., during mode-1, $V_{AB} = V_{cin}$ and during mode-2, $V_{AB} = -V_{cout}$. Hence, the output voltage before the filter is

equal to the difference of average voltage across the capacitor C_{in} and the average voltage across the capacitor C_{out}, as expressed in

$$V_{AB} = \langle V_{cin} \rangle - \langle V_{cout} \rangle \tag{3.1}$$

3.3 Voltage Gain of Converter

The proposed power circuit comprises of a photovoltaic module, a DC-DC boost converter followed by flying inductor inverter topology and a single-phase AC grid. Once the photovoltaic voltage is boosted to the DC link level, then it is inverted. Following assumptions are made to simplify the operation:

1) All the switches, inductors and capacitors are considered in an ideal state.
2) The output filter is set to obtain pure sinusoidal output voltage.

3.3.1 Steady-State Equations

Therefore, with the above-specified assumptions, the volt-second balance equation is applied by averaging voltages across inductors (L_{in}, L_{fly} and L_f) in steady state during one switching cycle to calculate following equations:

$$\int_0^{T_s} < V_{Lin} > dt = \int_0^{T_{on}} < V_{Lin} > dt + \int_{T_{on}}^{T_s} < V_{Lin} > dt \tag{3.2}$$

$$= 0$$

$$\frac{V_{in} * D * T_S + (V_{in} - V_{cin}) * (1 - D) * T_S}{T_S} \tag{3.3}$$

$$= 0$$

$$V_{cin} = \frac{V_{in}}{(1 - D)} \tag{3.4}$$

Similarly,

$$\int_0^{T_s} < V_{Lfly} > dt = \int_0^{T_{on}} < V_{Lfly} > dt + \int_{T_{on}}^{T_s} < V_{Lfly} > dt = 0 \tag{3.5}$$

$$\frac{(-V_{cout}) * D * T_S + V_{cin} * (1 - D) * T_S}{T_S} = 0 \tag{3.6}$$

$$V_{cout} = \frac{V_{Cin} * (1 - D)}{D} \tag{3.7}$$

and

$$\int_0^{T_s} < V_{Lf} > dt = \int_0^{T_{on}} < V_{Lf} > dt + \int_{T_{on}}^{T_s} < V_{Lfl} > dt = 0 \tag{3.8}$$

$$\frac{-(V_{cf} + V_{cout}) * D * T_S + (V_{cin} - V_{cf}) * (1-D) * T_S}{T_S} = 0 \tag{3.9}$$

Substituting (3.4) and (3.7) in (3.9)

$$V_{Cf} = \frac{(2D-1) * V_{in}}{D * (1-D)} = V_0 \tag{3.10}$$

where D=Duty ratio = $\frac{T_{on}}{T_s}$

Similarly applying charge balance by integrating current through capacitors (C_{in}, C_{out} and C_f) in steady state over one complete switching cycle, we get

$$\int_0^{T_s} < i_{Cin} > dt = \int_0^{T_{on}} < i_{Cin} > dt + \int_{T_{on}}^{T_s} < i_{Cin} > dt = 0 \tag{3.11}$$

$$\frac{-i_{L_f} * D * T_S + \left(i_{Lin} - i_{L_{fly}}\right) * (1-D) * T_S}{T_S} = 0 \tag{3.12}$$

$$-i_{L_f} * D + \left(i_{Lin} - i_{L_{fly}}\right) * (1-D) = 0 \tag{3.13}$$

Also,

$$\int_0^{T_s} < i_{C_{out}} > dt = \int_0^{T_{on}} < i_{C_{out}} > dt + \int_{T_{on}}^{T_s} < i_{C_{out}} > dt = 0 \tag{3.14}$$

$$\frac{i_{L_{fly}} * D * T_S + i_{L_f} * (1-D) * T_S}{T_S} = 0 \tag{3.15}$$

$$i_{L_{fly}} = -\frac{i_{L_f} * (1-D)}{d} \tag{3.16}$$

and

$$\int_0^{T_s} < i_{C_f} > dt = \int_0^{T_{on}} < i_{C_f} > dt + \int_{T_{on}}^{T_s} < i_{C_f} > dt = 0 \tag{3.17}$$

$$\frac{(i_{L_f} - I_O) * D * T_S + (i_{L_f} - I_O) * (1-D) * T_S}{T_S} = 0 \tag{3.18}$$

$$i_{L_f} = i_O \tag{3.19}$$

Substituting (3.16) and (3.19) in (3.13), we obtain

$$i_{Lin} = \frac{(2D-1) * i_O}{D * (1-D)} \tag{3.20}$$

3.3.2 *Variation of Voltage Gain with Duty Ratio*

Figure 3.4 depicts the voltage gain as a function of the duty cycle (D) derived from (3.22). It is observed that when the duty ratio is less than 0.5, then the voltage gain is negative. At D = 0.5, the voltage becomes zero and then as duty ratio goes above 0.5, the gain demonstrates a positive pattern. Thus proposed topology yields a symmetric behavior in voltage gain from D = 0.25 to D = 0.75. Thus, by varying the duty ratio in sinusoidal manner with respect to D = 0.5, the proposed converter provides the sinusoidal output voltage.

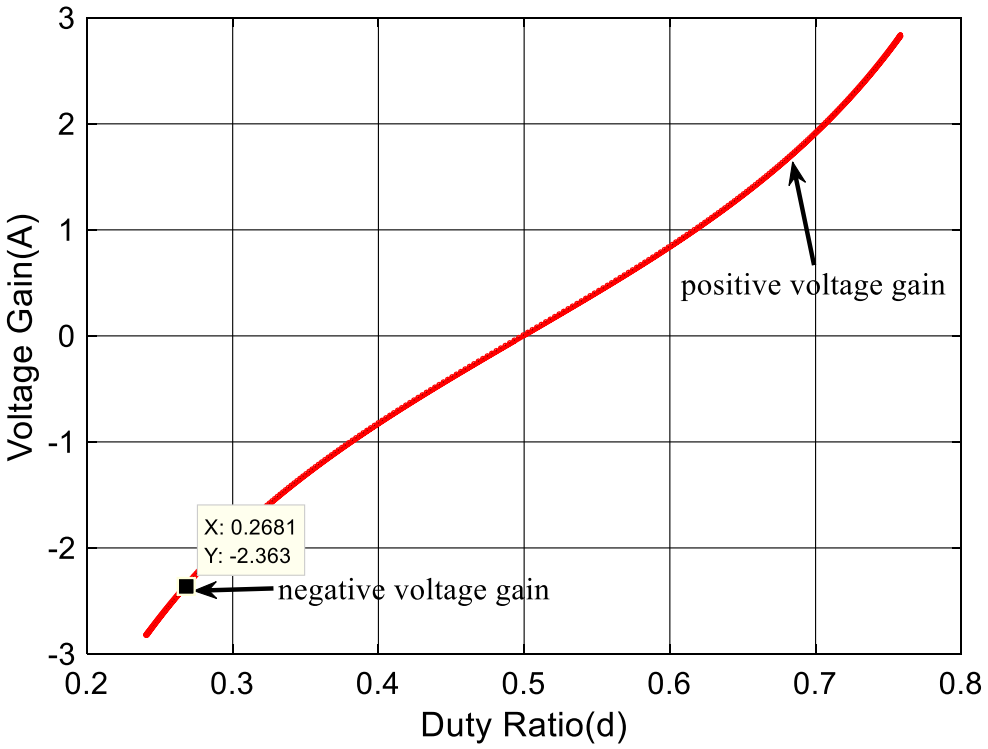

Figure 3.4 Variation of voltage gain versus Duty ratio

3.3.3 *Control Strategy*

Since the proposed inverter by default provides a bipolar voltage at the output before low-pass filter, any conventional bipolar or unipolar sinusoidal PWM methods can be used to obtain sinusoidal output voltage. Modulation strategy is a contributing factor in leakage current flow. Bipolar modulation results in lower ground current than unipolar modulation. Thus, it is followed for the operation of the proposed inverter. The control strategy adopted is explained in this section. The first stage (boost converter) has to be controlled in such a way that voltage across the DC-link capacitor (C_{in}) is a rectified sine wave.

The voltage gain of the proposed converter can be re-written as:

$$\frac{V_0}{V_{in}} = \frac{(2D-1)}{D*(1-D)} = ASin\theta \tag{3.21}$$

Assuming A = $\frac{V_m}{V_{in}}$ = voltage gain and $V_0 = V_m \sin\theta$.

After forming a quadratic equation from the above-mentioned formula, duty ratio D could be represented as:

$$D = \frac{1}{2} - \frac{2 \pm \sqrt{4 + (A * Sin\theta)^2}}{2 * A * Sin\theta} \tag{3.22}$$

where voltage gain is multiplied by $Sin\theta$ so that duty cycle varies as a function of θ and a pure sinusoidal output voltage can be obtained. On solving the above equation, there are two possible values of D. Since, one of them is negative, so the other positive value i.e. D = 0.75 is considered. Thus, the following equation is proposed as a control function.

$$D = \frac{1}{2} - \frac{2 - \sqrt{4 + (A * Sin\theta)^2}}{2 * A * Sin\theta} \tag{3.23}$$

This modulation technique aids in varying duty ratio in such a fashion that voltage gain varies in a symmetric fashion as shown in Figure 3.4. Figure 3.5 depicts the behavior of voltage gain for duty ratio less than 0.5 and greater than 0.5 respectively. V_{P1} and V_{P2} are the gate pulses applied to switches S_1 and S_2 respectively.

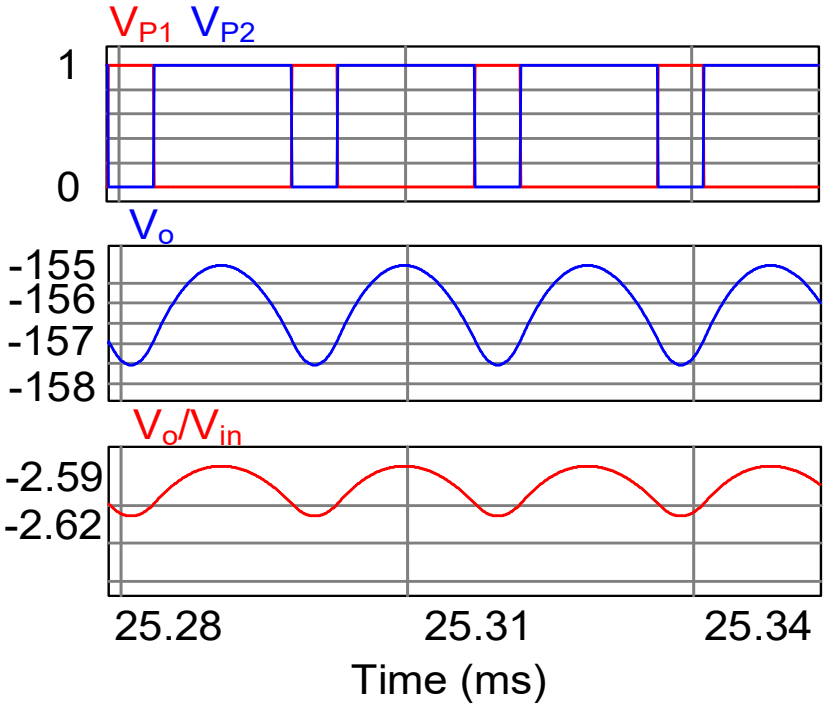

(a)

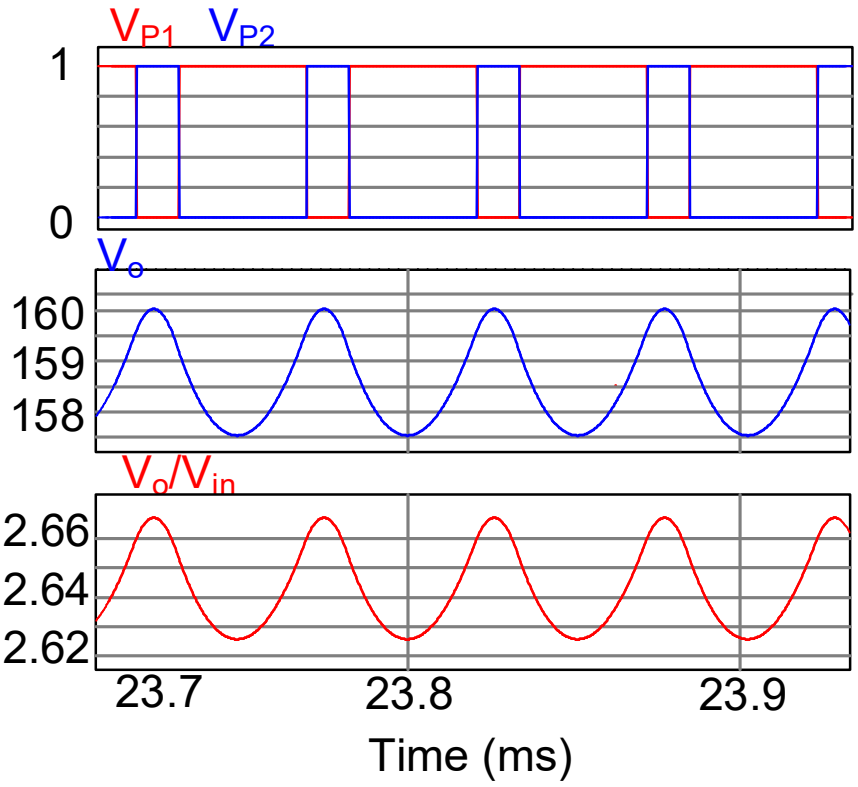

(b)

Figure 3.5 Converter output voltage for duty ratio (a) $D = 0.25$; (b) $D = 0.75$

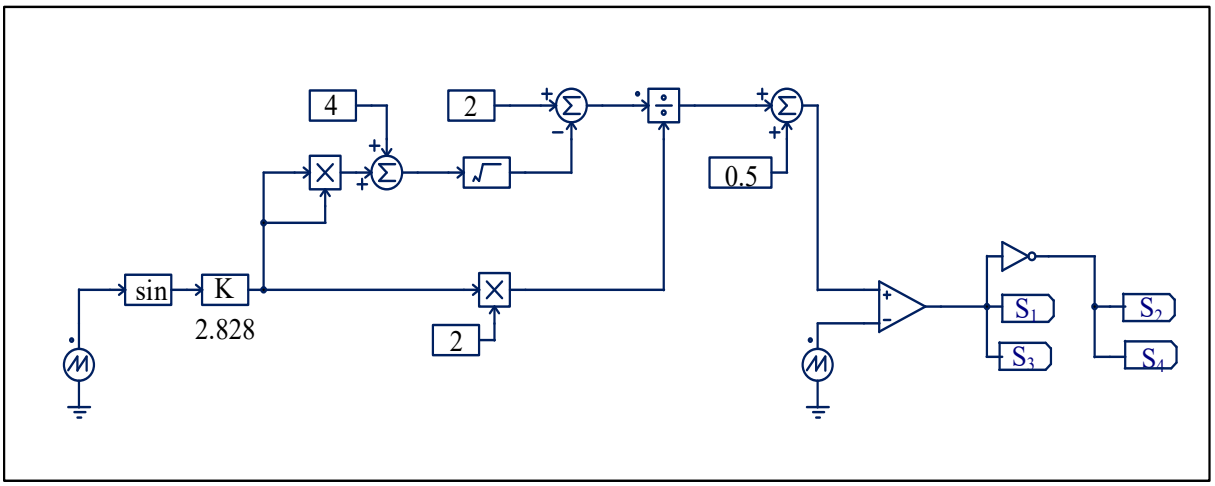

Figure 3.6 Control circuit for open loop operation of the proposed converter

3.4 Circuit Parameters Design

This section discusses the design of a 250W, 120V, 60 Hz single-phase DC-AC converter. With input and output voltage specified, the energy storage elements i.e. inductors and capacitors have to be designed. The output voltage is considered nearly equal to utility grid

voltage in case of high switching frequency and unity power factor (PF) operation. The specifications are given in Table 3.2.

3.4.1 Converter Main Specifications

Table 3.2 Input Parameters of Converter

Power Rating, P_o	250W
Input DC voltage, V_{in}	60V
Output Current, I_O	2.08A (from (7))
Grid Voltage, V_{out} or V_{grid}	120V rms
Switching frequency,f_s	50 kHz
Grid frequency, f_g	60 Hz

Thus, the impedance of the resistive load can be calculated from (3.24) and output current from (3.26).

$$R = \frac{V_{grid,rms}^2}{P_{max}} \tag{3.24}$$

$$R = \frac{(120)^2}{250} = 57.6\Omega \tag{3.25}$$

$$I_O = \frac{V_{out}}{R} = \frac{120}{57.6} = 2.08\ A \tag{3.26}$$

3.4.2 Boost Inductor (L_{in})

The first stage of the converter acts as a DC-DC boost converter and L_{in} is the boost inductor. It is connected in series with the input voltage to limit the input current ripple. It could prevent shoot-through issues. The inductor operates in continuous conduction mode (CCM), which ensures the injection of high-quality sinusoidal current into the AC grid [27]. As per (3.27), inductance is inversely proportional to the inductor current ripple and directly proportional to the voltage applied. Considering Mode 1 ($0<t<DT_s$), the value of L_{in} is:

$$v_{L_{in}} = V_{in} = -\frac{L_{in} di_{L_{in}}}{dt} \tag{3.27}$$

Therefore,

$$L_{in} = (V_{in}.D.T_s)/\Delta I_{L_{in},max} \tag{3.28}$$

$$L_{in} = \frac{60 * 0.75 * 20 * 10^{-6}}{0.74} = 1200\mu H \tag{3.29}$$

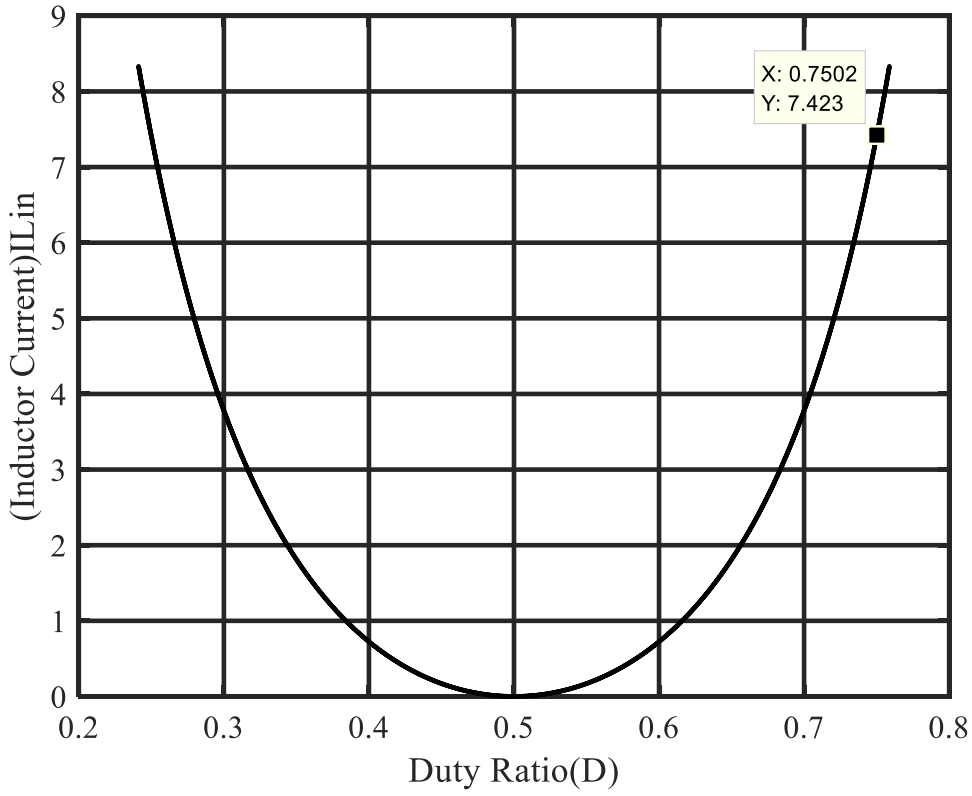

Figure 3.7 Inductor Current ($I_{L_{in}}$)versus Duty ratio (D)

where D=0.75

$I_{L_{in},max}$ = 7.4 A (shown in Figure 3.7).

$\Delta I_{L_{in},max}$ = 10 % of 7.4 A = 0.74 A.

3.4.3 DC-Link Capacitor (C_{in})

A small capacitor is used in DC link for power decoupling between the PV module and the utility grid. The value of this capacitor decides the maximum ripple amplitude in the PV array voltage that is allowed. In general, the film capacitors are preferred over electrolytic capacitors as they provide higher reliability and lower power dissipation. For Mode 1 (0<t<DT_s), DC-link capacitor current is the same as output current as specified in (3.30).

Thus, the value of C_{in} is

$$i_{C_{in}} = -i_{L_f} = -\frac{C_{in}\, dV_{C_{in}}}{dt} \tag{3.30}$$

Therefore,

$$C_{in} = -(i_{L_f} * D * T_s)/\Delta V_{C_{in}} \quad (3.31)$$

$$C_{in} = -\frac{3 * 0.75 * 20 * 10^{-6}}{12} = 3.75\mu F \quad (3.32)$$

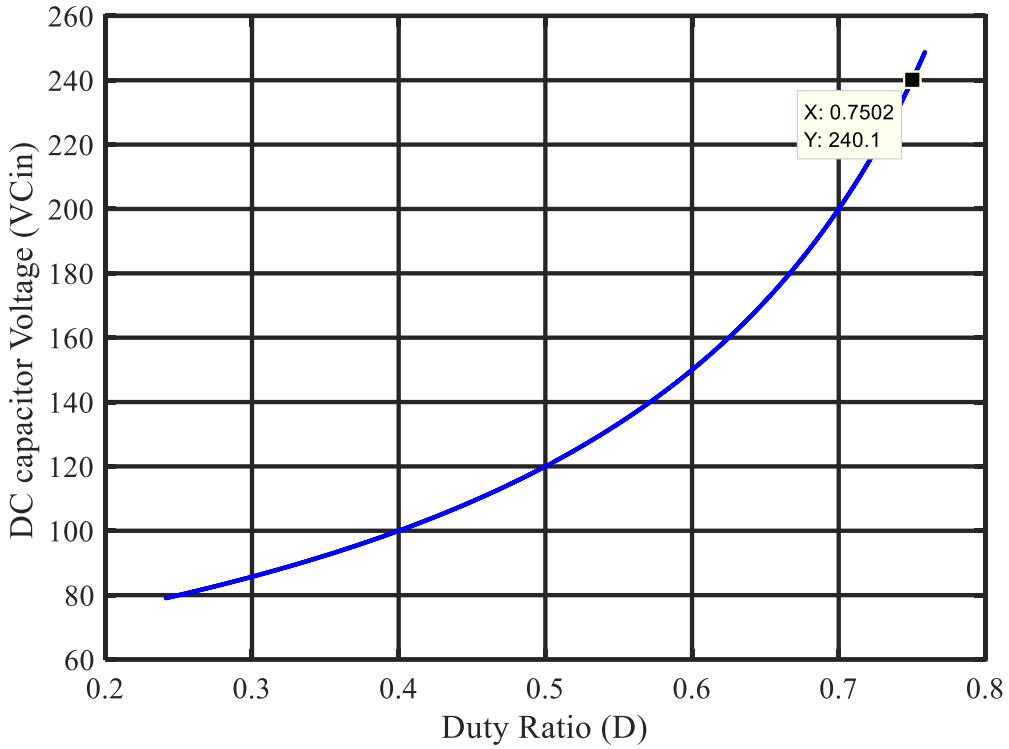

Figure 3.8 DC-link capacitor voltage ($V_{C_{in}}$) versus Duty ratio (D)

where

$V_{C_{in}}$ = 240 V (given in Figure 3.8)

5% of $V_{C_{in}}$ = 12V

A standard capacitor of 5 μF is selected for withstanding overvoltage and keeping capacitor safe.

3.4.4 C_{out} and L_{fly}

I. *Flying Inductor* (L_{fly}) is mainly used to prevent the DC fluctuations caused by the series connection between input and output as it is responsible for energy transfer [27]. It relies on permissible switching inductor current ripple ($\Delta I_{L_{fly},max}$). Considering Mode 2 (DT_s<t<T_s) the flying inductor V_{Lfly} will be equal to DC-link capacitor voltage ($V_{C_{in}}$) mentioned in

$$L_{fly} = \frac{v_{\mathrm{L_{fly}}}.(1-D).T_s}{\Delta I_{\mathrm{L_{fly}},max}} \tag{3.33}$$

$$L_{fly} = \frac{240 * (1-0.75) * \ 20 * 10^{-6}}{0.82} = 1304\ \mu H \tag{3.34}$$

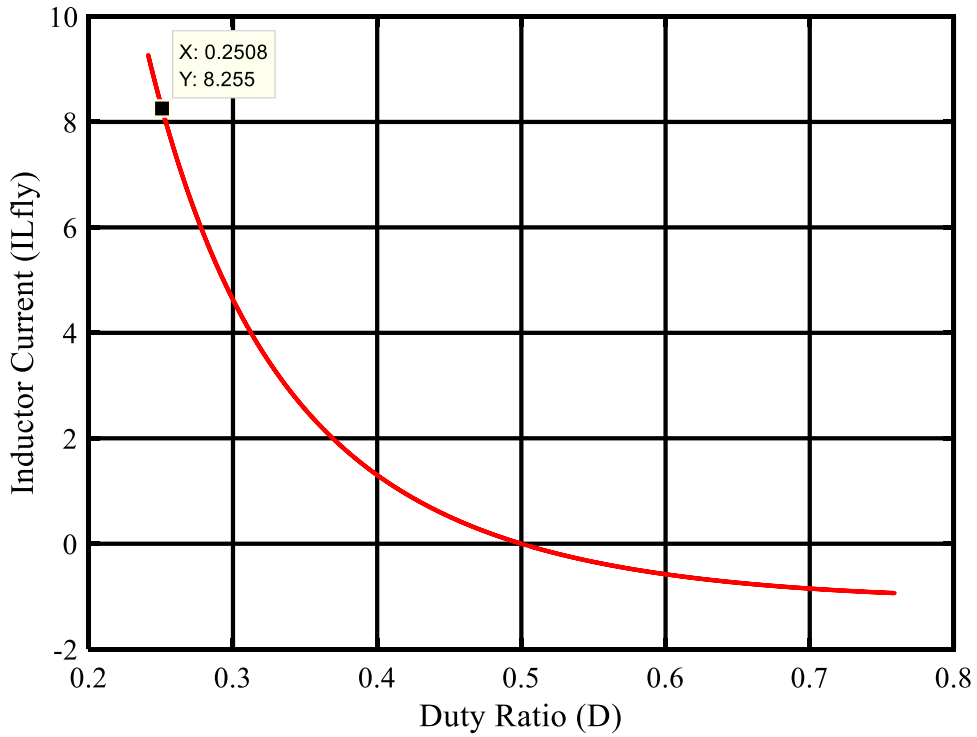

Figure 3.9 Inductor Current ($I_{i_{\mathrm{L_{fly}}}}$)versus Duty ratio (D)

where

$I_{\mathrm{L_{fly}},max}$ = 8.2 A (as per Figure 3.9)

$\Delta I_{L_{in},max}$ = 10 % of 8.2A = 0.82A

II. Output Capacitor (C_{out})

Considering Mode 2 (DT_s<t<T_s)

$$i_{\mathrm{C_{out}}} = i_{\mathrm{L_f}} = -\frac{\mathrm{C_{out}} * dV_{\mathrm{C_{out}}}}{dt} \tag{3.35}$$

$$\mathrm{C_{out}} = (i_{\mathrm{L_f}} * (1-D) * T_s)/\Delta V_{C_{out}} \tag{3.36}$$

$$\mathrm{C}_{out} = -\frac{3 * (1-0.75) * 20 * 10^{-6}}{12} = 1.25\mu F \tag{3.37}$$

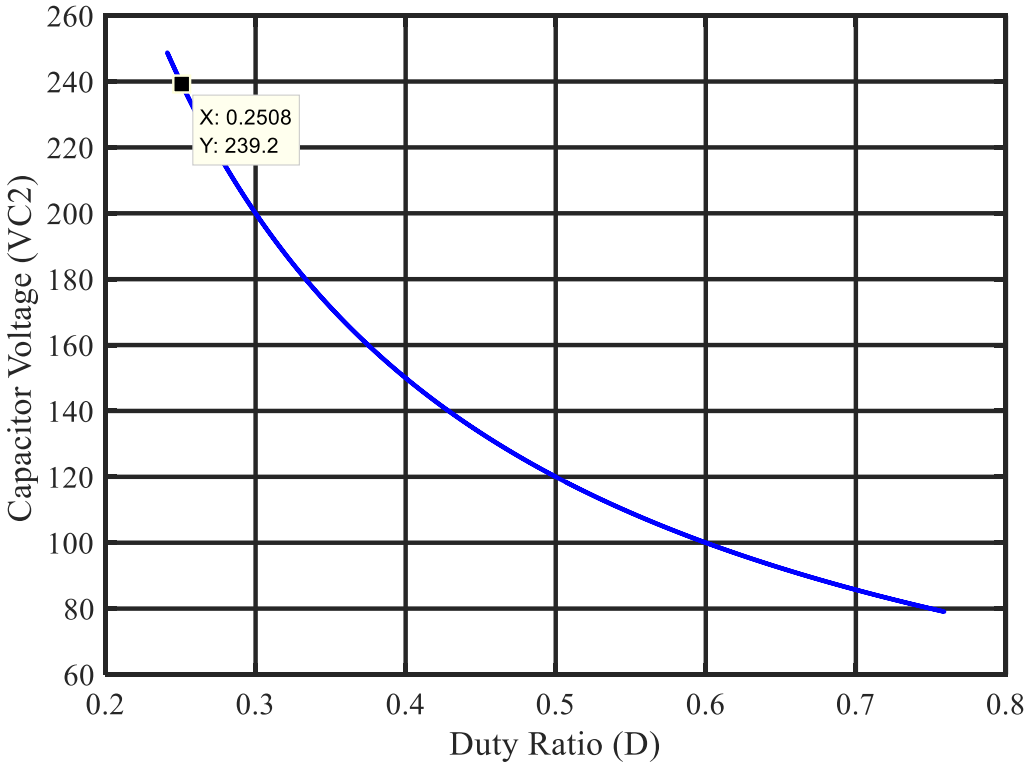

Figure 3.10 Output capacitor voltage versus Duty ratio (D)

where

$V_{C_{in}}$ = 240 V (as per MATLAB Figure 3.10)

5% of $V_{C_{out}}$ = 12V

A standard capacitor of 1.25 μF is selected for withstanding overvoltage and keeping capacitor safe.

3.4.5 Output Filter (L_f and C_f)

In order to reduce the current ripple introduced by PWM high-frequency switching and improvise total harmonic distortion (THD) of output current, the output filter is a must. The LC low pass filter is preferred as they are cost-effective, although there is a possibility of overvoltage due to filter resonance. The inductor attenuates the high-frequency component in output current which is about to be injected to the grid. The output current ripple is similar to inductor current ripple and as per the IEEE harmonic standard [28], 15-20% of the rated current is permissible. The parallel capacitor reduces size and losses due to the inductor. Hence, the resonant frequency (f_r) is chosen 10 times lesser than switching frequency (f_s) and well above fundamental grid frequency (f_g) as given in (3.38) [29].

$$10 * f_g \ < \ f_r \ < \frac{1}{10} f_s \tag{3.38}$$

The resonant frequency (f_r) is calculated from (3.38) and chosen as 5 kHz. Higher switching frequency aids in cutting down the size of the filter components. The inductor is placed between the inverter and the grid to eliminate the higher current harmonics caused by switching of MOSFETs. It ensures continuous active current is being injected to the grid. The filter inductor L_f can be calculated from (3.39) [30] and depends on:

$V_{C_{in}}$ = DC link voltage,

$\widehat{\Delta I_{L_f}}$ = peak filter inductor current ripple (25% of rated output current)

=25% of I_O(peak) =0.25* $\sqrt{2} * I_O(rms) = \ 0.74\ A$

$[I_O(rms) = \ 2.08\ A] from$ (3.26)

f_s = switching frequency i.e. 50 kHz

$$V_{L_f} = \frac{L_f * \Delta I_L}{D * T_s} \tag{3.39}$$

$$L_f = \frac{\left(V_{C_{in}} - V_O\right) * D * T_s}{\widehat{\Delta I_L}} \tag{3.40}$$

$$L_f = \frac{(240 - 170) * 0.75 * 20 * 10^{-6}}{0.74} = 1.4\ mH \tag{3.41}$$

$$f_r = \frac{1}{2\pi\sqrt{L_f * C_f}} \tag{3.42}$$

$$C_f = \frac{1}{(2 * \pi * 5 * 10^3)^2 * 1.4 * 10^{-3}} = 0.7\mu F \tag{3.43}$$

A standard inductor of 1.5 mH and capacitor of $1\mu F$ is selected.

3.5 Simulation and Experimental Results

3.5.1 Simulation Results

The converter is designed with the input parameters specified in Table 3.2. As calculated above, the design parameters for simulation are summarized in Table 3.3. For the simplification of converter design, input inductor (L_{in}) and flying inductor (L_{fly}) are kept the same. The simulation results of the proposed converter are depicted in Figure 3.11. Figure 3.11(a) shows the converter input current. The input current drawn from the converter is DC

with second harmonic grid frequency oscillation. Figure 3.11(b) shows the converter output current and output voltage. The output voltage is pure sinusoidal and the output current is following output voltage since the converter is tested with resistive load. Figure 3.11(c) shows the voltages across capacitors 'C_{in}', and 'C_{out}'. It is observed that during the positive half cycle, the voltage across capacitor 'C_{in}' is having a sinusoidal envelope, while during the negative half cycle, the voltage across capacitor 'C_{out}' is having a sinusoidal envelope. The voltage ripple is as expected. Figure 3.11(d) reflects the behavior of switch voltages, S_1 and S_2 during the entire switching scheme and for clarity purpose, the zoomed version is shown as well. The maximum voltage appeared across switch is the V_{Cin} peak voltage, which is in good agreement with the analysis. Figure 3.11(e) shows the voltage across AB terminals before the low-pass filter. It can be observed that at a given instant, the voltage across 'AB' terminals is bipolar in nature, and the output voltage is the difference of the voltage across capacitor 'C_{in}' and the voltage across capacitor 'C_{out}', which validates the analysis of the proposed converter. It also displays the current flowing through flying inductor, it is following the same envelope of V_{Cout}, since it is responsible to maintain the negative sinusoidal envelope.

Table 3.3 Designed Parameters for proposed Converter

Input inductor, L_{in}	390 μH
Flying inductor, L_{fly}	390 μH
Output filter inductor, L_f	1.2 mH
Capacitor in, C_{in}	5 μF
Capacitor out, C_{out}	5 μF
Filter capacitor, C_f	1 μF

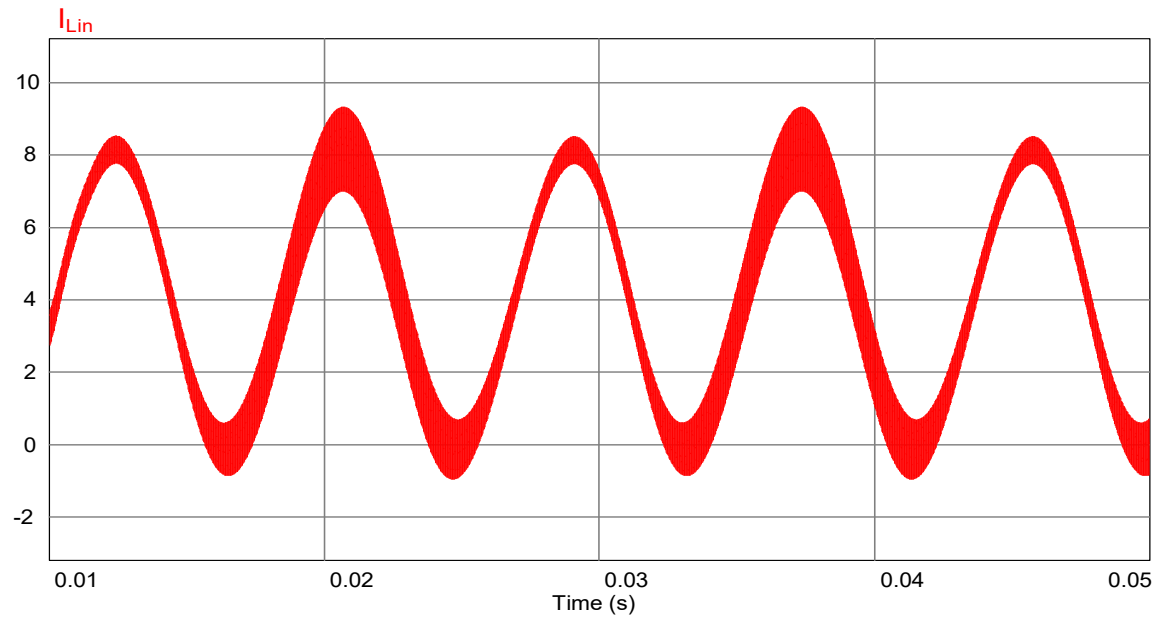
I_{Lin}
10
8
6
4
2
0
-2
0.01
0.02
0.03
0.04
0.05
Time (s)

(a)

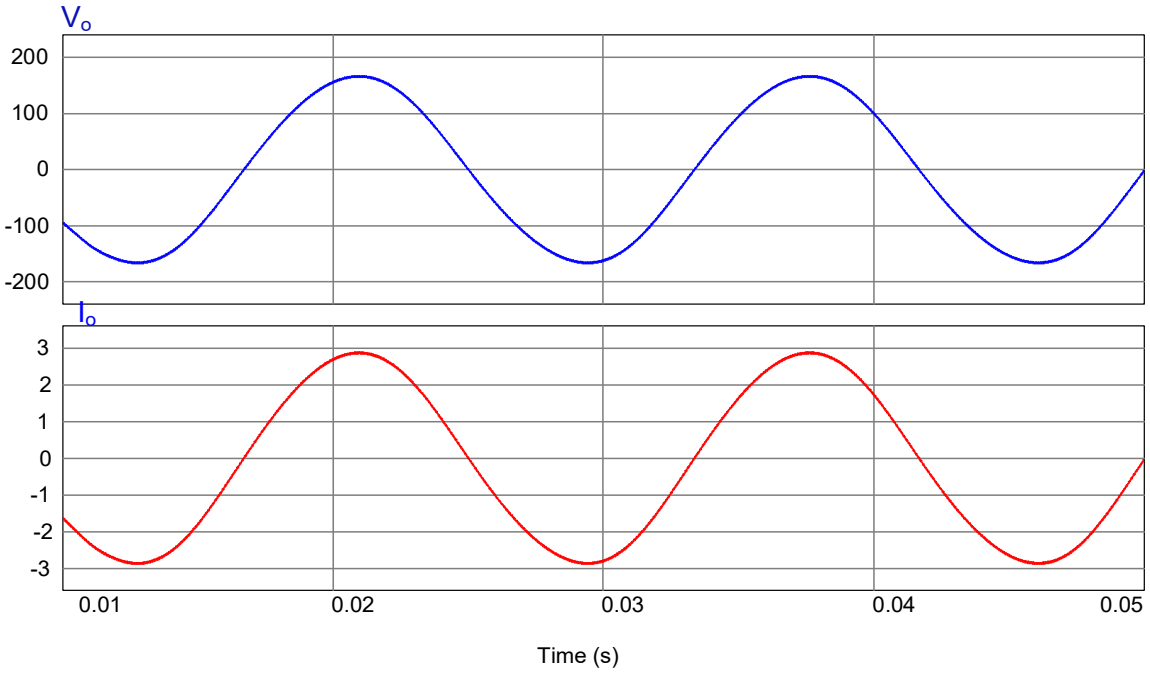
V_o
200
100
0
-100
-200
I_o
3
2
1
0
-1
-2
-3
0.01
0.02
0.03
0.04
0.05
Time (s)

(b)

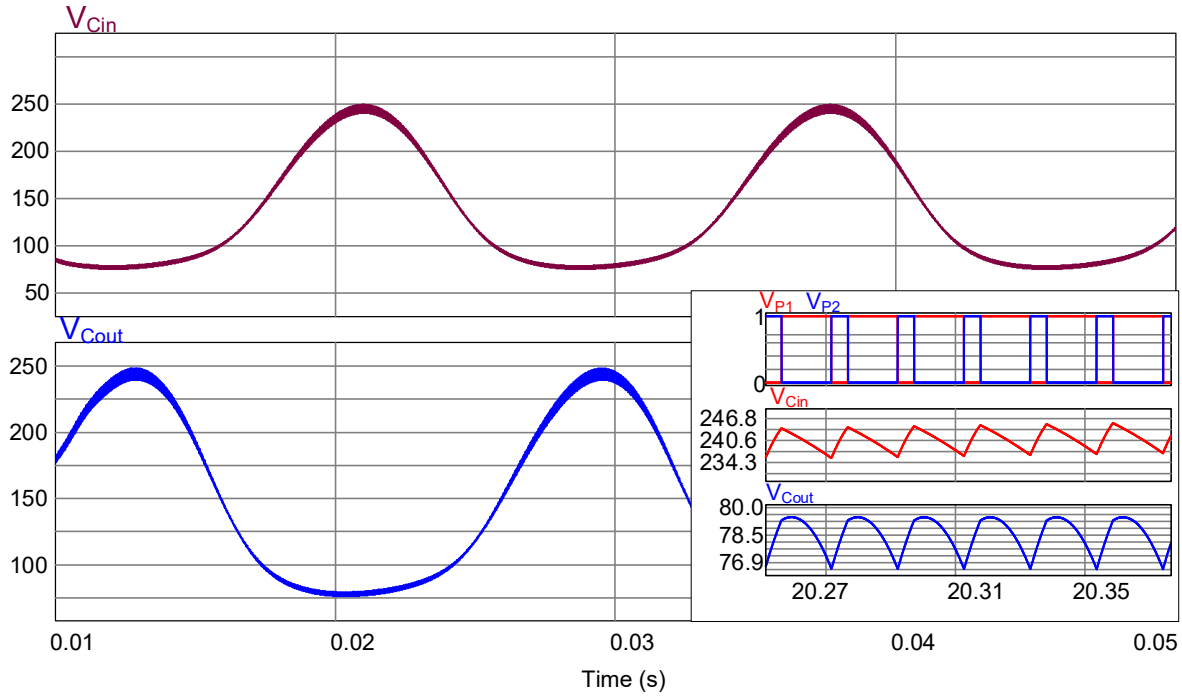
VCin
250
200
150
100
50
VCout
250
200
150
100
VP1 VP2
1
0
VCin
246.8
240.6
234.3
VCout
80.0
78.5
76.9
20.27
20.31
20.35
0.01
0.02
0.03
0.04
0.05
Time (s)

(c)

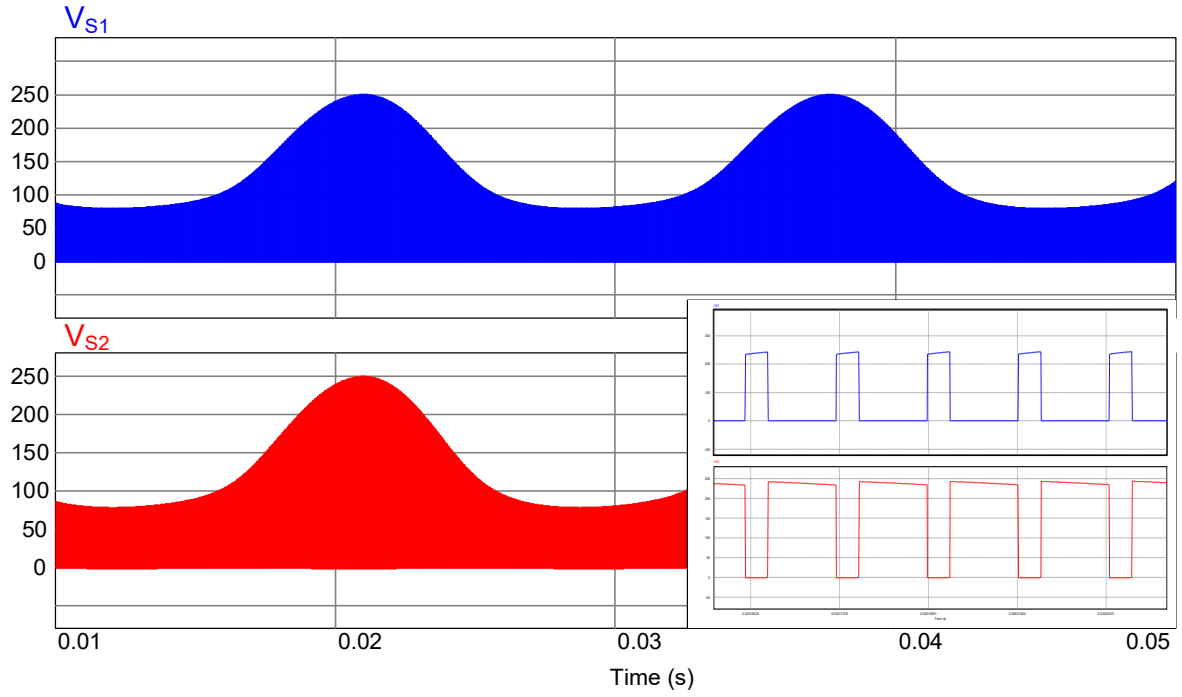
VS1
250
200
150
100
50
0
VS2
250
200
150
100
50
0
0.01
0.02
0.03
0.04
0.05
Time (s)

(d)

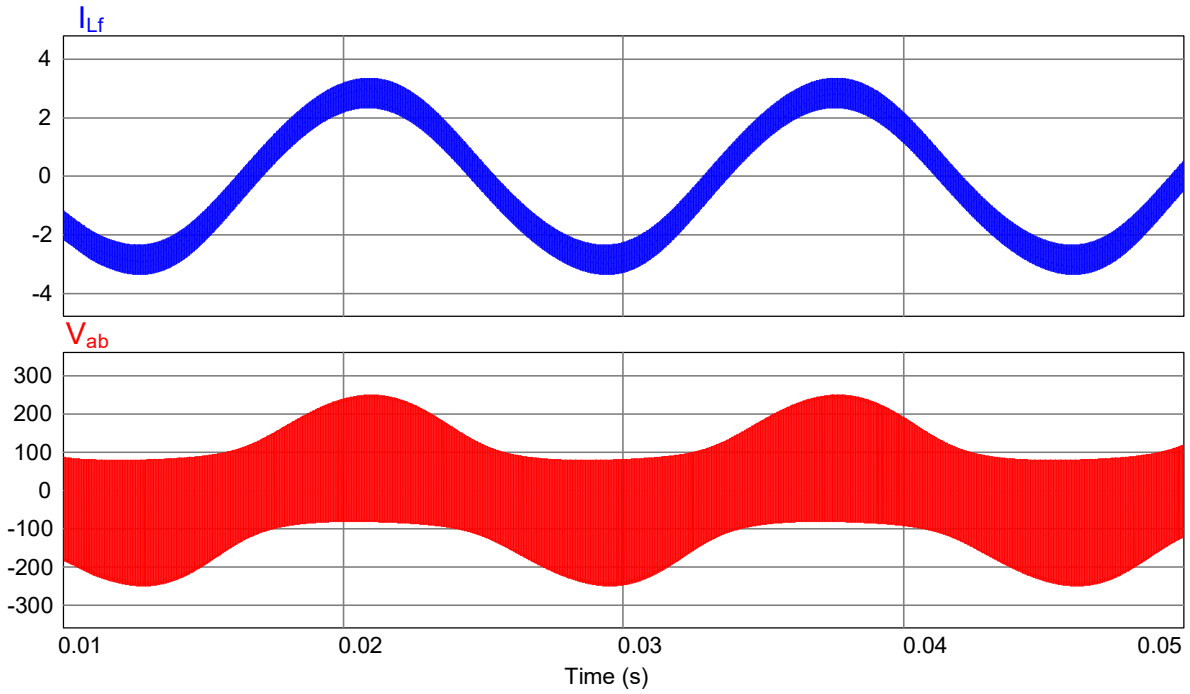

(e)

Figure 3.11 Simulated steady-state results of proposed topology, (a) input current; (b) output current, and output voltage; (c) voltages across capacitors 'C_{in}', and 'C_{out}'; (d)) voltage across switches; (e) current through filter inductor and the voltage across AB terminals before filter;

3.5.2 Experimental Results

A proof-of-concept 250 W hardware prototype of the proposed solar inverter was built as shown in Figure 3.12. by considering similar simulation parameters given in Table 3.3 are considered for developing the hardware. The input DC voltage is 60 V and the AC output voltage is 120 V (rms). The control strategy was implemented in DSP TMS320F28335 through Code Composer Studio (CCS) to generate gating pulses for the inverter. The switching frequency has been chosen 50 kHz. Complementary gating pulses are given to (S_1, S_3) and (S_2,S_4) The components used for the experimental set-up are given in Table 3.4.

The experimental results in the open loop are displayed in Figure 3.13, showing the steady-state performance of the proposed inverter. Figure 3.13 (a) displays input current which is dc with the second harmonic pulsation of inverter output. Figure 3.13 (b) shows peak output voltage is 169 V which reflects complete utilization of the duty cycle in the proposed inverter. Inverter output voltage and current maintain high quality with low distortion and harmonic content. The voltage across the two capacitors ($V_{C_{in}}$ and $V_{C_{out}}$) follow the sinusoidal pattern and that is reflected at the inverter output because of the switching scheme. The voltages across

the output and capacitors are shown in Figure 3.13 (b) and (c) respectively. The voltage across the switches follow the sinusoidal envelope as shown in Figure 3.13 (d).

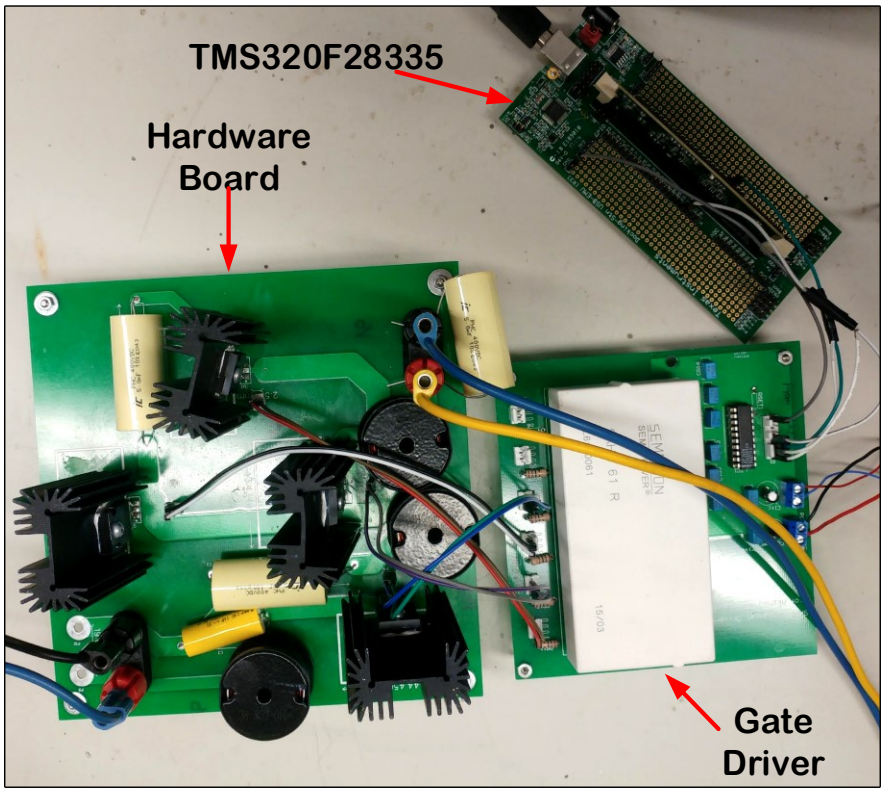

Figure 3.12 Hardware Experimental Prototype

Table 3.4 Experimental Component Specifications

Digital Control	TMS320F28335
MOSFETS(S1-S4)	SiHP065N60E(600V, 40A)
Inductors (L_{in} ,L_{fly})	1140-391K-RC
DC Capacitor(C_{in} ,C_{out})	598-505PHC400K
Filter Inductor(L_f)	1140-122K-RC
Filter Capacitor(C_f)	C4GAFUB4100AA0J

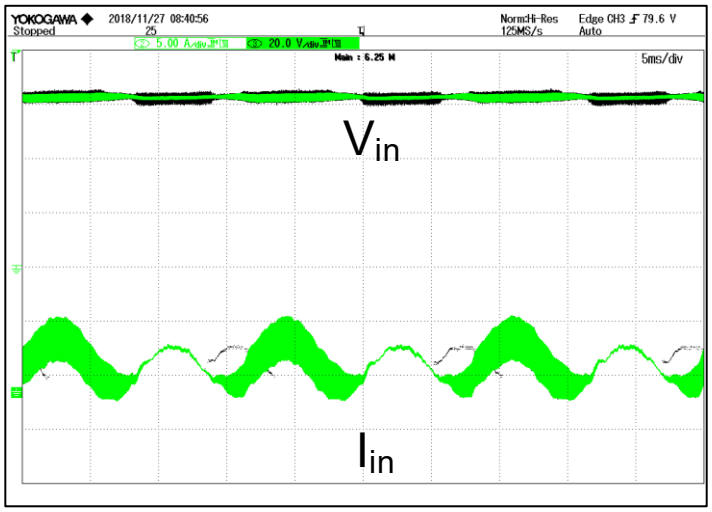
YOKOGAWA
2018/11/27 08:40:56
Stopped
25
Norm:Hi-Res
125MS/s
Edge CH3 79.6 V
Auto
5.00 A/div
20.0 V/div
Main : 6.25 M
5ms/div
Vin
Iin

(a)

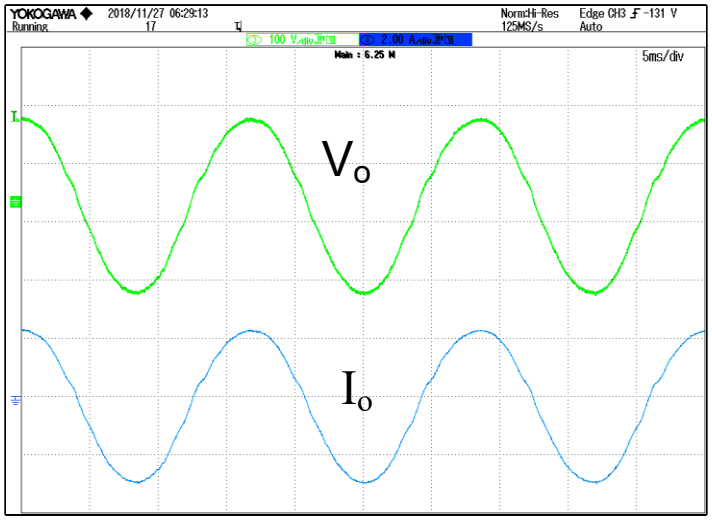
YOKOGAWA
2018/11/27 06:29:13
Running
17
Norm:Hi-Res
125MS/s
Edge CH3 -131 V
Auto
100 V/div
2.00 A/div
Main : 6.25 M
5ms/div
Vo
Io

(b)

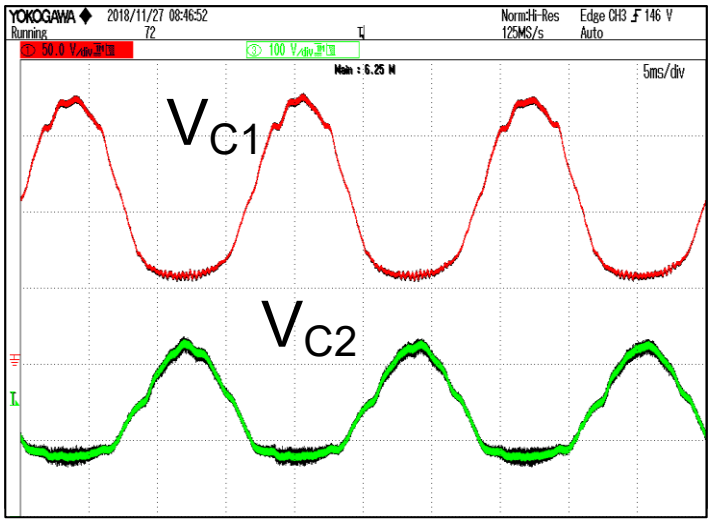

(c)

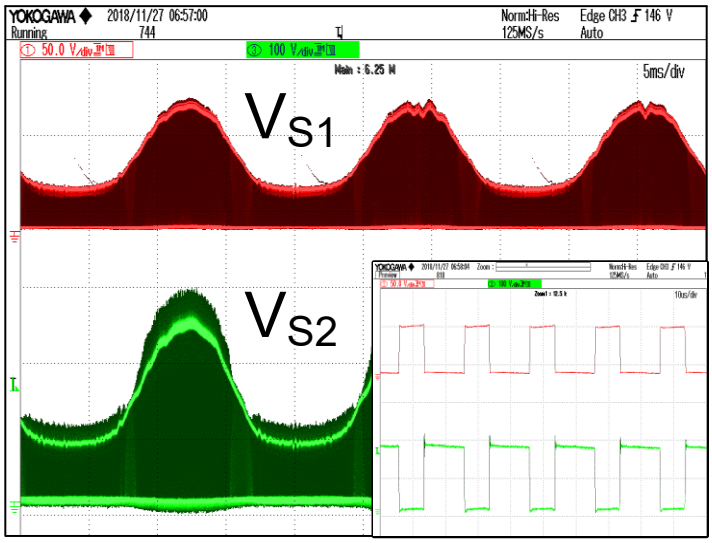

(d)

Figure 3.13 Experimental results of the proposed inverter, (a) input voltage (20 V/div), and input current (5.0 A/div); (b) output voltage (100 V/div), output current (2.0 A/div); (c) voltage across capacitors 'C_{in}' (50 V/div), and 'C_{out}' (100 V/div); (d) voltage across switches 'S_1' (50 V/div), and 'S_2' (100 V/div).

3.6 Conclusion

In this chapter, the modes of operation of the proposed inverter have been explained in detail which is followed by designing and calculation of passive elements. The control strategy has been derived for the duty cycle. The proposed inverter provides symmetrical voltage to

gain both positive and negative through a unique and simple modulation strategy and is successfully implemented. The waveforms captured in experimental results are observed quite similar to simulation results. Hence, it is showed that the results are in good agreement with the proposed analysis.

Chapter 4 **Small-Signal Model of the Solar Inverter**

4.1 Introduction

The DC-AC Inverter plays a crucial role in controlling the power factor by maintaining sinusoidal current injected into the utility grid. With respect to the grid-tied PV systems, the inverter has to be designed to attain high efficiency and low total harmonic distortion (THD) of grid current fed into the grid are the requirements to be taken into consideration [31]. As per IEEE 1547 and IEC 61727, THD has to be maintained below 5% and DC current injected can be up to 1% of current. Since the converter operates in continuous conduction mode (CCM) with varying duty cycle, the output voltage alters with the input voltage and load variations from its designated value. Thus, the inverter has to ensure stable sinusoidal output voltage irrespective of the load connected to it. For this purpose, a fast and accurate closed loop controller is required to regulate the output voltage.

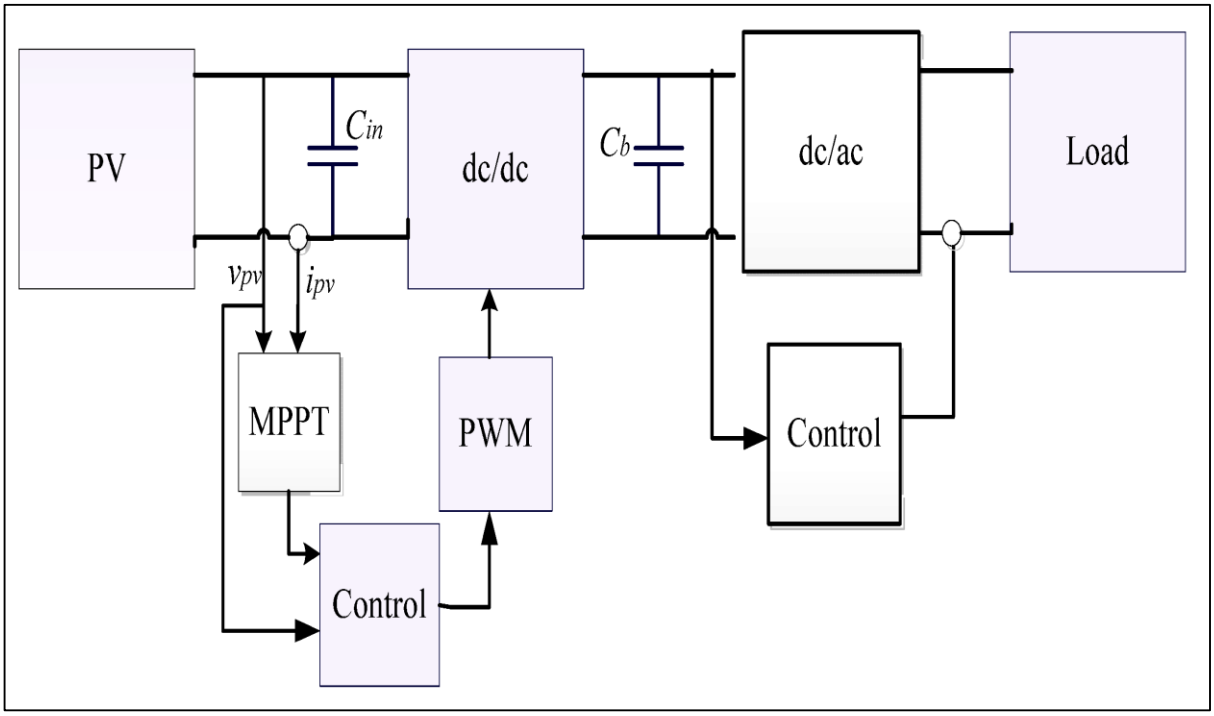

Figure 4.1 Closed loop control of grid-tied PV inverter [32]

Closed loop operation adjusts the duty cycle to regulate the load voltage despite any variations in input voltage or load. The small signal analysis of the converter derives the transfer functions which is required to design the closed-loop control circuit [33]. For grid-interfaced systems, the injected grid current can be controlled via a current sensor. Generally, inverter uses the control strategy of output current control to attain grid stability. Thereupon,

the end purpose of the current controller is to maintain unity power factor (UPF) during steady state and inject high-quality current into the grid.

4.1.1 Dynamic Modeling of Proposed Inverter

Modeling could be defined as depicting a physical phenomenon through mathematical expressions. It requires approximations to be considered for simplification which are generally achieved by averaging inductor voltage and capacitor current over one switching period in order to remove high frequency switching ripples. As per the principle of inductor volt-second balance and capacitor-charge balance, it estimates inductor current and capacitor voltage to be zero when the converter operates in an equilibrium state. Since these state-space equations are a set of non-linear differential equations, it must be linearized by applying few standard linear methods like Laplace transform [34]. State-space averaging and circuit averaging are two renowned techniques for ac modeling.

4.1.2 State-space Averaged Model

As this converter is non-linear and time-variant, small-signal modeling of state-space average technique is applied for designing a linear controller [35]. This small-signal model is useful for extracting open loop transfer function like control to output, output to input. Since switches are responsible for introducing switching harmonics, therefore the circuit model is derived by averaging the switch waveforms [34]. This model analyzes the small deviations around the steady-state operating point known as a perturbation. The technique is used by converting the converter circuit into a simple electric circuit in which all the energy storage elements (inductor current and capacitor voltage) are the state variables. Hence, for "n "independent storage elements, there are "n "state variables. Thus, six passive elements in this converter mean six state variables. The state-space equations can be obtained from Table 3.1 and state-space averaged expressions for state variables are as follows:

$$\frac{L_{in}\, di_{\mathrm{L_{in}}}}{dt} = v_{in} - v_{\mathrm{C_{in}}}(1-d) \tag{4.1}$$

$$\frac{\mathrm{C_{in}}\, dV_{\mathrm{C_{in}}}}{dt} = i_{L_{in}}(1-d) - i_{L_f}d + i_{L_{fly}}(d-1) \tag{4.2}$$

$$\frac{L_{fly}\, di_{\mathrm{L_{fly}}}}{dt} = -v_{\mathrm{C}_{out}}d + v_{\mathrm{C_{in}}}(1-d) \tag{4.3}$$

$$\frac{\mathrm{C_{out}}\, dV_{\mathrm{C_{out}}}}{dt} = i_{L_{fly}}.d + i_{L_f}(1-d) \tag{4.4}$$

$$\frac{L_f\, di_{\mathrm{L_f}}}{dt} = v_{\mathrm{C_{in}}} d - v_{\mathrm{C}_{out}}(1-d) - v_O \tag{4.5}$$

$$\frac{\mathrm{C_f}\, dV_{\mathrm{C_f}}}{dt} = i_{L_f} - i_0 \tag{4.6}$$

Here, the elements are assumed to be ideal and at zero initial conditions. Perturbation is introduced in the state variables and duty cycle can be listed as follows:

$$i_{\mathrm{L_{in}}} = I_{\mathrm{L_{in}}} + \hat{\imath}_{\mathrm{L_{in}}}, i_{\mathrm{L_{fly}}} = I_{\mathrm{L_{fly}}} + \hat{\imath}_{\mathrm{L_{fly}}}, i_{\mathrm{L_f}} = I_{\mathrm{L_f}} + \hat{\imath}_{\mathrm{L_f}} \tag{4.7}$$

$$v_{\mathrm{C_{in}}} = V_{\mathrm{C_{in}}} + \hat{v}_{\mathrm{C_{in}}}, v_{\mathrm{C}_{out}} = V_{\mathrm{C_{out}}} + \hat{v}_{\mathrm{C}_{out}}, v_O = v_{\mathrm{C_f}} = V_{\mathrm{C_f}} + \hat{v}_{\mathrm{C_f}},$$

$$d = D + \hat{d}$$

where $I_{\mathrm{L_{in}}}, I_{\mathrm{L_{fly}}}, I_{\mathrm{L_f}}, V_{\mathrm{C_{in}}}, V_{\mathrm{C_{out}}}\ and\ V_{\mathrm{C_f}}$ denote DC values and variables with hat($\widehat{\ }$) indicates perturbation (AC variation around steady-state operating point). After substituting these variables as mentioned in (4.7) into (4.1) – (4.6) and neglecting higher order equations, we can obtain following small-signal AC model in matrix form as given in (4.10). The input voltage perturbation has been neglected for simplification purpose.

The dynamic or state space equations of the converter can be written as [36]:

$$\dot{X} = AX + BU \tag{4.8}$$

$$Y = CX + DU \tag{4.9}$$

where A- system matrix

B- Input matrix

C- Output matrix

D- Feedback matrix

There are two modes in the proposed converter: the on- mode (t_{on}) and the off-mode (t_{off}). Thus, below are the system of the equation obtained when S_1, S_3 are ON and S_2, S_4 are OFF for this converter in CCM would be:

$$\begin{bmatrix} i'_{L_{in}} \\ i'_{L_{fly}} \\ i'_{L_f} \\ v'_{C_{in}} \\ v'_{C_{out}} \\ v'_O \end{bmatrix} = \begin{bmatrix} 0 & 0 & 0 & 0 & 0 & 0 \\ 0 & 0 & 0 & 0 & \frac{-1}{L_{fly}} & 0 \\ 0 & 0 & 0 & \frac{1}{L_f} & 0 & \frac{-1}{L_f} \\ 0 & 0 & \frac{-1}{C_{in}} & 0 & 0 & 0 \\ 0 & \frac{1}{C_{out}} & 0 & 0 & 0 & 0 \\ 0 & 0 & \frac{1}{C_f} & 0 & 0 & \frac{-1}{(RC_f)} \end{bmatrix} \times \begin{bmatrix} \hat{\imath}_{L_{in}} \\ \hat{\imath}_{L_{fly}} \\ \hat{\imath}_{L_f} \\ \hat{v}_{C_{in}} \\ \hat{v}_{C_{out}} \\ \hat{v}_O \end{bmatrix} + \begin{bmatrix} \frac{1}{L_{in}} \\ 0 \\ 0 \\ 0 \\ 0 \\ 0 \end{bmatrix} \times [\hat{v}_{in}] + \begin{bmatrix} \frac{V_{C_{in}}}{L_{in}} \\ \frac{-(V_{C_{in}} + V_{C_{out}})}{L_{fly}} \\ \frac{(V_{C_{in}} + V_{C_{out}})}{L_f} \\ \frac{-(I_{L_{in}} + I_{L_f} - I_{L_{fly}})}{C_{in}} \\ \frac{(I_{L_{fly}} - I_{L_f})}{C_{out}} \\ 0 \end{bmatrix} \times [\hat{d}] \tag{4.10}$$

The system of the equation obtained when S_2, S_4 are ON and S_1, S_3 are OFF for this converter:

$$\begin{bmatrix} i'_{Lin} \\ i'_{Lfly} \\ i'_{Lf} \\ v'_{C_{in}} \\ v'_{C_{out}} \\ v'_O \end{bmatrix} = \begin{bmatrix} 0 & 0 & 0 & \frac{-1}{L_{in}} & 0 & 0 \\ 0 & 0 & 0 & \frac{1}{L_{fly}} & 0 & 0 \\ 0 & 0 & 0 & 0 & \frac{-1}{L_f} & \frac{-1}{L_f} \\ \frac{1}{C_{in}} & \frac{-1}{C_{in}} & 0 & 0 & 0 & 0 \\ 0 & 0 & \frac{1}{C_{out}} & 0 & 0 & 0 \\ 0 & 0 & \frac{1}{C_f} & 0 & 0 & \frac{-1}{(RC_f)} \end{bmatrix} \times \begin{bmatrix} \hat{\imath}_{L_{in}} \\ \hat{\imath}_{L_{fly}} \\ \hat{\imath}_{L_f} \\ \hat{v}_{C_{in}} \\ \hat{v}_{C_{out}} \\ \hat{v}_O \end{bmatrix} + \begin{bmatrix} \frac{1}{L_{in}} \\ 0 \\ 0 \\ 0 \\ 0 \\ 0 \end{bmatrix} \times [\hat{v}_{in}] + \begin{bmatrix} \frac{V_{C_{in}}}{L_{in}} \\ \frac{-(V_{C_{in}} + V_{C_{out}})}{L_{fly}} \\ \frac{(V_{C_{in}} + V_{C_{out}})}{L_f} \\ \frac{-(I_{L_{in}} + I_{L_f} - I_{L_{fly}})}{C_{in}} \\ \frac{(I_{L_{fly}} - I_{L_f})}{C_{out}} \\ 0 \end{bmatrix} \times [\hat{d}] \tag{4.11}$$

The complete bilinear model is achieved by [19]:

$$X' = [A_1 d + A_2(1-\mathrm{d})]\widehat{\mathrm{X}} + [B_1 d + B_2(1-d)]\hat{v}_{in} + [(A_1 - A_2)X + (B_1 - B_2)v_{in}]\hat{d} \quad (4.12)$$

where d is the duty cycle

A_1, B_1 and A_2, B_2 are the system and input matrix obtained from (4.10)and (4.11) respectively. Therefore, the full model of the converter is given by

$$\begin{bmatrix} i'_{Lin} \\ i'_{Lfly} \\ i'_{Lf} \\ v'_{\mathrm{C_{in}}} \\ v'_{\mathrm{C}_{out}} \\ v'_{O} \end{bmatrix} = \begin{bmatrix} 0 & 0 & 0 & \frac{d-1}{L_{in}} & 0 & 0 \\ 0 & 0 & 0 & \frac{1-d}{L_{fly}} & \frac{-d}{L_{fly}} & 0 \\ 0 & 0 & 0 & \frac{d}{L_f} & \frac{d-1}{L_f} & \frac{-1}{L_f} \\ \frac{1-d}{\mathrm{C_{in}}} & \frac{d-1}{\mathrm{C_{in}}} & \frac{-d}{\mathrm{C_{in}}} & 0 & 0 & 0 \\ 0 & \frac{d}{\mathrm{C}_{out}} & \frac{1-d}{\mathrm{C}_{out}} & 0 & 0 & 0 \\ 0 & 0 & \frac{1}{\mathrm{C}_f} & 0 & 0 & \frac{-1}{RC_f} \end{bmatrix} \times \begin{bmatrix} \hat{\imath}_{\mathrm{L_{in}}} \\ \hat{\imath}_{\mathrm{L_{fly}}} \\ \hat{\imath}_{\mathrm{L_f}} \\ \hat{v}_{\mathrm{C_{in}}} \\ \hat{v}_{\mathrm{C}_{out}} \\ \hat{v}_{O} \end{bmatrix} + \begin{bmatrix} \frac{1}{L_{in}} \\ 0 \\ 0 \\ 0 \\ 0 \\ 0 \end{bmatrix} \times [v_{in}] + \begin{bmatrix} \frac{V_{\mathrm{C_{in}}}}{L_{in}} \\ \frac{-(V_{\mathrm{C_{in}}} + V_{\mathrm{C_{out}}})}{L_{fly}} \\ \frac{(V_{\mathrm{C_{in}}} + V_{\mathrm{C_{out}}})}{L_f} \\ \frac{-(I_{\mathrm{L_{in}}} + I_{\mathrm{L_f}} - I_{\mathrm{L_{fly}}})}{\mathrm{C_{in}}} \\ \frac{(I_{\mathrm{L_{fly}}} - I_{\mathrm{L_f}})}{\mathrm{C}_{out}} \\ 0 \end{bmatrix} \times [\hat{d}] \quad (4.13)$$

Our aim is to derive a transfer function between the control input $d(s)$ to filter inductor current $i_{L_f}(s)$, known as plant transfer function can be obtained by using

$$\mathrm{T(s)} = \frac{i_{L_f}(s)}{d(s)} = \mathrm{C.\,(SI - A)^{-1}.}\,B \quad (4.14)$$

where, I is the identity matrix, A=$A_1 + A_2$ is the system matrix and B = $B_1 + B_2$ is the input matrix. It can be obtained from dynamic equations (4.8) and (4.9). C is the output matrix shown below:

$$C = [0 \quad 0 \quad 1 \quad 0 \quad 0 \quad 0] \tag{4.15}$$

4.1.3 Transfer function

Due to six state variables, a sixth order AC model is obtained in (4.13), represented in matrix form. After substituting the matrix A, B and C in (4.14), we get the optimized plant transfer function $G_p(s)$ by using MATLAB given as

$$G_p(s) = \frac{i_{L_f}(s)}{d(s)} \tag{4.16}$$
$$= \frac{35 \times 10^4\, s^5 + 2.65 \times 10^9 s^4 + 1.55 \times 10^{14} s^3 + 1.2 \times 10^{18} s^2 + 4.85 \times 10^{21}\, s + 4.9 \times 10^{28}}{4.5\, s^6 + 4 \times 10^4\, s^5 + 6 \times 10^9\, s^4 + 2 \times 10^{13} s^3 + 1.5 \times 10^{18}\, s^2 + 1.2 \times 10^{21} s + 3.5 \times 10^{25}}$$

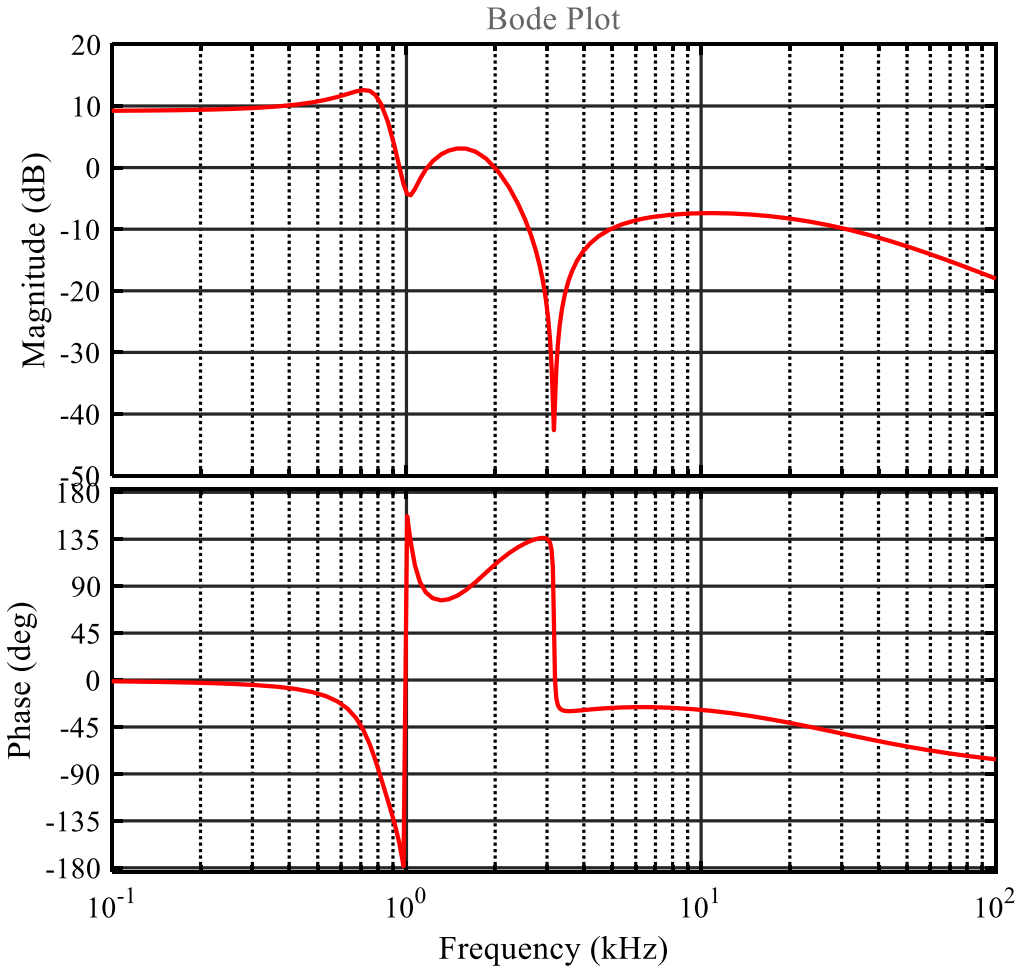

Figure 4.2 Bode plot of the plant transfer function

D=0.75 is used for calculation of $G_p(s)$. The value of the input (L_{in})and the flying inductor (L_{fly}) have been kept the same for simplification of converter design. Similarly, C_{in} and C_{out} have been kept the same. The uncompensated plant transfer function is shown in Figure 4.2 with the help of a bode plot.

With (4.13), the transfer function between filter inductor current (i_{L_f}) to the output voltage (v_O) can also be computed as follows:

$$T(s) = \frac{v_O(s)}{i_{L_f}(s)} = C.(SI - A)^{-1}.B \tag{4.17}$$

$$C = [0 \quad 0 \quad 0 \quad 0 \quad 0 \quad 1] \tag{4.18}$$

$$B = [0 \quad 0 \quad 1 \quad 0 \quad 0 \quad 0] \tag{4.19}$$

Where C and B are the output and input matrix respectively.

Thus, the transfer function is

$$G_p(s) = \frac{v_O(s)}{i_{L_f}(s)} = \frac{10^6 s^4 + 4 \times 10^{14} s^2 + 9.6 \times 10^{21}}{s^6 + 18 \times 10^3 s^5 + 13.5 \times 10^8 s^4 + 82 \times 10^{11} s^3 + 34 \times 10^{16} s^2 + 56 \times 10^{19} s + 8 \times 10^{24}} \tag{4.20}$$

4.2 Controller Design Consideration

The objectives of a controller are to accurately track reference current, reduce the steady-state error and minimize harmonics in the grid current. It comprises of a fast internal current loop and a slow external voltage loop. The filter inductor current (i_{L_f}) is controlled in the inner loop and the output voltage is regulated in an outer feedback loop. The current controller contributes to the quality of grid current and attaining fast dynamic response significantly whereas the voltage controller is mainly for stability and optimal regulation [31]. Hence, it is essential that the controller provides an optimal quality sinusoidal output current with minimum harmonics to prevent distortion [37]. The outer voltage loop is slower than the inner current loop. Thus, the bandwidth of the inner current loop is higher than that of the outer voltage loop.

4.3 Types of Current Controllers

There are various types of controllers such as linear, non-linear, robust, predictive, adaptive and intelligent controllers. They are briefly described in Table 4.1. The linear

controller will be discussed in detail as they are implied in the inverter for control. They are drafted based on the feedback control theory [31].

Table 4.1 Characteristics of various current controllers [31]

Current Controller	Details
Linear	Mainly based on classical linear systems and control science.
Non-linear	Remarkable in performance, improved performance in transforming non-linear to partially or fully linear systems.
Robust	Provides sturdy performance, manages non-linear constraints and ensures stability in closed loop systems.
Predictive	Anticipates behavior of parameters by utilizing a system model and yields fast dynamic response.
Adaptive	Control of the system is altered as per the operating conditions
Intelligent	Troubleshoots control system issues by computerization in biological intelligence.

4.3.1 Linear Controllers

This group of linear controller mainly consists of Proportional Integral (PI), Proportional Integral Derivative (PID), Proportional-Derivative (PD) and Proportional (P) controller based on the dynamics of a linear system.

- Proportional Integral (PI) Controller: It is the most commonly used controller in current controlled VSI and can be designed using Ziegler-Nicholas, Pole-placement and frequency response methods. Despite this, they have two major shortcomings: incapability to track sinusoidal reference with zero steady-state error and poor disturbance rejection. It can perfectly track dc signals but not the sine reference due to high rise and settling time. This makes these controllers inappropriate for AC systems in the high-frequency range [2]. The synchronous reference frame PI controller excels over the stationary reference frame controller as the latter undergo potential amplitude and phase error due to gain limitations at the fundamental frequency. But PI controller implementation becomes complex due to the signal

transformation from stationary to synchronous frame [38]. This leads to the introduction of P + Resonant (PR) controller for tracking sinusoidal current in the stationary frame. It can be obtained by transforming an ideal synchronous PI controller to a stationary frame.

$$G_{PI}(s) = K_p + \frac{K_i}{s} \tag{4.21}$$

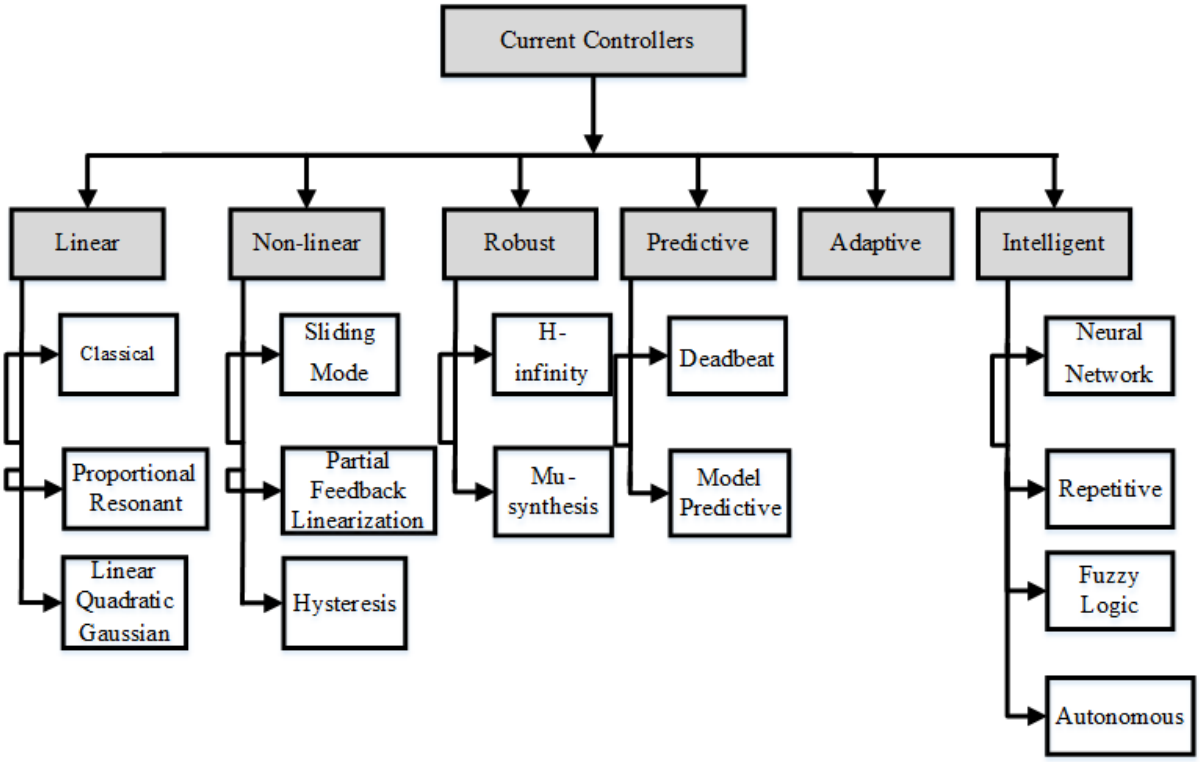

Figure 4.3 Types of current controllers [31]

4.3.2 Proportional Resonant (PR) Controller

The Proportional Resonant (PR) controller is preferred to augment the tracking performance of the converter and replace the conventional PI controller. They are highly suited for generating sinusoidal reference as required in grid-connected PV inverter. In addition to it, the PR controller delivers similar performance as a PI controller in the synchronous reference frame. It has the main function of introducing infinite gain at selected resonant frequency (grid frequency) for zero steady-state error and almost no gain and phase-shift at other frequencies [39]. Thus, it can be considered as PI controller with a resonant portion as a double generalized

AC integrator (GI). Thus, the PR controller is tuned at a grid frequency of 60 Hz to ensure high gain at grid frequency. The transfer function $G_{PR}(s)$ of an ideal PR controller is given as

$$G_{PR}(s) = K_p + \frac{2K_i s}{s^2 + \omega_0^2} \tag{4.22}$$

where K_p, K_i are gain constants and ω_0 $(= 2\pi \times 60 \frac{rad}{s})$ is the grid frequency.

4.3.3 Linear Quadratic Gaussian (LQG) Controllers

It is an outcome of the linear quadratic regulator and Kalman filter. It is applicable for both time-varying and time in varying systems.

4.4 Single Phase PV Inverter Control

A control strategy for PV inverter control mainly depends on the mode of operation. In the grid-tied mode, PV inverter behaves as a current controlled source to generate output current as per the reference current whereas, in off-grid mode (stand-alone mode), PV inverter serves as a voltage-controlled source to produce output voltage based on reference voltage [40]. These controllers are adapted to ensure that all the problems related to leakage current, DC current injection are kept within limits to maintain grid current quality. The feedback controller has to ensure

- Grid synchronization
- Extracting maximum power from PV panels
- Injection of active power in a controlled manner
- Reactive power support

The closed loop control is a combination of the inner current loop and outer voltage loop to provide zero steady-state error and harmonic compensation [41].

4.4.1 Inner Current Loop

The inner current loop is responsible for grid current control which is achieved by stabilizing current through filter inductor (I_{Lf}). Since it is a grid-interfaced PV inverter, thus the assumption has been made that grid voltage remains constant i.e. $120V, rms$.

For grid-tied PV inverter, the grid side inductor i.e. filter inductor is very crucial as it is designed to attenuate the high-frequency currents from inverter to grid [40]. Thus, the output

current is compared with the current reference$I_{Lf,peak} \times Sin\,\theta$ and the error generated is fed to the PR controller which yields a change in duty ratio. The output of the current controller is a sinusoidal modulating signal, which is compared with the carrier triangular wave for the generation of gating pulses for the converter. Thus, the inductor current is sensed and the duty cycle is controlled. Generally, a unit delay is taken into consideration for digital implementation as modulating signal will not update until the next switching cycle. This controller acts as a compensator for the inner loop.

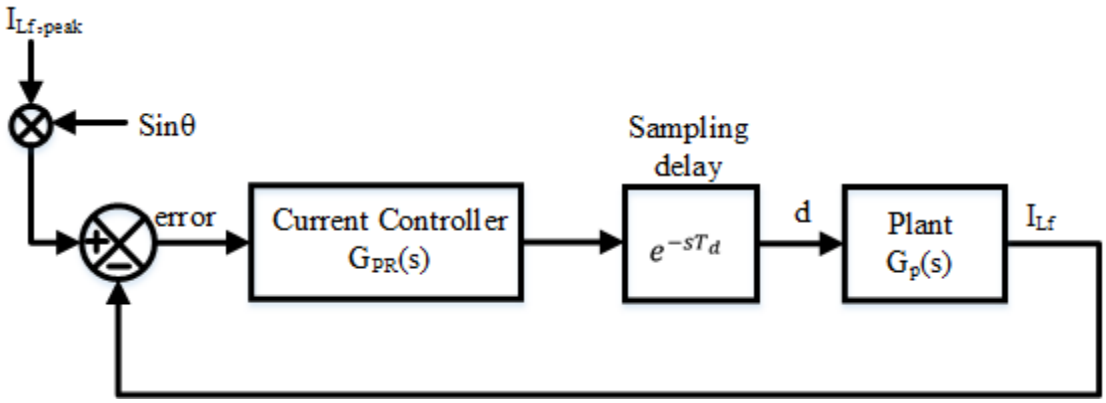

Figure 4.4 Block diagram of the current control loop

The purpose of the PR controller is to obtain high gain at grid frequency ($w_0 = 377\,rad/s$). The transfer function given in (4.22) is an ideal transfer function of the PR controller which gives infinite gain at ω_0 and may lead to stability issues. Thus, the PR controller is made non-ideal by introducing damping and its frequency response is given as:

$$G_{PR}(s) = K_p\left(1 + \frac{2K_i \times \omega_r s}{(s^2 + \omega_r\, s + \omega_0^2)}\right); \quad K_i = \frac{K_p}{\tau_i} \tag{4.23}$$

where ω_r is the resonant cut-off frequency and is generally in the range of 1-10 rad/s. It is more realizable in the digital domain due to finite precision. The proportional gain K_p is similar to the PI controller and determines the dynamics of a system i.e. bandwidth, phase and gain margins. A procedure has been followed to determine the time constant (τ_i), controller gain constants K_p and K_i [27].

1. The gain equation is given as $G(s) = G_{PR}(s) \times e^{-sT_d} \times G_p(s)$.
2. At crossover frequency (ω_c), the desired phase margin (PM) denoted as $\emptyset_m$ can be expressed as:

$$G_{PR}(j\,\omega_c) \times e^{-j\,\omega_c T_d} \times G_P(j\,\omega_c) = -\pi + \emptyset_m \tag{4.24}$$

$$\emptyset_m \cong \omega_c T_d + \tan^{-1}\left(\tau_i \times \frac{\omega_c}{2\omega_r}\right) \tag{4.25}$$

3. Some estimations in (4.25) lead us to the following equation from where ω_{cmax} can be calculated as:

$$\omega_{cmax} = \frac{(90° - \emptyset_m)}{T_d} \times \frac{\pi}{180}° \tag{4.26}$$

4. Considering the desired phase margin of 40° and delay time $T_d = 0.75T_s$ where $T_s = 20\mu s$ is the switching time (corresponding to 50 KHz), ω_{cmax} is computed to be 58178 rad/s.
5. Next step is to calculate the time constant τ_i from the following formula:

$$\tan^{-1}\left(\tau_i \times \frac{\omega_{cmax}}{2\omega_r}\right) = \emptyset_m - \omega_c T_d \tag{4.27}$$

$$\tau_i = \frac{(\tan 85 \times 10)}{58178} = 1.96 \times 10^{-3}\ sec. \tag{4.28}$$

6. Now, K_p can be calculated by equating $G(s)$ to unity at the maximum crossover frequency ω_{cmax}. The plant transfer function $G_P(s)$can be obtained from (4.16).

$$1 = K_p\left(1 + \frac{2K_i \times \omega_r \times j\omega_{cmax}}{((j\omega_{cmax})^2 + \omega_r \times j\omega_{cmax} + \omega_0^2)}\right) \times e^{-j\,\omega_{cmax}T_d} \times G_P(j\,\omega_{cmax}) \tag{4.29}$$

7. After solving the above calculations, K_p is derived as 0.4 and K_i is 200. The integral gain K_i must be high enough to enforce small steady-state error [37]. It is observed that the magnitude of the base of the PR controller rises with the K_i and an increase in K_p rises the resonant part of the controller. Thus, the PR controller transfer function is derived as follows:

$$G_{PR}(s) = 0.4\left(1 + \frac{200 \times 10s}{(s^2 + 5s + 1.4 \times 10^5)}\right) \tag{4.30}$$

The bode plots of the plant transfer function $G_P(s)$, controller $G_{PR}(s)$and $G(s)$ are shown in Figure 4.5. A high gain of $49dB$ has been noticed at grid frequency (60Hz). Henceforth, the steady-state error which is inverse of this gain is determined to be 0.35%. This proves that the PR controller has been tuned to absolutely track the current reference.

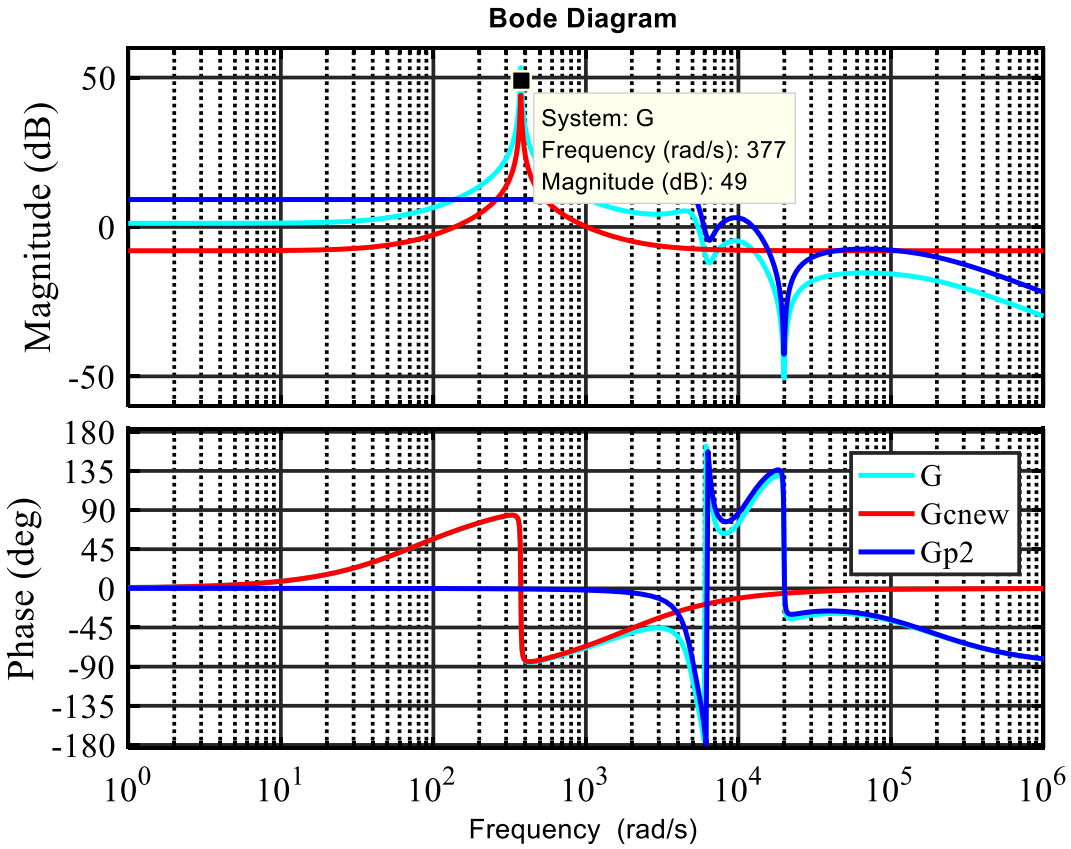

Figure 4.5 Bode plots of the transfer function

4.4.2 Reference Current ($i_{L_{f,ref}}$) Generation

The control block diagram of the proposed solar inverter is shown in Figure 4.6. It has a voltage controller which provides the peak value of reference output current to be injected into a grid based on the error between the sensed grid voltage and the reference grid voltage.

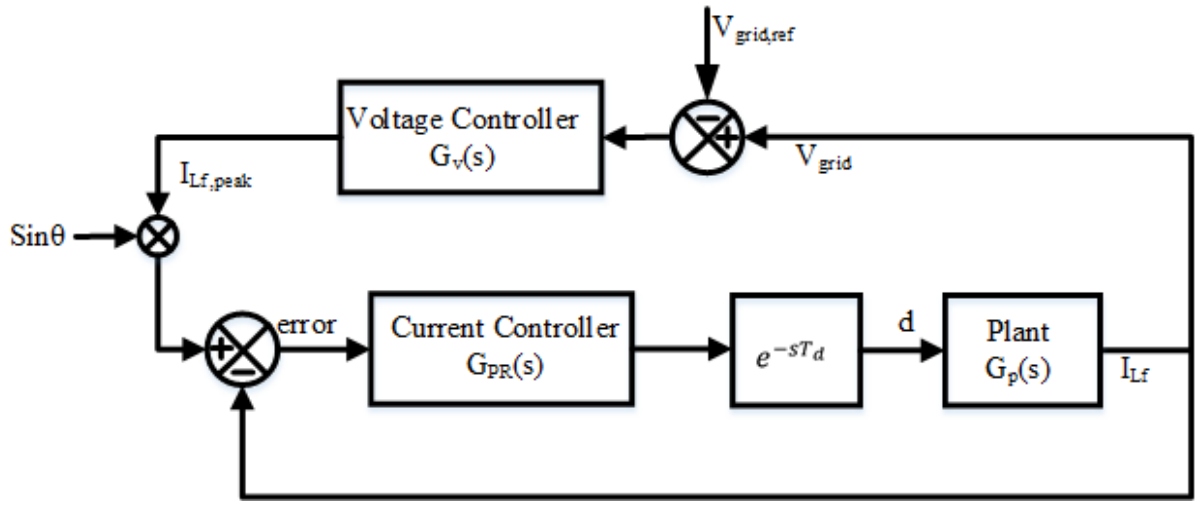

Figure 4.6 Block diagram of the implemented control strategy [27]

The filter inductor current (i_{L_f}) to the output voltage $v_O(s)$ transfer function is given in (4.20). Using the same approach as for the inner current loop, the PR controller for the outer loop is designed and calculated to be:

$$G_{PR2}(s) = 0.04\left(\frac{(s^2 + 3780s + 1.4 \times 10^5}{(s^2 + 30s + 1.4 \times 10^5)}\right) \quad (4.31)$$

4.5 Simulation and Experimental Results

4.5.1 Simulation Results

The performance of the developed closed-loop control is verified by simulating it in PSIM software as shown in Figure 4.7. A 250 W grid-tied PV inverter was modeled with DC source as input and connected with similar parameters as used for open loop analysis. It is operated at 50 kHz of switching frequency and interfaced to 60 Hz grid supply. It is designed to inject sinusoidal current to a grid having $120V, rms$. The reference current $i_{L_f}, peak$ was generated as 1.414 A and 2.828 A for 50% and full load respectively. The input inductor current ($I_{L_{in}}$) which limits the current ripple across the PV module is shown in Figure 4.7 (a). The grid voltage and current have been shown along with the capacitor voltages ($V_{C_{in}}$ and $V_{C_{out}}$) at 50% load in Figure 4.7 (b) and (c). Figure 4.7 (d) and (e) demonstrates that filter inductor current (i_{Lf}) trails the reference current absolutely at 50% load and full load respectively. Its output is then fed to the modulator for switching the inverter. Frequency analysis of the grid current has also been shown in Figure 4.7 (f). The proposed inverter leakage current is almost zero less than 2 mA as shown in Figure 4.7 (g). The simulation results for both 50% load and full load conditions have been analyzed to verify the control. The transient response of output current has also been evaluated by varying load from 50% to full load.

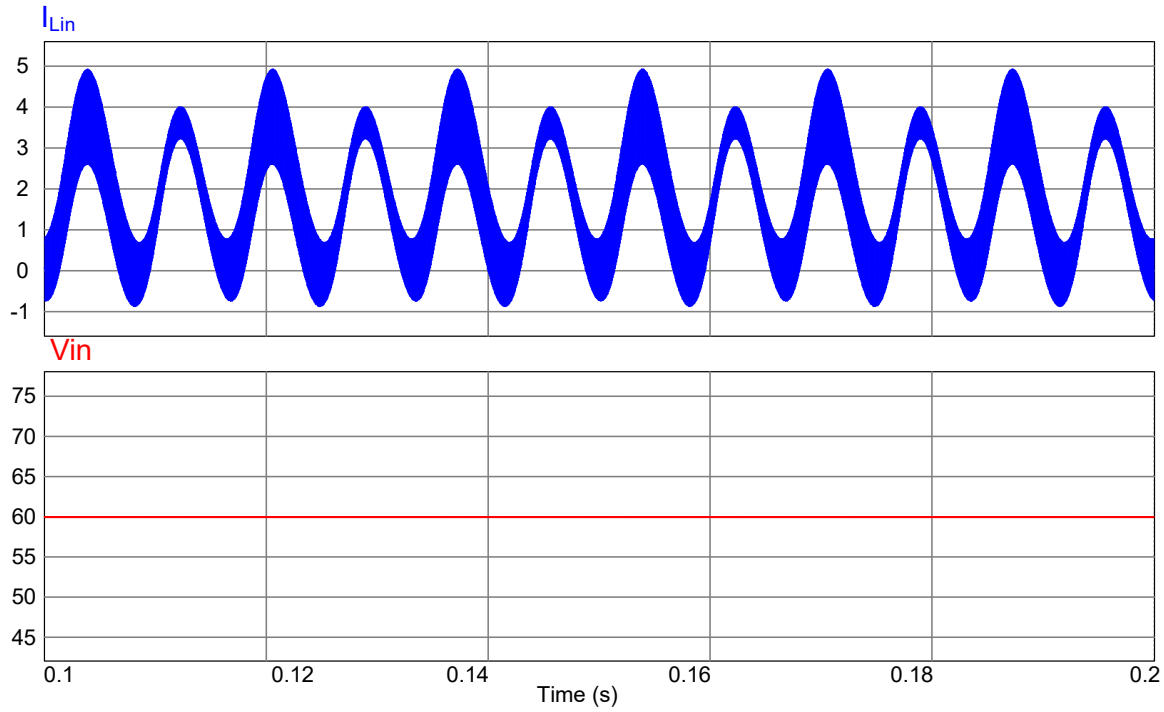
I_{Lin}
5
4
3
2
1
0
-1
Vin
75
70
65
60
55
50
45
0.1
0.12
0.14
0.16
0.18
0.2
Time (s)

(a)

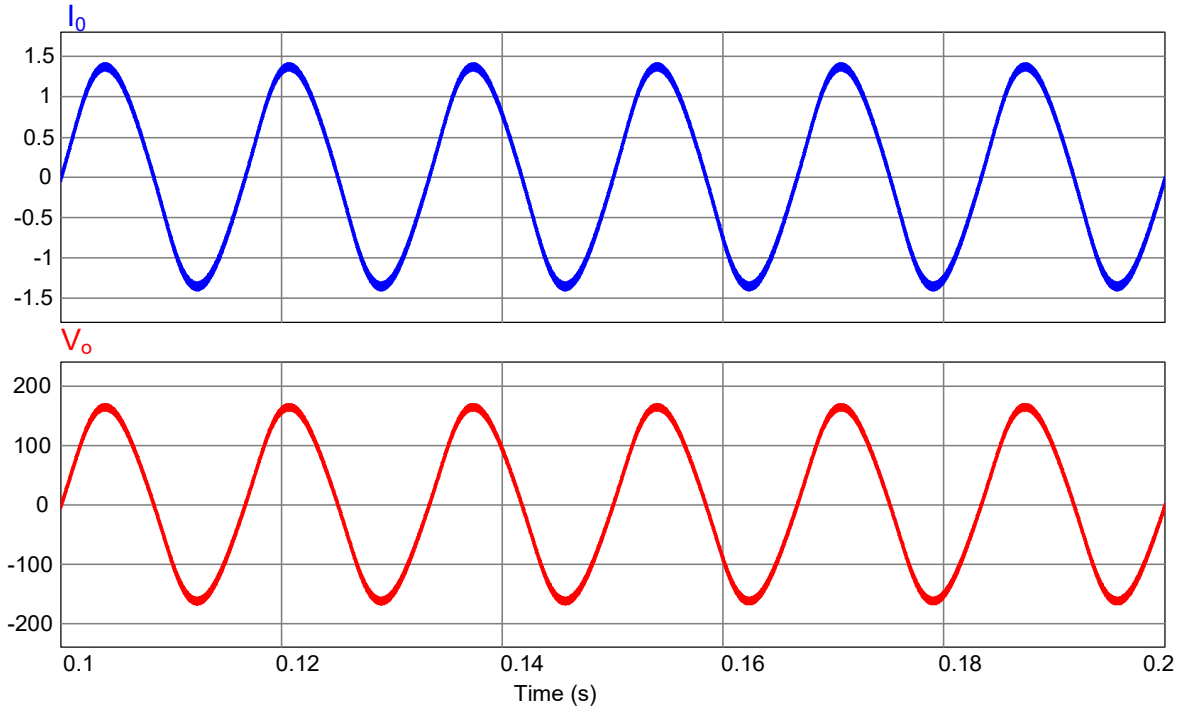
I_0
1.5
1
0.5
0
-0.5
-1
-1.5
V_o
200
100
0
-100
-200
0.1
0.12
0.14
0.16
0.18
0.2
Time (s)

(b)

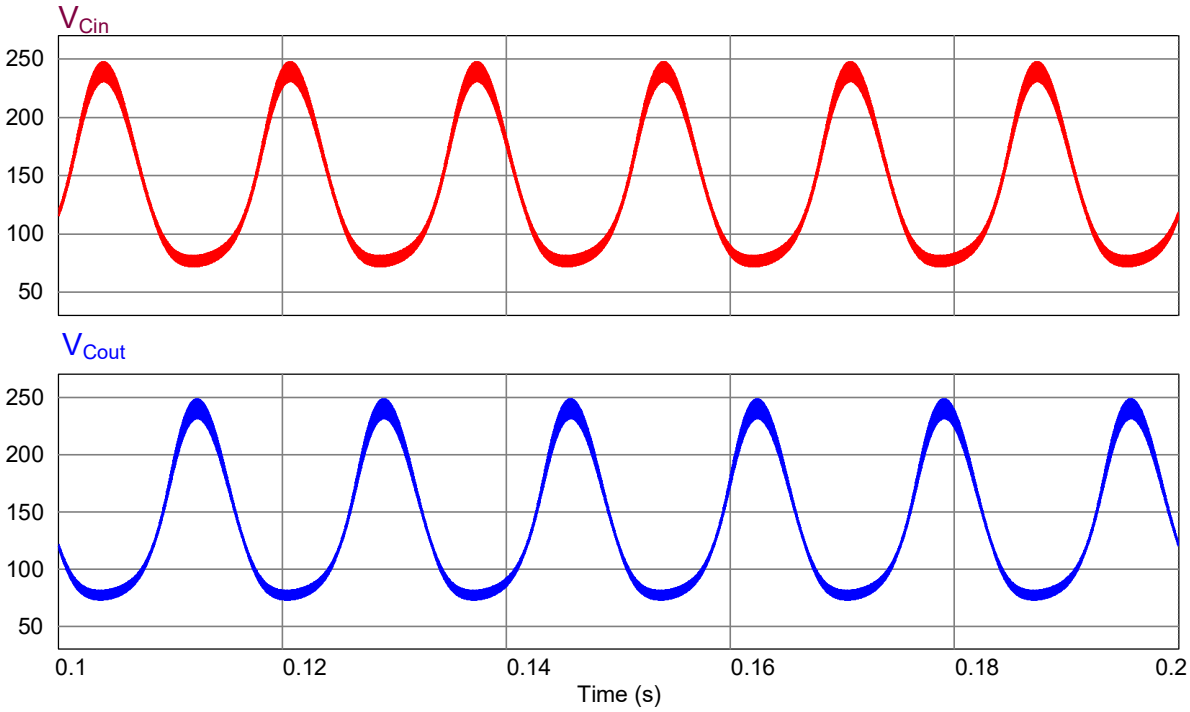
V_Cin
250
200
150
100
50
V_Cout
250
200
150
100
50
0.1
0.12
0.14
0.16
0.18
0.2
Time (s)

(c)

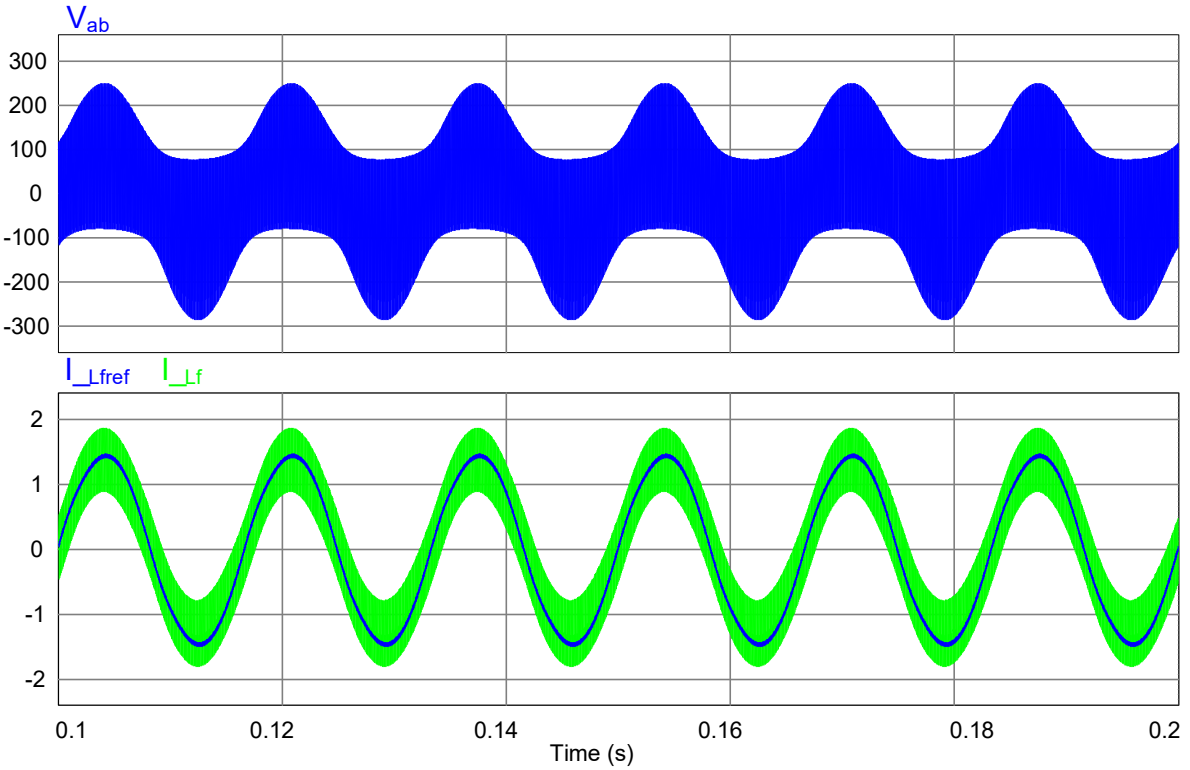
V_ab
300
200
100
0
-100
-200
-300
I_Lfref
I_Lf
2
1
0
-1
-2
0.1
0.12
0.14
0.16
0.18
0.2
Time (s)

(d)

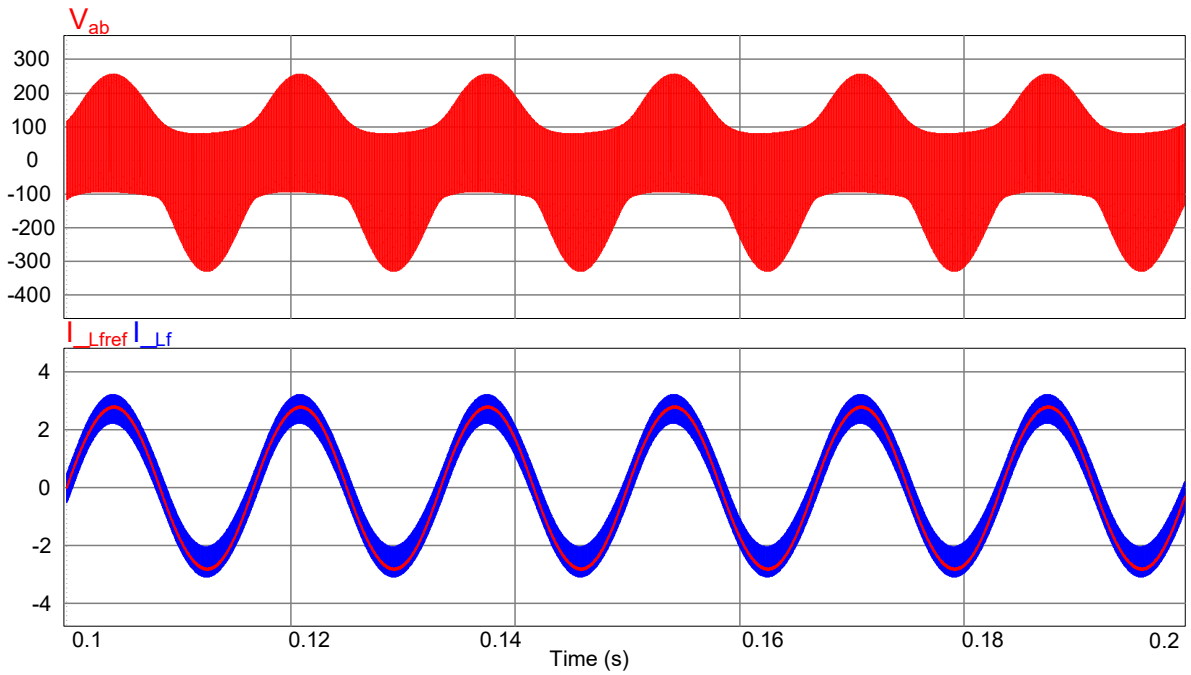
Vab
300
200
100
0
-100
-200
-300
-400
I_Lfref
I_Lf
4
2
0
-2
-4
0.1
0.12
0.14
0.16
0.18
0.2
Time (s)

(e)

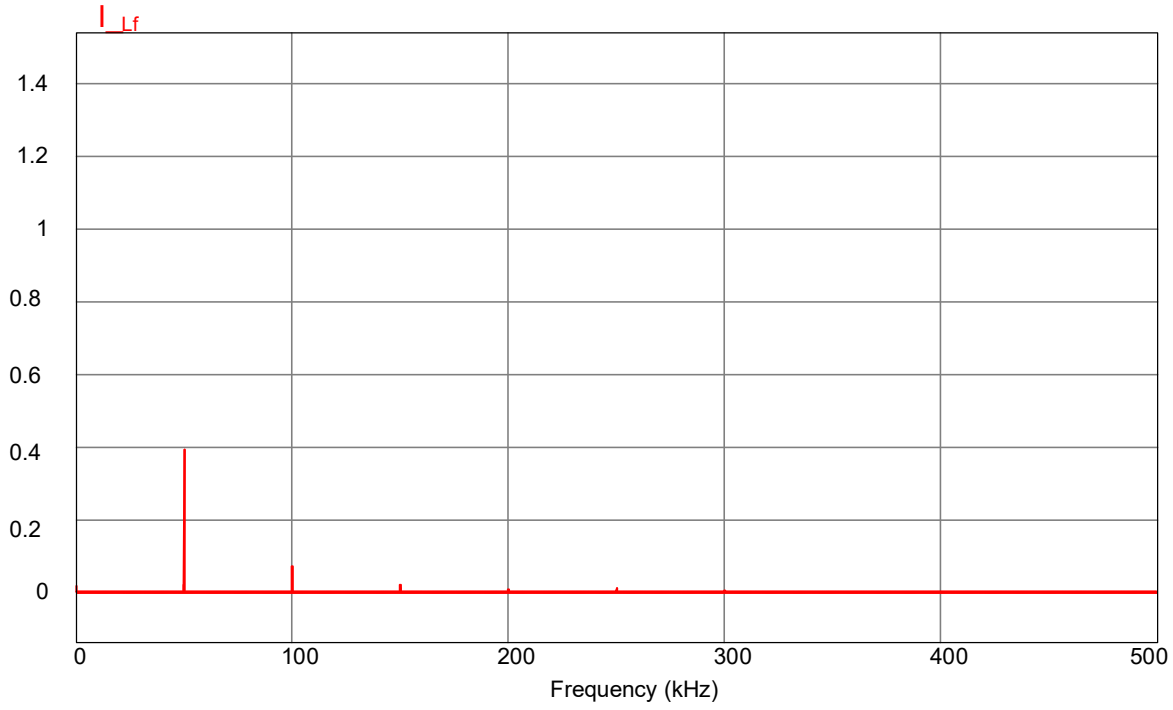
I_Lf
1.4
1.2
1
0.8
0.6
0.4
0.2
0
0
100
200
300
400
500
Frequency (kHz)

(f)

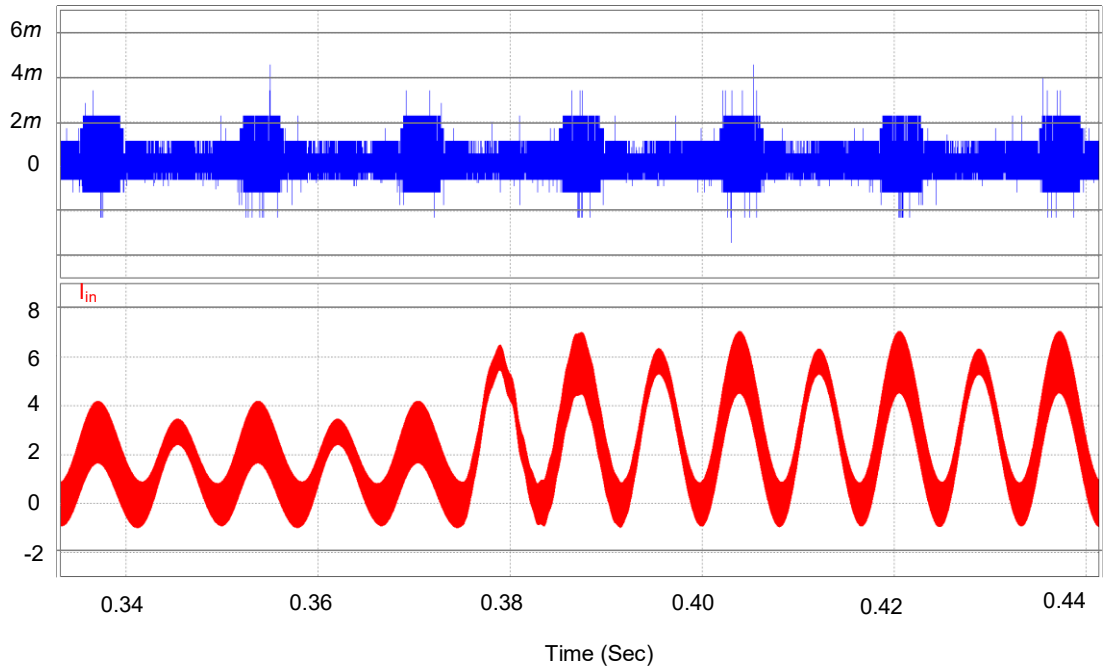

(g)

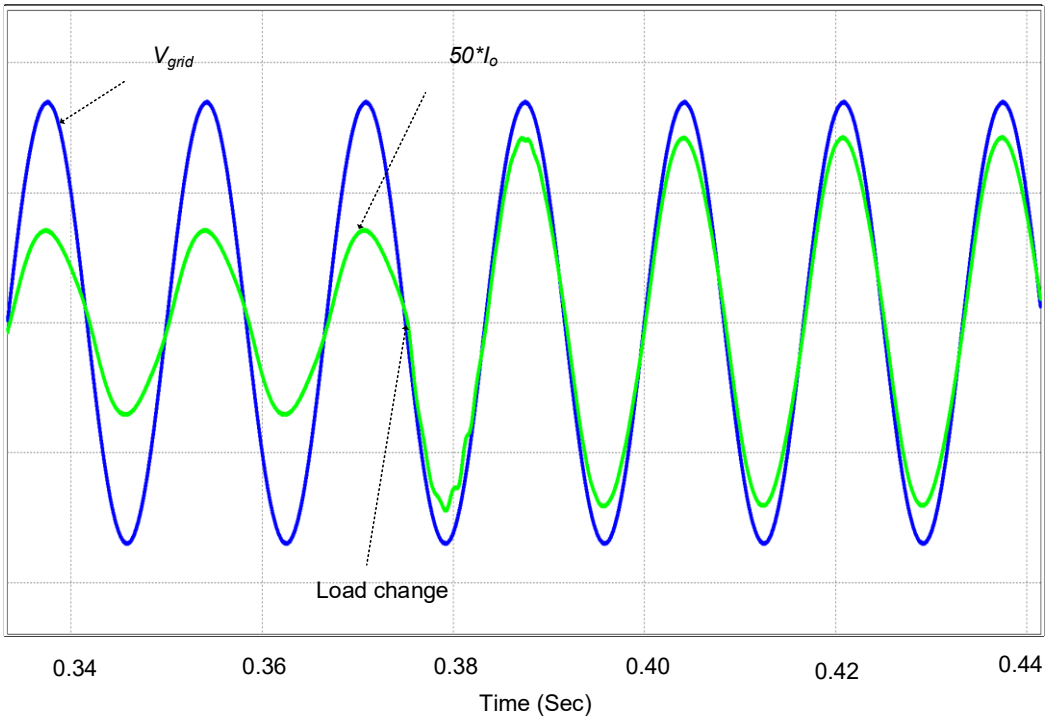

(h)

Figure 4.7 Simulated steady-state results of proposed topology, (a) input current and voltage; (b) output current, and output voltage; (c) voltages across capacitors 'C_{in}', and 'C_{out}'; (d) filter inductor current tracking reference current @ 50% load and the voltage across AB terminals before filter; (e) filter inductor current tracking reference current @ 100% load and voltage across AB terminals before filter; (f) FFT of grid current ; (g) inverter leakage current and input current; (h) transient response of output current from 50% load to full load.

4.5.2 Experimental Results

A 250W single-phase PV inverter hardware prototype was designed and developed in the lab to verify the control experimentally. The inverter is developed with the same parameters used in the simulation. A DC supply is used instead of a PV panel for simplicity. The hardware results are presented in Figure 4.8. A fixed-point TMS320F28335 was programmed for control platform. The pulses are generated through the internal pulse generator of the digital signal platform (DSP).

The hall-effect sensors LV-20P and LA-55P are used to sense grid voltage and output inductor current respectively. The output inverter voltage was scaled down to be less than 3.3V to make it compatible with the DSP. Operational amplifier LM324 has been used for the same. Voltage and current signals are measured using the internal analog-to-digital converter in DSP. The sampling frequency of 50 kHz and dead time of $1\mu s$ has been chosen. The waveforms for output voltage, output current, and the voltage across capacitors (C_{in} *and* C_{out}) are in agreement with simulations and theoretical claims as shown in Figure 4.8 (b) and (c). The measured voltage across AB terminals and the measured filter current and their zoomed version are shown in Figure 4.8 (d). The transient performance of the converter is also checked by changing load from 50 % to 100% and vice-versa as depicted in Figure 4.8 (e) and (f). Henceforth, the controller response is instantaneous as the change in load current is responded by PV inverter.

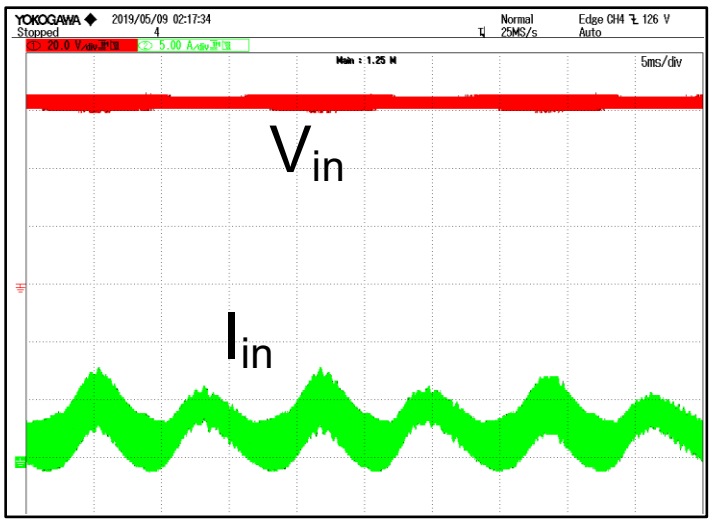

(a)

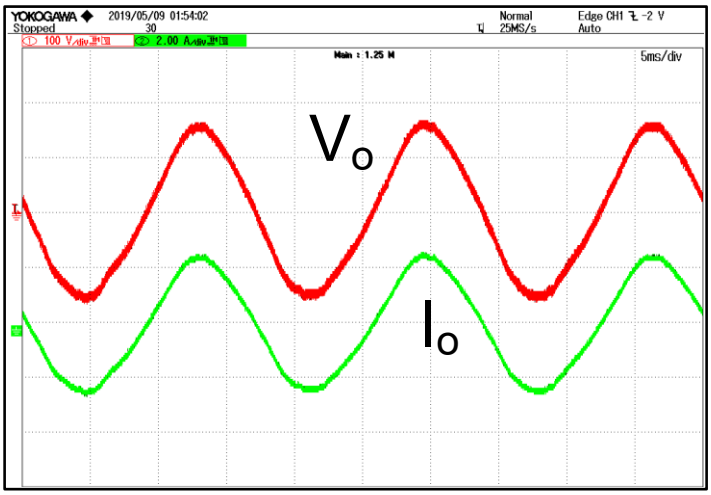
YOKOGAWA
2019/05/09 01:54:02
Stopped
30
Normal
25MS/s
Edge CH1 -2 V
Auto
100 V/div
2.00 A/div
Main : 1.25 M
5ms/div
Vo
Io

(b)

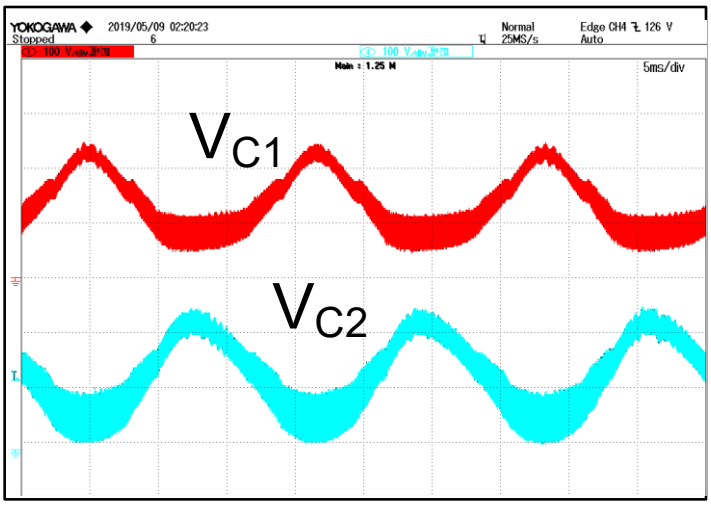
YOKOGAWA
2019/05/09 02:20:23
Stopped
6
Normal
25MS/s
Edge CH4 126 V
Auto
100 V/div
100 V/div
Main : 1.25 M
5ms/div
Vc1
Vc2

(c)

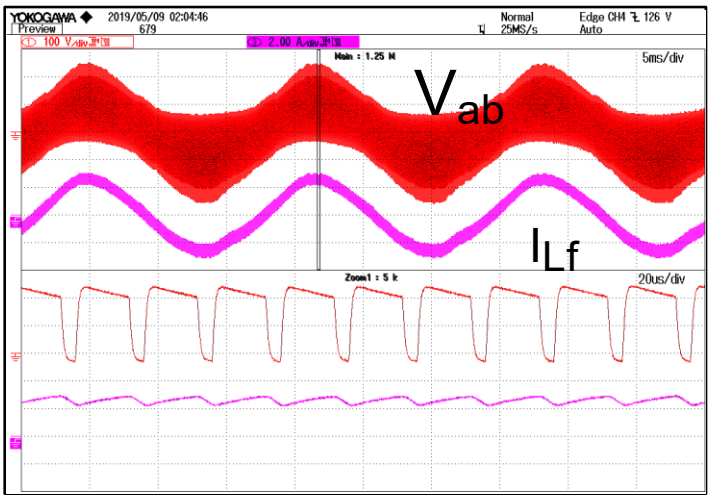
YOKOGAWA
2019/05/09 02:04:46
Preview
679
Normal
25MS/s
Edge CH4 126 V
Auto
100 V/div
2.00 A/div
Main : 1.25 M
5ms/div
Vab
ILf
Zoom1 : 5 k
20us/div

(d)

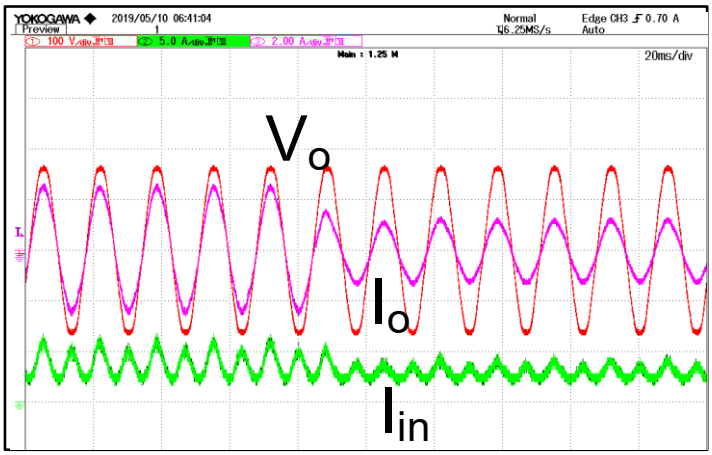

(e)

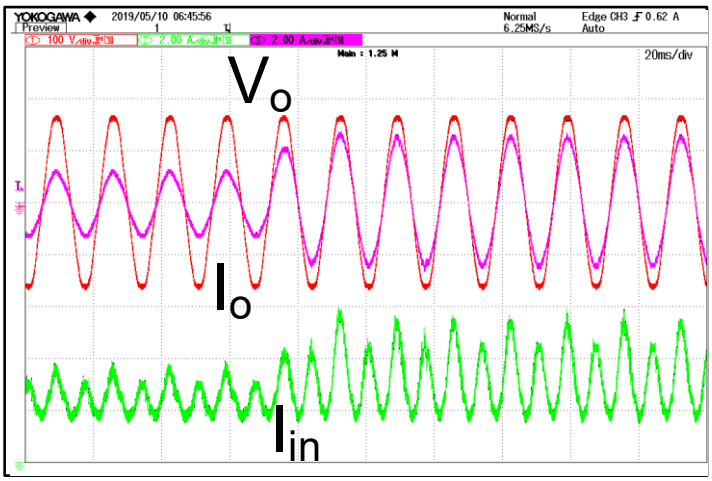

(f)

Figure 4.8 Experimental results of the proposed inverter, (a) input voltage (20 V/div), and input current (5.0 A/div); (b) output voltage (100 V/div), output current (2.0 A/div); (c) voltage across capacitors 'C_{in}' (100 V/div), and 'C_{out}' (100 V/div); (d) filter inductor current (2A/div), and voltage across AB terminals before filter (100 V/div); (e) &(f) Dynamic response of injected grid current on load change.

It is observed that the inverter output current is injected in-phase with the grid voltage, which validates the robustness of the designed controller and inverter. These experimental results are following the simulation results, and they are validating the theory and the inverter design with the expected output.

4.6 Conclusion

This Chapter explains the small-signal modeling of the proposed PV inverter. A sixth order small-signal AC model for this converter is developed utilizing the six energy storage elements which act as state variables. A step by step procedure to compute the transfer function of the plant is explained. Control (d) to filter inductor current (i_{L_f}) transfer function has been derived and bode plot shows the behavior of plant transfer function in the frequency domain. To reduce the steady-state error, the controller to be designed is discussed. In addition, closed-loop analysis of this inverter has been carried out and various kinds of controllers for grid-interfaced application are discussed. PR controller has been proven successful in controlling current and injecting sinusoidal current in phase with the grid voltage. The simulation results at first and later the experimental results which are in good agreement are presented. Therefore, the theoretical claims are also verified.

Chapter 5 **Conclusion and Future Work**

5.1 Summary

In this thesis, a novel transformerless PV inverter has been proposed. The motivation to limit the extensive usage of conventional energy resources owing to the environmental concerns and increasing global demand in power generation has been expressed. This has led to an increment in the contribution by clean energy resources (like wind, hydro, solar and other RES) to the total energy consumed in the world. The reasons behind solar energy gaining exceptional importance as one of the emerging technologies are discussed. The importance of the power electronic converters as a medium of power conversion between RES and distribution grid has been highlighted in Chapter 1. It is followed by the categorization of the PV system based on the mode of operation. Different kinds of PV inverter for grid-tied systems are detailed.

In Chapter 2, a literature review has been presented showing the benefits of eliminating the transformer. This trending topic has attracted a lot of researchers in the past few decades and single-phase non-isolated PV inverters are categorized based on numerous factors such as types of power decoupling stages, number of power processing stages, with or without a transformer and types of grid-interfaces. A detailed study on prevailing transformerless inverters has been done. Different attributes like cost, complexity, number of devices, additional branches and number of passive elements have been considered. The concerns on removing a transformer (generation of leakage current due to the galvanic connection between PV panel and the grid) have been brought into notice and how an inverter topology can ensure that the flow of leakage current is maintained within limits (less than 300 mA) specified by German standard VDE 0126-1-1.

In Chapter 3, based on the overview and analysis of aforementioned inverter topologies, a novel transformerless PV inverter is proposed with a reduced number of semiconductor devices and no additional auxiliary components for disconnecting PV source from the grid which helps in minimizing leakage current. Since the negative rail of the PV module is directly connected with the utility grid in the proposed inverter, it a common-ground type inverter and thus minimal leakage current should be observed. Steady-state analysis of the proposed inverter topology has been reported in detail. The various modes of operation in the

proposed inverter are explained and then by application of volt-second balance and capacitor-charge balance, the voltage gain is derived. A unique control strategy was designed from the voltage gain expression. It depicted a symmetric duty cycle with respect to voltage gain and sinusoidal output waveforms as desired. It is observed that voltage gain is negative and positive for duty ratio less than 0.5 and greater than 0.5 respectively. The analysis of the converter was validated by simulating on PSIM software. A 250W prototype was build and the experimental results appeared to be in close agreement with the simulation results. Thus, open-loop analysis of proposed PV inverter was verified. It should be underlined that this performance was achieved by using only four switches and without any complex control circuit.

In Chapter 4, the dynamic modeling of the inverter was done. The state-space model, considering the uncertainties of state variables, was established. The closed-loop analysis begins with calculating the transfer function of the plant which is done in MATLAB using *minreal* function. A step-by-step procedure has been shown to compute the control input $d(s)$ to filter inductor current $i_{L_f}(s)$ transfer function. Since the proposed inverter is considered for grid-connected PV systems, current control technique has to be implied which is generally a double loop structure with outer-loop generating output current reference and inner-loop for regulating grid current as per the reference generated. Later, various types of current controllers are studied and PR controllers are considered to be the most suitable for the generation of sinusoidal reference and achieving zero steady-state error. The derivation for computation of the controller transfer function has been explained. The transfer function for the inner and outer loop has been determined and the absolute tracking of the sinusoidal reference has been observed. The closed loop operation of this inverter has been validated through simulation results in PSIM software and hardware implementation is done to verify the simulation results. These results demonstrate a promising and practical inverter for a grid-connected PV system.

5.2 Contribution of the thesis

1. Steady-state analysis and designing a new circuit topology for DC/AC conversion; single-stage direct conversion.
2. Small-signal modeling and closed-loop control and design of the proposed topology.

5.3 Suggestions for Future Work

a) Stand-alone or off-grid mode of operation:

Since this work is focused on the grid-tied solar inverters, its operation in grid isolation mode can also be tested. As future work, this would contribute to further expansion of the PV system for both modes of operation.

In addition, efficiency analysis of the proposed topology with other single-phase single-stage transformerless inverter topologies can be done to estimate the accuracy and losses of this inverter with respect to existing transformerless inverter topologies.

b) Three-phase circuit operation, analysis, and design:

This single-phase inverter can be further examined by extending it to three- phase system and the performance of the inverter can be observed.

REFERENCES

[1] A. Y. Saber and G. K. Venayagamoorthy, "Plug In Vehicles and Renewable Energy Sources for Cost and Emmision Reductions," *IEEE Transactions on Industrial Electronics,* vol. 58, no. 4, pp. 1229-1238, 2011.

[2] "www.nrcan.gc.ca," [Online]. Available: https://www.nrcan.gc.ca/energy/facts/renewable-energy/20069.

[3] S. Shinde , K. Patil, S. Khairnar and W. Gandhare, "The role of power electronics in renewable energy systems research and development," in *Second International Conference on Emerging Trends in Engineering & Technology*, Nagpur, India, 2009.

[4] A. Chatterjee and K. B. Mohanty, "Current Control strategies for single phase grid integrated inverters for photovoltaic applications-a review," *Renewable and Sustainable Energy Reviews,* vol. 92, pp. 554-569, 2018.

[5] J.-S. Lai, "Power electronics applications in renewable energy systems," in *IECON'03.29th Annual Conference of the IEEE Industrial Electronics Society*, Roanoke, VA, USA, 2003.

[6] J. M. Carrasco, L. G. Franquelo, J. Bialasiewicz, E. Galvan, R. PortilloGuisado, M. Prats, J. Leon and N. Moreno-Alfonso, "Power-Electronics Systems for the Grid Integration of Renewable Energy Sources:A Survey," vol. 53, no. 4, pp. 1002-1016, August 2006.

[7] "wikipedia," [Online]. Available: https://en.wikipedia.org/wiki/Growth_of_photovoltaics.

[8] S. Alepuz, S. Busquets-Monge, J. Bordonau, J. Gago, D. Gonzalez and J. Balcells, "Interfacing renewable eneregy sources to the utility grid using a three level inverter," *IEEE Transactions on Industrial Electronics,* vol. 53, no. 5, pp. 1504-1511, October 2006.

[9] R. Hasan, S. Mekhilef, M. Seyedmahmaoudian and B. Horan , "Grid-connected isolated PV microinverters:A review," *Renewable and Sustainable Energy Reviews,* vol. 67, pp. 1065-1080, January 2017.

[10] S. Kjaer, J. Pedersen and F. Blaabjerg, "A Review of Single Phase Grid connected Inverters for Photovoltaic modules," *IEEE Transactions on Industry Applications,* vol. 41, no. 5, pp. 1292-1306, 2005.

[11] R. Akikur, R. Saidur, H. Ping and K. Ullah, "Comparative study of stand-alone and hybrid solar energy systems suitable for off-grid rural electrification: A review," *Renewable and Sustainable Energy Reviews,* vol. 27, pp. 738-752, November 2013.

[12] "International Energy Agency (IEA).World Energy Outlook 2018-Executive summary - English version," [Online]. Available: https://www.iea.org/publications/freepublications/.

[13] K. Zipp, "Available:https://www.solarpowerworldonline.com/2012/07/reliability-in-solar-inverter-design/," 27 July 2012. [Online].

[14] M. Calais, J. Myrzik, T. Spooner and V. Agelidis, "Inverters for single-phase grid connected photovoltaic systems-an overview," in *2002 IEEE 33rd Annual IEEE Power Electronics Specialists Conference*, Cairns, Qld., Australia, Australia, 2002.

[15] "https://www.energymatters.com.au/components/micro-string-central-inverters/," [Online].

[16] S. Deshpande and N. Bhasme, "A review of topologies of inverter for grid connected PV systems," in *2017 Innovations in Power and Advanced Computing Technologies (i-PACT)*, Vellore, India.

[17] N. Panwar, S. Kaushik and S. Kothari, "Role of Renewable Energy Sources in Environmental Pollution: a Review," *Renewable and Sustainable Energy Reviews,* vol. 15, no. 3, pp. 1513-1524, 2010.

[18] Q.-C. Zhong and T. Hornik, Control of Power Inverters in Renewable Energy and Smart Grid Integration, 2012.

[19] N. Vazquez, M. Rosas, C. Hernandez, E. Vazquez and F. Perez-Pinal, "A New Common-Mode Transformerless Photovoltaic Inverter," vol. 62, pp. 6381-6391, 2015.

[20] T. Salmi, M. Bouzguenda, A. Gastli and A. Masmoudi, "A Novel Transformerless Inverter Topology without Zero-Crossing Distortion," *International Journal of Renewable Energy Research,* vol. 2, pp. 140-146, 2012.

[21] T. Kerekes, R. Teodorescu and U. Borup, "Transformerless Photovoltaic Inverters Connected to the Grid," in *APEC 07 - Twenty-Second Annual IEEE Applied Power Electronics Conference and Exposition,* , Anaheim, CA, USA, 2007.

[22] R. Gonzalez, E. Gubia, J. Lopez and L. Marroyo, "Transformerless Single-Phase Multilevel-Based Photovoltaic Inverter," *IEEE Transactions on Industrial Electronics,* vol. 55, no. 7, pp. 2694-2702, July 2008.

[23] S. V. Araujo, P. Zacharias and R. Mallwitz, "Highly Efficient Single-Phase Transformerless Inverters for Grid-Connected Photovoltaic Systems," *IEEE Transactions on Industrial Electronics,* vol. 57, no. 9, pp. 3118-3128, 2010.

[24] K. S. Y. X. a. M. X. L. Zhang, "H6 Transformerless Full-Bridge PV Grid-Tied Inverters," *IEEE Transactions on Power Electronics,* vol. 29, no. 3, pp. 1229-1238, March 2014.

[25] L. Zhang, K. Sun, Y. Xing and M. Xing, "H6 Transformerless Full-Bridge PV Grid-Tied Inverters," *IEEE Transactions on Power Electronics,* vol. 29, no. 3, pp. 1229-1238, 2014.

[26] Y. Siwakoti and F. Blaabjerg, "Common-Ground-Type Transformerless Inverters for Single-Phase Solar Photovoltaic Systems," *IEEE Transactions on Industrial Electronics,* vol. 65, no. 3, pp. 2100-2111, March 2018.

[27] M. Rajeev and V. Agarwal, "Analysis and Control of a Novel Transformer-Less Microinverter for PV-Grid Interface," *IEEE Journal of Photovoltaics,* vol. 8, no. 4, pp. 1110-1118, July 2018.

[28] *IEEE Recommended Practice and Requirements for Harmonic Control in Electric Power Systems,* IEEE Std 519-2014(Revision of IEEE Std 519-1992), 2014, pp. 1-29.

[29] T. Habetler, R. Naik and T. Nondahl, "Design and implementation of an inverter output LC filter used for dv/dt reduction," *IEEE Transactions on Power Electronics,* vol. 17, no. 3, pp. 327-331, 2002.

[30] K. Ahmed, S. Finney and B. Williams, "Passive Filter Design for Three-Phase Inverter Interfacing in Distributed Generation," in *Compatibility in Power Electronics*, Gdansk, Poland, 2007.

[31] K. Zeb and e. al, "A comprehensive review on inverter topologies and control strategies for grid connected photovoltaic system," *Renewable and Sustainable Energy Reviews,* vol. 94, pp. 1120-1141, October 2018.

[32] P. Andrea Ortiz Valencia and C. Andres Ramos-Paja, "Sliding-Mode Controller for Maximum Power Point Tracking in Grid-Connected Photovoltaic Systems," *Energies 2015,* vol. 8, no. 11, pp. 12363-12387, 2015.

[33] A. K. Rathore, A. K. S. Bhat, S. Nandi and R. Oruganti, "Small signal analysis and closed loop control design of active-clamped zero-voltage switched two inductor current-fed isolated DC-DC converter," *IET Power Electronics,* vol. 4, no. 1, pp. 51 - 62, 2011.

[34] R. W. Erickson and D. Maksimovic, Fundamentals of Power Electronics, 2004.

[35] H. Abdel-Gawad and V. Sood, "Small-signal analysis of boost converter, including parasitics, operating in CCM," in *2014 6th IEEE Power India International Conference (PIICON)*, Delhi, India, 2014.

[36] V. Ramanarayan, Switched Mode Power Conversion., 2nd ed., 2007.

[37] D. Zammit, C. S. Staines, M. Apap and J. Licari, "Design of PR current control with selective harmonic compensators using Matlab," *Journal of Electrical Systems and Information Technology,* vol. 4, no. 3, pp. 347-358, December 2017.

[38] T.-K. Vu and S.-J. Seong, "Comparison of PI and PR Controller Based Current Control Schemes for Single-Phase Grid-Connected PV Inverter," *Journal of the Korea Academia-Industrial cooperation Society,* vol. 11, no. 8, pp. 2968-2974, August 2010.

[39] R. Teodorescu, F. Blaabjerg, M. Liserre and P. Loh, "Proportional-resonant controllers and filters for grid-connected voltage-source converters," *IEE Proceedings - Electric Power Applications,* vol. 153, no. 5, pp. 750-762, 2006.

[40] A. Panda, M. Pathak and S. Srivastava, "A single phase photovoltaic inverter control for grid connected system," *Indian Academy of Sciences,* vol. 41, no. 1, pp. 15-30, January 2016.

[41] Y. Kafle, G. Town, X. Guochun and S. Gautam, "Performance comparison of single-phase transformerless PV inverter systems," in *2017 IEEE Applied Power Electronics Conference and Exposition (APEC)*, Tampa, US, 2017.

[42] "User's Guide for Digitally Controlled Solar Micro Inverter Design using C2000 Piccolo Microcontroller," Texas Instruments, June 2017. [Online]. Available: http://www.ti.com/lit/ug/tidu405b/tidu405b.pdf.